A COMPARISON OF FRACTURE GROWTH IN INTACT AND MICRO-FRACTURED LAC DU BONNET BATHOLITH GRANITE

BY

JASON BLAIR MARTINO

A Thesis
Submitted to the Faculty of Graduate Studies
in Partial Fulfillment of the Requirements
for the Degree of

MASTER OF SCIENCE

Department of Civil and Geological Engineering
University of Manitoba
Winnipeg, Manitoba

ISBN 0-612-13346-X

Canada

Name Jason Blair Martino

Dissertation Abstracts International is arranged by broad, general subject categories. Please select the one subject which most nearly describes the content of your dissertation. Enter the corresponding four-digit code in the spaces provided.

A Comparison of Fracture Growth in Intact and Micro-Fractured Lac du Bonnet Batholith Granite SUBJECT TERM

0	5	4	3

SUBJECT CODE

U·M·I

Subject Categories

THE HUMANITIES AND SOCIAL SCIENCES

COMMUNICATIONS AND THE ARTS
Architecture 0729
Art History 0377
Cinema 0900
Dance 0378
Fine Arts 0357
Information Science 0723
Journalism 0391
Library Science 0399
Mass Communications 0708
Music 0413
Speech Communication 0459
Theater 0465

EDUCATION
General 0515
Administration 0514
Adult and Continuing 0516
Agricultural 0517
Art 0273
Bilingual and Multicultural 0282
Business 0688
Community College 0275
Curriculum and Instruction 0727
Early Childhood 0518
Elementary 0524
Finance 0277
Guidance and Counseling 0519
Health 0680
Higher 0745
History of 0520
Home Economics 0278
Industrial 0521
Language and Literature 0279
Mathematics 0280
Music 0522
Philosophy of 0998
Physical 0523
Psychology 0525
Reading 0535
Religious 0527
Sciences 0714
Secondary 0533
Social Sciences 0534
Sociology of 0340
Special 0529
Teacher Training 0530
Technology 0710
Tests and Measurements 0288
Vocational 0747

LANGUAGE, LITERATURE AND LINGUISTICS
Language
- General 0679
- Ancient 0289
- Linguistics 0290
- Modern 0291

Literature
- General 0401
- Classical 0294
- Comparative 0295
- Medieval 0297
- Modern 0298
- African 0316
- American 0591
- Asian 0305
- Canadian (English) 0352
- Canadian (French) 0355
- English 0593
- Germanic 0311
- Latin American 0312
- Middle Eastern 0315
- Romance 0313
- Slavic and East European 0314

PHILOSOPHY, RELIGION AND THEOLOGY
Philosophy 0422
Religion
- General 0318
- Biblical Studies 0321
- Clergy 0319
- History of 0320
- Philosophy of 0322

Theology 0469

SOCIAL SCIENCES
American Studies 0323
Anthropology
- Archaeology 0324
- Cultural 0326
- Physical 0327

Business Administration
- General 0310
- Accounting 0272
- Banking 0770
- Management 0454
- Marketing 0338

Canadian Studies 0385
Economics
- General 0501
- Agricultural 0503
- Commerce-Business 0505
- Finance 0508
- History 0509
- Labor 0510
- Theory 0511

Folklore 0358
Geography 0366
Gerontology 0351
History
- General 0578
- Ancient 0579
- Medieval 0581
- Modern 0582
- Black 0328
- African 0331
- Asia, Australia and Oceania 0332
- Canadian 0334
- European 0335
- Latin American 0336
- Middle Eastern 0333
- United States 0337

History of Science 0585
Law 0398
Political Science
- General 0615
- International Law and Relations 0616
- Public Administration 0617

Recreation 0814
Social Work 0452
Sociology
- General 0626
- Criminology and Penology ... 0627
- Demography 0938
- Ethnic and Racial Studies 0631
- Individual and Family Studies 0628
- Industrial and Labor Relations 0629
- Public and Social Welfare 0630
- Social Structure and Development 0700
- Theory and Methods 0344

Transportation 0709
Urban and Regional Planning 0999
Women's Studies 0453

THE SCIENCES AND ENGINEERING

BIOLOGICAL SCIENCES
Agriculture
- General 0473
- Agronomy 0285
- Animal Culture and Nutrition 0475
- Animal Pathology 0476
- Food Science and Technology 0359
- Forestry and Wildlife 0478
- Plant Culture 0479
- Plant Pathology 0480
- Plant Physiology 0817
- Range Management 0777
- Wood Technology 0746

Biology
- General 0306
- Anatomy 0287
- Biostatistics 0308
- Botany 0309
- Cell 0379
- Ecology 0329
- Entomology 0353
- Genetics 0369
- Limnology 0793
- Microbiology 0410
- Molecular 0307
- Neuroscience 0317
- Oceanography 0416
- Physiology 0433
- Radiation 0821
- Veterinary Science 0778
- Zoology 0472

Biophysics
- General 0786
- Medical 0760

EARTH SCIENCES
Biogeochemistry 0425
Geochemistry 0996
Geodesy 0370
Geology 0372
Geophysics 0373
Hydrology 0388
Mineralogy 0411
Paleobotany 0345
Paleoecology 0426
Paleontology 0418
Paleozoology 0985
Palynology 0427
Physical Geography 0368
Physical Oceanography 0415

HEALTH AND ENVIRONMENTAL SCIENCES
Environmental Sciences 0768
Health Sciences
- General 0566
- Audiology 0300
- Chemotherapy 0992
- Dentistry 0567
- Education 0350
- Hospital Management 0769
- Human Development 0758
- Immunology 0982
- Medicine and Surgery 0564
- Mental Health 0347
- Nursing 0569
- Nutrition 0570
- Obstetrics and Gynecology .. 0380
- Occupational Health and Therapy 0354
- Ophthalmology 0381
- Pathology 0571
- Pharmacology 0419
- Pharmacy 0572
- Physical Therapy 0382
- Public Health 0573
- Radiology 0574
- Recreation 0575
- Speech Pathology 0460
- Toxicology 0383

Home Economics 0386

PHYSICAL SCIENCES
Pure Sciences
Chemistry
- General 0485
- Agricultural 0749
- Analytical 0486
- Biochemistry 0487
- Inorganic 0488
- Nuclear 0738
- Organic 0490
- Pharmaceutical 0491
- Physical 0494
- Polymer 0495
- Radiation 0754

Mathematics 0405
Physics
- General 0605
- Acoustics 0986
- Astronomy and Astrophysics 0606
- Atmospheric Science 0608
- Atomic 0748
- Electronics and Electricity 0607
- Elementary Particles and High Energy 0798
- Fluid and Plasma 0759
- Molecular 0609
- Nuclear 0610
- Optics 0752
- Radiation 0756
- Solid State 0611

Statistics 0463

Applied Sciences
Applied Mechanics 0346
Computer Science 0984
Engineering
- General 0537
- Aerospace 0538
- Agricultural 0539
- Automotive 0540
- Biomedical 0541
- Chemical 0542
- Civil 0543
- Electronics and Electrical 0544
- Heat and Thermodynamics ... 0348
- Hydraulic 0545
- Industrial 0546
- Marine 0547
- Materials Science 0794
- Mechanical 0548
- Metallurgy 0743
- Mining 0551
- Nuclear 0552
- Packaging 0549
- Petroleum 0765
- Sanitary and Municipal 0554
- System Science 0790

Geotechnology 0428
Operations Research 0796
Plastics Technology 0795
Textile Technology 0994

PSYCHOLOGY
General 0621
Behavioral 0384
Clinical 0622
Developmental 0620
Experimental 0623
Industrial 0624
Personality 0625
Physiological 0989
Psychobiology 0349
Psychometrics 0632
Social 0451

Nom _____

Dissertation Abstracts International est organisé en catégories de sujets. Veuillez s.v.p. choisir le sujet qui décrit le mieux votre thèse et inscrivez le code numérique approprié dans l'espace réservé ci-dessous.

_____ ☐☐☐ U·M·I

SUJET — CODE DE SUJET

Catégories par sujets

HUMANITÉS ET SCIENCES SOCIALES

COMMUNICATIONS ET LES ARTS
Architecture 0729
Beaux-arts 0357
Bibliothéconomie 0399
Cinéma 0900
Communication verbale 0459
Communications 0708
Danse 0378
Histoire de l'art 0377
Journalisme 0391
Musique 0413
Sciences de l'information 0723
Théâtre 0465

ÉDUCATION
Généralités 515
Administration 0514
Art 0273
Collèges communautaires 0275
Commerce 0688
Économie domestique 0278
Éducation permanente 0516
Éducation préscolaire 0518
Éducation sanitaire 0680
Enseignement agricole 0517
Enseignement bilingue et multiculturel 0282
Enseignement industriel 0521
Enseignement primaire. 0524
Enseignement professionnel 0747
Enseignement religieux 0527
Enseignement secondaire 0533
Enseignement spécial 0529
Enseignement supérieur 0745
Évaluation 0288
Finances 0277
Formation des enseignants 0530
Histoire de l'éducation 0520
Langues et littérature 0279
Lecture 0535
Mathématiques 0280
Musique 0522
Orientation et consultation 0519
Philosophie de l'éducation 0998
Physique 0523
Programmes d'études et enseignement 0727
Psychologie 0525
Sciences 0714
Sciences sociales 0534
Sociologie de l'éducation 0340
Technologie 0710

LANGUE, LITTÉRATURE ET LINGUISTIQUE
Langues
- Généralités 0679
- Anciennes 0289
- Linguistique 0290
- Modernes 0291

Littérature
- Généralités 0401
- Anciennes 0294
- Comparée 0295
- Médiévale 0297
- Moderne 0298
- Africaine 0316
- Américaine 0591
- Anglaise 0593
- Asiatique 0305
- Canadienne (Anglaise) 0352
- Canadienne (Française) 0355
- Germanique 0311
- Latino-américaine 0312
- Moyen-orientale 0315
- Romane 0313
- Slave et est-européenne 0314

PHILOSOPHIE, RELIGION ET THÉOLOGIE
Philosophie 0422
Religion
- Généralités 0318
- Clergé 0319
- Études bibliques 0321
- Histoire des religions 0320
- Philosophie de la religion 0322

Théologie 0469

SCIENCES SOCIALES
Anthropologie
- Archéologie 0324
- Culturelle 0326
- Physique 0327

Droit 0398
Économie
- Généralités 0501
- Commerce-Affaires 0505
- Économie agricole 0503
- Économie du travail 0510
- Finances 0508
- Histoire 0509
- Théorie 0511

Études américaines 0323
Études canadiennes 0385
Études féministes 0453
Folklore 0358
Géographie 0366
Gérontologie 0351
Gestion des affaires
- Généralités 0310
- Administration 0454
- Banques 0770
- Comptabilité 0272
- Marketing 0338

Histoire
- Histoire générale 0578
- Ancienne 0579
- Médiévale 0581
- Moderne 0582
- Histoire des noirs 0328
- Africaine 0331
- Canadienne 0334
- États-Unis 0337
- Européenne 0335
- Moyen-orientale 0333
- Latino-américaine 0336
- Asie, Australie et Océanie 0332

Histoire des sciences 0585
Loisirs 0814
Planification urbaine et régionale 0999
Science politique
- Généralités 0615
- Administration publique 0617
- Droit et relations internationales 0616

Sociologie
- Généralités 0626
- Aide et bien-être social 0630
- Criminologie et établissements pénitentiaires 0627
- Démographie 0938
- Études de l' individu et de la famille 0628
- Études des relations interethniques et des relations raciales 0631
- Structure et développement social 0700
- Théorie et méthodes. 0344
- Travail et relations industrielles 0629

Transports 0709
Travail social 0452

SCIENCES ET INGÉNIERIE

SCIENCES BIOLOGIQUES
Agriculture
- Généralités 0473
- Agronomie. 0285
- Alimentation et technologie alimentaire 0359
- Culture 0479
- Élevage et alimentation 0475
- Exploitation des pâturages 0777
- Pathologie animale 0476
- Pathologie végétale 0480
- Physiologie végétale 0817
- Sylviculture et faune 0478
- Technologie du bois 0746

Biologie
- Généralités 0306
- Anatomie 0287
- Biologie (Statistiques) 0308
- Biologie moléculaire 0307
- Botanique 0309
- Cellule 0379
- Écologie 0329
- Entomologie 0353
- Génétique 0369
- Limnologie 0793
- Microbiologie 0410
- Neurologie 0317
- Océanographie 0416
- Physiologie 0433
- Radiation 0821
- Science vétérinaire 0778
- Zoologie 0472

Biophysique
- Généralités 0786
- Medicale 0760

SCIENCES DE LA TERRE
Biogéochimie 0425
Géochimie 0996
Géodésie 0370
Géographie physique 0368
Géologie 0372
Géophysique 0373
Hydrologie 0388
Minéralogie 0411
Océanographie physique 0415
Paléobotanique 0345
Paléoécologie 0426
Paléontologie 0418
Paléozoologie 0985
Palynologie 0427

SCIENCES DE LA SANTÉ ET DE L'ENVIRONNEMENT
Économie domestique 0386
Sciences de l'environnement 0768
Sciences de la santé
- Généralités 0566
- Administration des hôpitaux 0769
- Alimentation et nutrition 0570
- Audiologie 0300
- Chimiothérapie 0992
- Dentisterie 0567
- Développement humain 0758
- Enseignement 0350
- Immunologie 0982
- Loisirs 0575
- Médecine du travail et thérapie 0354
- Médecine et chirurgie 0564
- Obstétrique et gynécologie 0380
- Ophtalmologie 0381
- Orthophonie 0460
- Pathologie 0571
- Pharmacie 0572
- Pharmacologie 0419
- Physiothérapie 0382
- Radiologie 0574
- Santé mentale 0347
- Santé publique 0573
- Soins infirmiers 0569
- Toxicologie 0383

SCIENCES PHYSIQUES
Sciences Pures
Chimie
- Généralités 0485
- Biochimie 487
- Chimie agricole 0749
- Chimie analytique 0486
- Chimie minérale 0488
- Chimie nucléaire 0738
- Chimie organique 0490
- Chimie pharmaceutique 0491
- Physique 0494
- PolymÈres 0495
- Radiation 0754

Mathématiques 0405
Physique
- Généralités 0605
- Acoustique 0986
- Astronomie et astrophysique 0606
- Électronique et électricité 0607
- Fluides et plasma 0759
- Météorologie 0608
- Optique 0752
- Particules (Physique nucléaire) 0798
- Physique atomique 0748
- Physique de l'état solide 0611
- Physique moléculaire 0609
- Physique nucléaire 0610
- Radiation 0756

Statistiques 0463

Sciences Appliqués Et Technologie
Informatique 0984
Ingénierie
- Généralités 0537
- Agricole 0539
- Automobile 0540
- Biomédicale 0541
- Chaleur et thermodynamique 0348
- Conditionnement (Emballage) 0549
- Génie aérospatial 0538
- Génie chimique 0542
- Génie civil 0543
- Génie électronique et électrique 0544
- Génie industriel 0546
- Génie mécanique 0548
- Génie nucléaire 0552
- Ingénierie des systèmes 0790
- Mécanique navale 0547
- Métallurgie 0743
- Science des matériaux 0794
- Technique du pétrole 0765
- Technique minière 0551
- Techniques sanitaires et municipales 0554
- Technologie hydraulique 0545

Mécanique appliquée 0346
Géotechnologie 0428
Matières plastiques (Technologie) 0795
Recherche opérationnelle 0796
Textiles et tissus (Technologie) 0794

PSYCHOLOGIE
Généralités 0621
Personnalité 0625
Psychobiologie 0349
Psychologie clinique 0622
Psychologie du comportement 0384
Psychologie du développement 0620
Psychologie expérimentale 0623
Psychologie industrielle 0624
Psychologie physiologique 0989
Psychologie sociale 0451
Psychométrie 0632

A COMPARISON OF FRACTURE GROWTH IN INTACT AND MICRO-FRACTURED LAC DU BONNET BATHOLITH GRANITE

BY

JASON BLAIR MARTINO

A Thesis submitted to the Faculty of Graduate Studies of the University of Manitoba in partial fulfillment of the requirements for the degree of

MASTER OF SCIENCE

TABLE OF CONTENTS

ABSTRACT

At the Underground Research Laboratory of Atomic Energy of Canada Limited in Manitoba, Canada, a 3.5-m-diameter circular tunnel was excavated into a pre-instrumented block of rock to determine the response of the rock mass to the excavation of the tunnel. In support of this project, physical models of the circular tunnel were tested in the laboratory under uniaxial and biaxial loading conditions. The rock blocks were instrumented to detect the nucleation and propagation of tensile cracks with increasing load. This thesis documents and interprets the fracture patterns in the rock blocks.

Two types of rocks were used in the study: pink unfractured granite and microfractured grey granite. Predictably, fractures formed and propagated at lower loads in the microfractured grey granite, however, the fracture pattern and sequence of fracturing are similar for both granites: primary fractures, followed by remote cracks with the process terminating with sidewall slabbing. The final length of the primary crack was shorter in the grey granite than in the pink granite (40 mm in the grey granite as compared to 125 mm in the pink granite for the uniaxial case). The length in both decreased with increased confining pressure. The remote crack lengths remained approximately the same at all confining pressures. The load causing the various fracture processes increased with confining pressure, although not as much as expected from theoretical studies.

ACKNOWLEDGMENTS

I wish to thank my Kelly, for all her patience and support while I prepared this thesis and my parents for their encouragement in pursuing my education.

I would also like to thank the following people.

Dr. Emery Lajtai for his guidance and advice.

Mr. Wojciech Grajewski and Mr. Wayne Pitura for their assistance in preparation of the physical models.

Dr. Brian Stimpson and Dr. Ian Ferguson for their constructive reviews and helpful comments on my work.

Finally, I would like to thank AECL and Mr. Gary Simmons in particular, for giving me time to work on my degree and thesis.

LIST OF FIGURES

LIST OF TABLES

CHAPTER 1

INTRODUCTION

The understanding of the mechanism of fracture development around underground openings is important for the design of a safe and stable opening. This is true for mining and civil engineering works as well as nuclear waste disposal vaults. AECL Research (Atomic Energy of Canada Limited) has developed an Underground Research Laboratory (URL) in the southeastern corner of Manitoba in the Lac du Bonnet Batholith to study the response of in situ rock to conditions that would exist in an underground waste disposal vault. Access to the rock to a depth of 440 m has allowed in situ and laboratory testing of brittle rock from different depths and stress regimes. There are two types of granite at the URL site, pink and grey. The rock is pink to a depth of 220 m at the URL shaft. At depth the rock is grey, except around water conducting fracture zones where it is pink. Above a major shallow dipping fracture zone (270 m depth at the URL shaft) the rock is jointed, below it joints are few to non-existent. However, the grey granite displays numerous microcracks around excavations.

In order to observe the behaviour of both pink and grey granite under controlled laboratory conditions, physical model testing of rectangular rock blocks with centrally drilled holes (representing a circular tunnel) was carried out at the University of Manitoba. The program was designed as a laboratory component of the Mine-by Experiment at the URL. The latter was designed to measure the rock mass response to the excavation of a circular tunnel along the intermediate stress direction (Read and Martin 1991). The former was done to test simplified models of the tunnel under controlled conditions to

assist in understanding the in situ response and to compare fracture development between the intact (pink) and micro-fractured (grey) granite. The properties of the pink granite are well known so they provided a point of comparison for the behaviour of the grey granite.

Both uniaxial and biaxial conditions were used in the block testing. Samples of both pink granite, from the near surface or shallow region, and grey granite, from the deep region were obtained from sites on the Lac du Bonnet batholith. The pink granite was obtained from Cold Spring Quarries, the grey from the 420 Level of the URL.

CHAPTER 2

GEOTECHNICAL SETTING

All samples used in this study come from one of two sites in the Lac du Bonnet Batholith. Pink granite block samples were excavated from the Cold Spring Quarry, which is a commercial operation producing building and decorative stone (Figure 2.1). The grey samples come from the URL. The URL is a center for large scale, in situ experiments related to the disposal of nuclear fuel wastes. The two sites are located about 20 km apart (Figure 2.2).

The URL shaft was collared in 1982, this was followed by the construction of the head frame. The shaft was excavated from 1983 March to 1985 April to 255 m as a rectangular, 4.8 X 2.9 m shaft. The shaft was extended from 1987 July to 1988 August to 443 m depth using full-face drill and blast excavation techniques. The extension is circular and 4.6-m in diameter. The 240 Level was developed from 1985 to 1987 and the 420 Level was completed in 1990 (Figure 2.3). A major experiment, the Mine-by Experiment was carried out from 1991 September to 1992 August. During this time a circular 3.5-m-diameter tunnel (Room 415) was excavated using a non-explosive, mechanical rock breaking technique (Onagi et al. 1992) into a pre-instrumented volume of rock.

The source rock for the grey granite samples was mechanically (without explosives) excavated in two large blocks, approximately one metre from the northwest sidewall of Room 415 in Room 414. The tunnel size was later increased to the configuration shown (Figure 2.4) so that the tunnel wall now touches the sample site. The block faces were aligned perpendicular to the Room 415 wall; the tunnel runs along azimuth 45° and the block faces are along azimuth 135°. The blocks had 45-mm-diameter pilot holes drilled

around their perimeter and these holes were then reamed with a 100-mm-diameter bit to remove the rock webs between the holes and free the blocks.

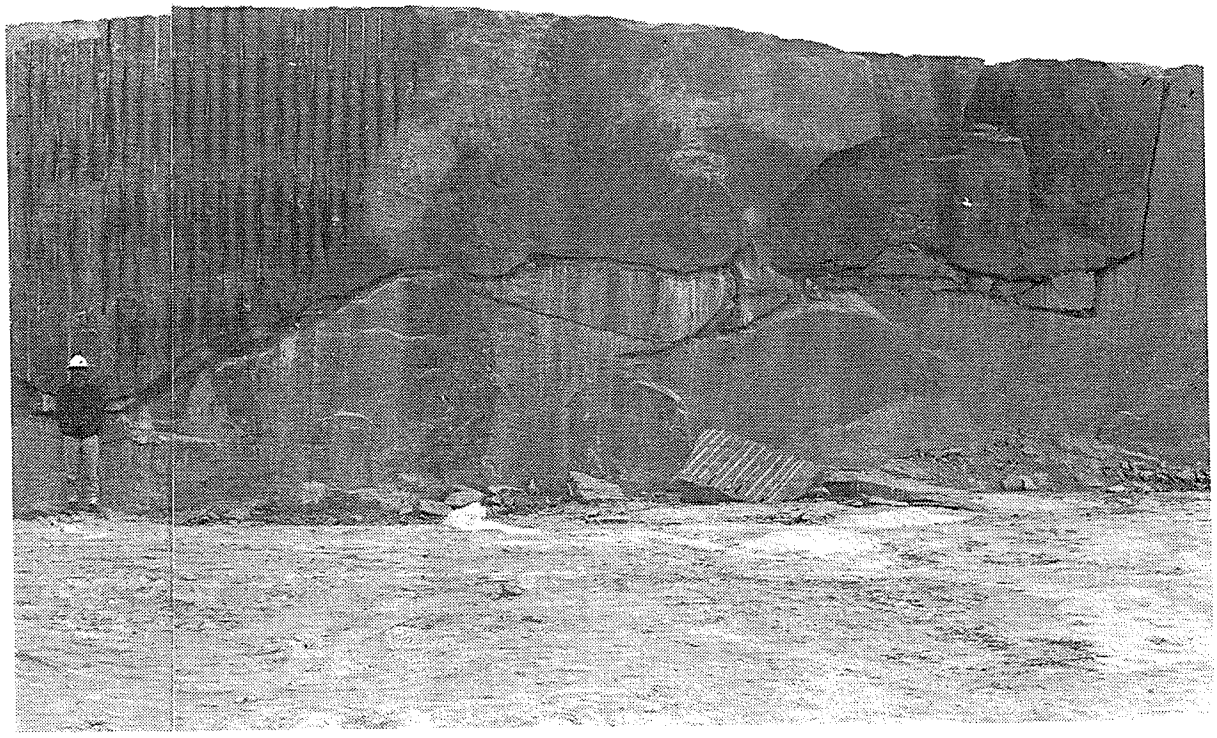

FIGURE 2.1: Photograph Shows a Sub-Horizontal Joint at the Cold Spring Quarry

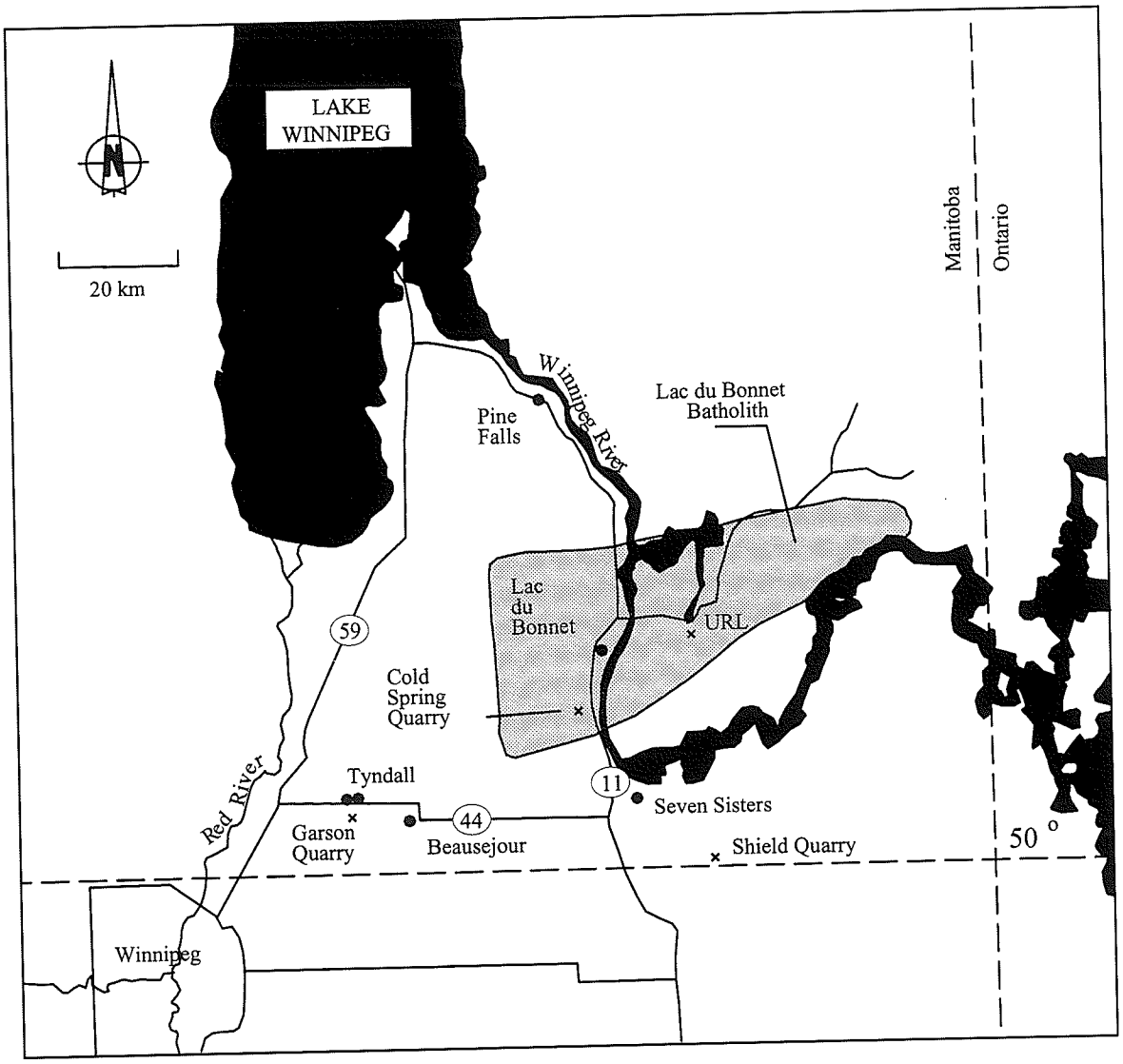

FIGURE 2.2: Location of the URL and the Cold Spring Quarry

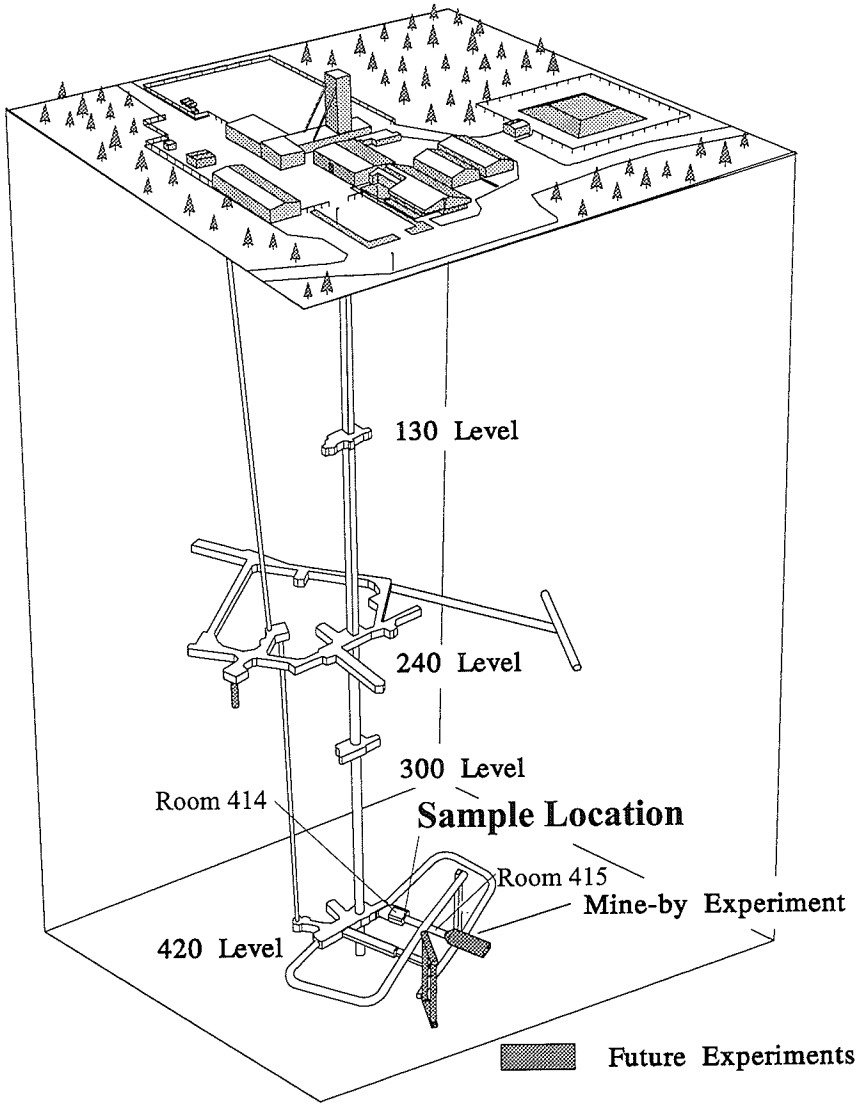

FIGURE 2.3: The Underground Layout of the URL

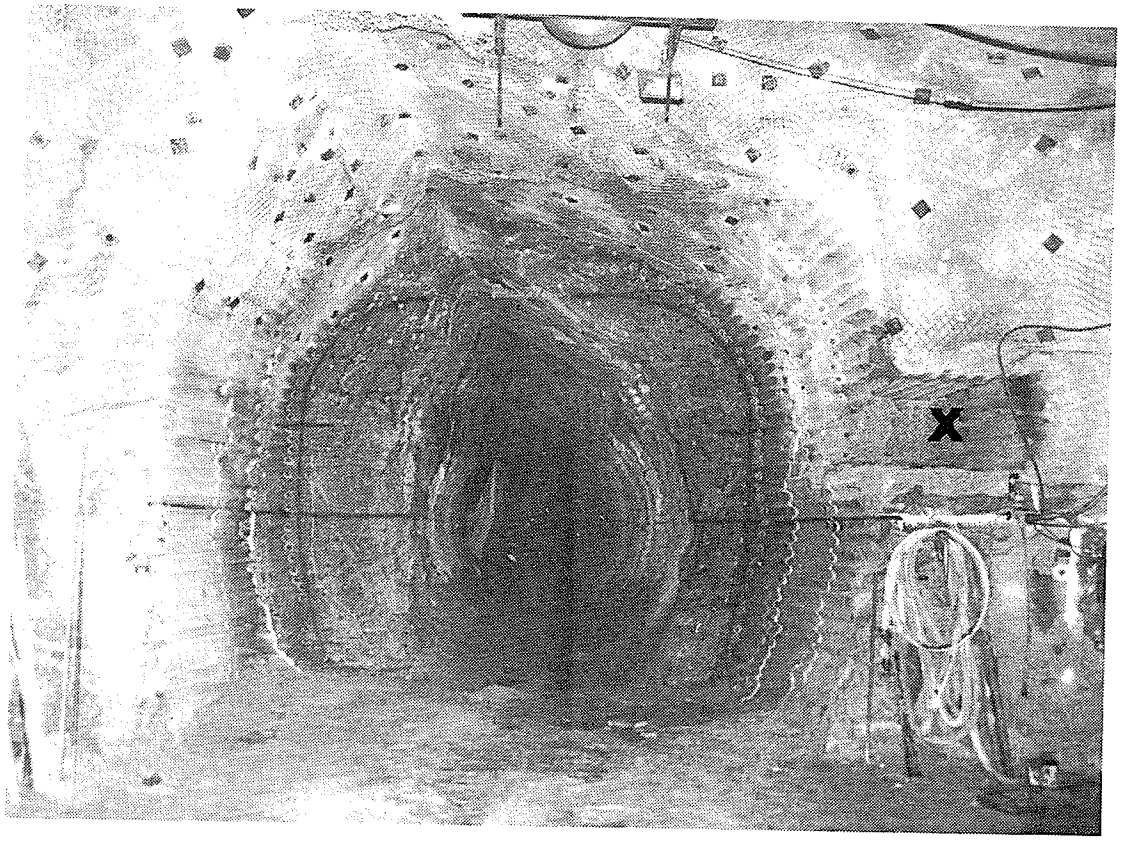

FIGURE 2.4: Location of the Grey Granite Block Samples, on the Northwest Sidewall of Room 415 on the 420 Level of the URL (marked by a X). The tunnel runs Azimuth 45-225°. The test block faces were perpendicular to the tunnel axis and the central hole in each block was drilled parallel to the tunnel axis.

2.1 Regional Geology

The Lac du Bonnet Batholith is located in the Bird River and Winnipeg River Batholithic sub-provinces in the English River gneissic belt of the Superior Province at the western edge of the Canadian Shield approximately 100 km east of Winnipeg in the southeastern corner of Manitoba. The batholith runs roughly east-northeast, has a surficial expression of over 1400 km^2 on surface, an additional 400 km^2 under Phanerozoic cover and extends from 6 to 25 km in depth. The Lac du Bonnet Batholith (LDBB) was emplaced approximately 2680$\pm$81 million years ago during the Kenoran Orogeny (Brown et al. 1989, Everitt et al. 1990).

The batholith is mainly composed of massive porphyritic granite. The granite colour is pink at surface and gradually turns to grey at depth. The grey colour represents the unaltered rock mass; the pink colour results from either a concentration of volatiles during crystallization causing leaching of iron and local deposition of iron oxide or from deutric alteration (Brown et al. 1989). The granite is medium to coarse grained and relatively uniform in texture, although it displays some local sub-horizontal gnessic banding and some xenolithic zones. Low dipping thrust faults cut through the batholith and have associated north-northeast trending joint sets (Figure 2.5). The joints sets are sub-vertical and the frequency of the joints becomes less with increasing depth (Martin and Chandler 1993).

2.2 Local Geology

Excavation at the Cold Spring Granite quarry is into an outcrop of the batholith which has a slightly higher relief than the surrounding land. It is located entirely in the pink surficial

granite. The rock mass is intersected by subvertical joint sets and a few subhorizontal joints. The subhorizontal joints are filled with clay gouge and show weathering of the joint walls.

The URL spans several lithologic and structural domains from pink, jointed granite at surface to massive unjointed grey granite at depth. The shaft intersects (Figure 2.5) two major low-dipping thrust faults, Fracture Zone 3 and 2, as well as splays of Fracture Zone 2 (Fracture Zones 2.5 and 1.9). These fracture zones are characterized by chloritic slip surfaces which grade into cataclastic zones. The cataclastic zones consist of 20 to 100 mm of breccia and clay gouge. The fracture zones show displacement on the order of a few metres to tens of metres and act as the primary ground water transportation conduits in the batholith (Everitt et al. 1990).

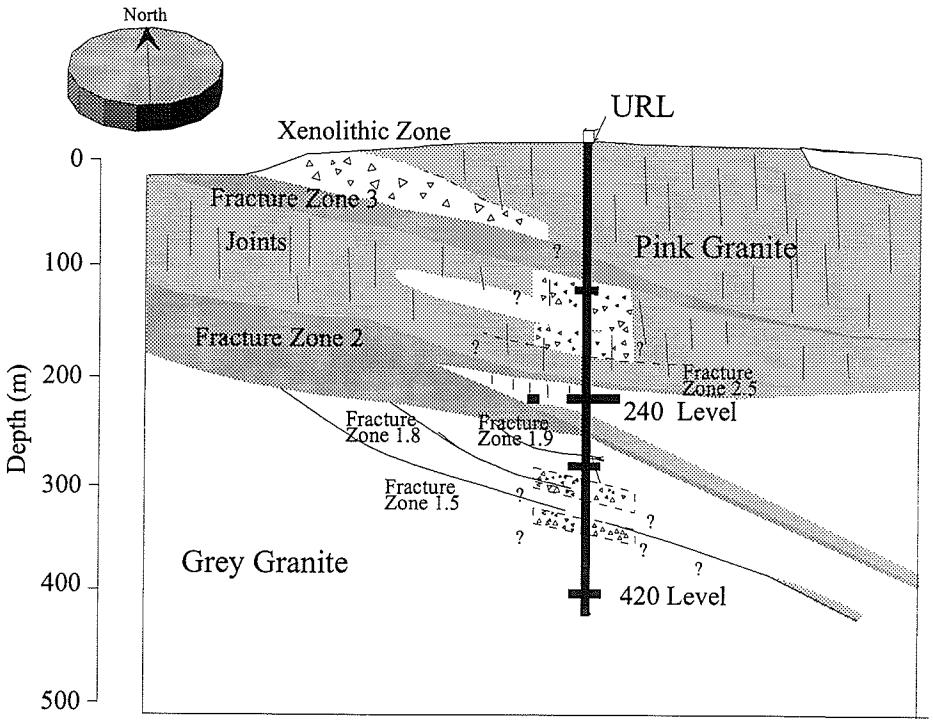

FIGURE 2.5: Geology of the Lac du Bonnet Batholith at the URL

From the surface to Fracture Zone 2.5 the rock is pink and is a medium to coarse grained granite. Tammemagi et al. (1980) classify the pink granite as granitic to granodioritic in composition under the (International Union of Geological Scientists) IUGS classification system. The most prominent joint set strikes at azimuth 020° at surface and 040° at the 240 Level. A second less prominent sub-vertical set strikes at 150-180° azimuth. Below Fracture Zone 2.5 the rock is massive unjointed grey granite except around the fracture zones where the rock is altered to pink in colour. The grey granite is classified as a granite under the IUGS classification system for igneous rocks (Kelly et al. 1993) and is coarse grained and inequigranular. The samples studied showed the rock has undergone strain as witnessed by annealed textures, cuspate/lobate grain boundaries and quartz with undulatory extinction. Chernis (1984) found core samples from the Lac du Bonnet Batholith showed an increase in porosity with depth which were attributed to the presence of microcracks that in turn may have originated on the removal of the samples from their in situ stress state.

2.3 Stress Conditions

In general, stress conditions determined at the URL are the same as those found elsewhere in the Canadian Shield with σ_1 (the maximum principal stress) being sub horizontal and σ_3 (the minimum principal stress) subvertical. Overcore stress determinations have been used extensively at the URL. However, below the 240 Level (Figure 2.3), the traditional methods of determining in situ stress, i.e. overcoring stress determinations and hydraulic fracturing, cannot adequately determine the stress conditions because the samples are microcracked and no longer elastic. Instead, interpretations using tunnel convergence and acoustic emissions have been employed to determine the stress conditions at depth (Martin 1993).

The horizontal stress falls into two domains at the URL (Martin 1989). The first domain runs from the surface to Fracture Zone 2 where σ_1 is oriented parallel to a major sub-vertical joint set which strikes at azimuth 040°. The second extends below Fracture Zone 2 where σ_1 is oriented parallel to the dip direction of Fracture Zone 2 at 130°, a rotation of 90° (Figure 2.6). This is the orientation of the tectonic maximum principal stress that caused the thrust faults. The orientation of σ_1 in the second domain matches the expected orientation of stresses in the Canadian Shield in this area (Herget 1980). The horizontal stress below the fracture zone is relatively constant with depth at about 55 MPa from Fracture Zone 2 to about 500 m and the magnitudes above the fracture zone are considerably less (Figure 2.7).

The vertical stress at the URL also changes with depth. The vertical stress is close to what one would expect from the overlying rock away from the fracture zones (Martin 1993) with a gradient of 0.026 MPa/m of depth. However, the presence of Fracture Zone 2 causes an increase in the vertical stresses because of stress concentrations at points where the fracture zone narrows (Martin and Chandler 1993).

Therefore, at the quarry, the in situ stress conditions are: a maximum horizontal stress of about 10 MPa trending 040° with a vertical stress of less than 0.25 MPa, based on extrapolation from the URL and other test sites on the batholith. At the 420 Level the maximum subhorizontal stress of 55 MPa (σ_1) dips 10° towards 130° azimuth and the subvertical stress is about 14 MPa (σ_3). The secondary principal stress (σ_2), is subhorizontal and about 48 MPa in magnitude.

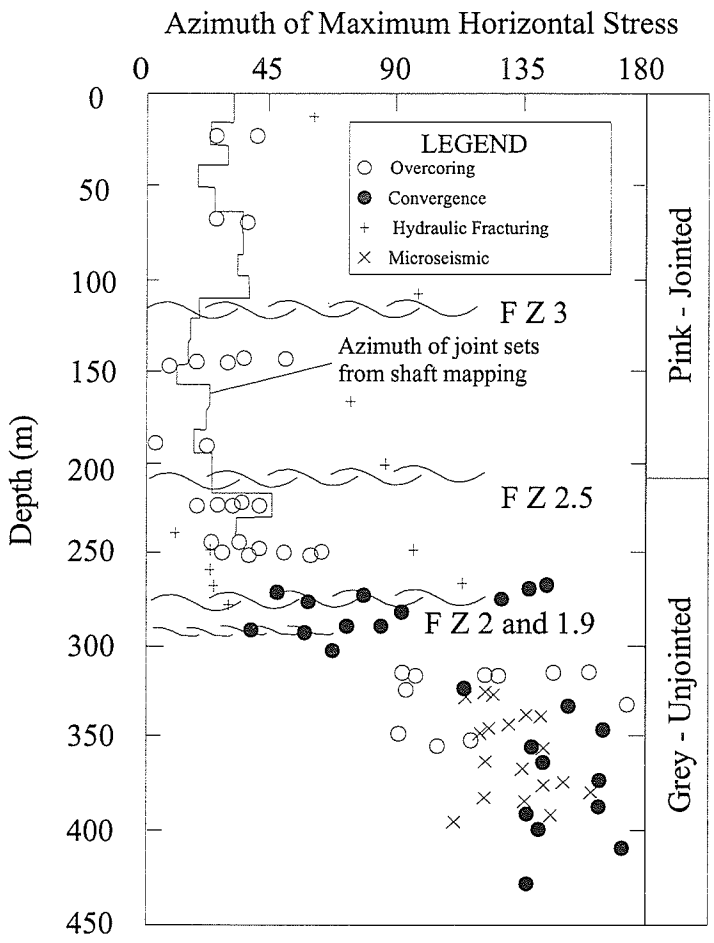

FIGURE 2.6: Variation of Maximum Horizontal Stress Orientation with Depth. The orientation of the maximum horizontal stress rotates 90° from above to below Fracture Zone 2 (after Martin 1989).

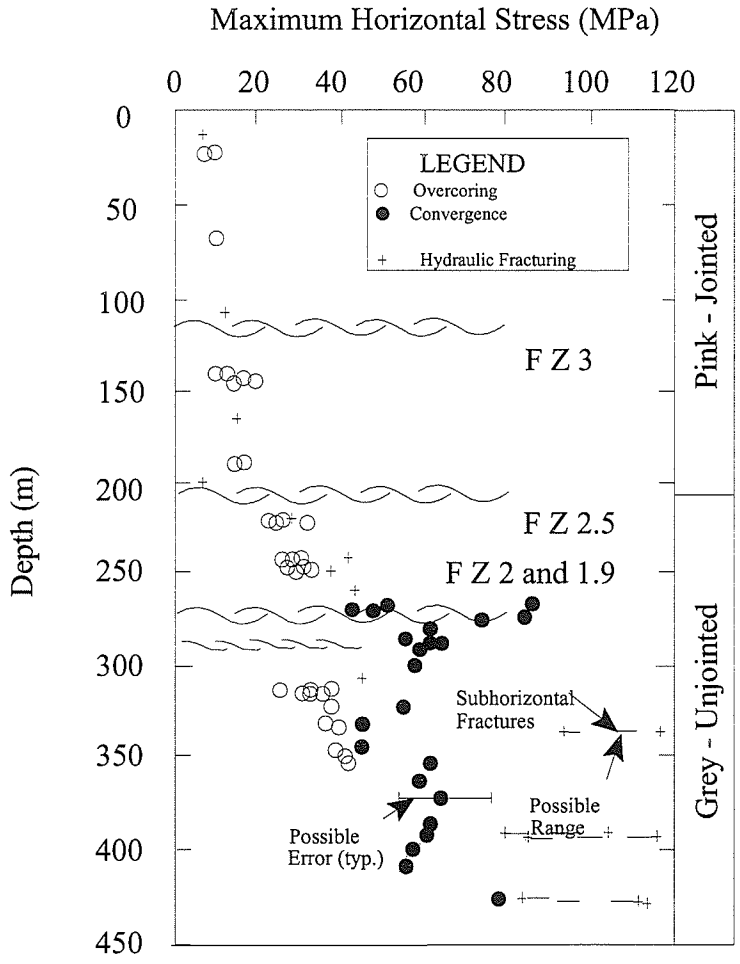

FIGURE 2.7: Maximum Horizontal Stress Increases with Depth Above Fracture Zone 2 but Remains Relatively Consistent with Depth Below Fracture Zone 2 (after Martin 1989).

CHAPTER 3

ROCK PROPERTIES

Extensive testing has been done on the pink and grey granite by the University of Manitoba, AECL and the Canada Centre for Mineral and Energy Technology (CANMET). The Cold Spring Quarry samples have been tested primarily by the University of Manitoba while samples from the URL have been primarily tested by AECL and CANMET. Martin (1993) has compiled a detailed summary of laboratory properties from the 1980s to 1993 and he indicates the Lac du Bonnet granite is a standard granite in comparison with other granites around the world, based on Deere's classification system (Deere 1980). It should be noted that both the pink and grey granites fall within this range although, based on laboratory properties, the grey granite is substantially weaker (Figure 3.1). This section provides a summary of basic rock properties.

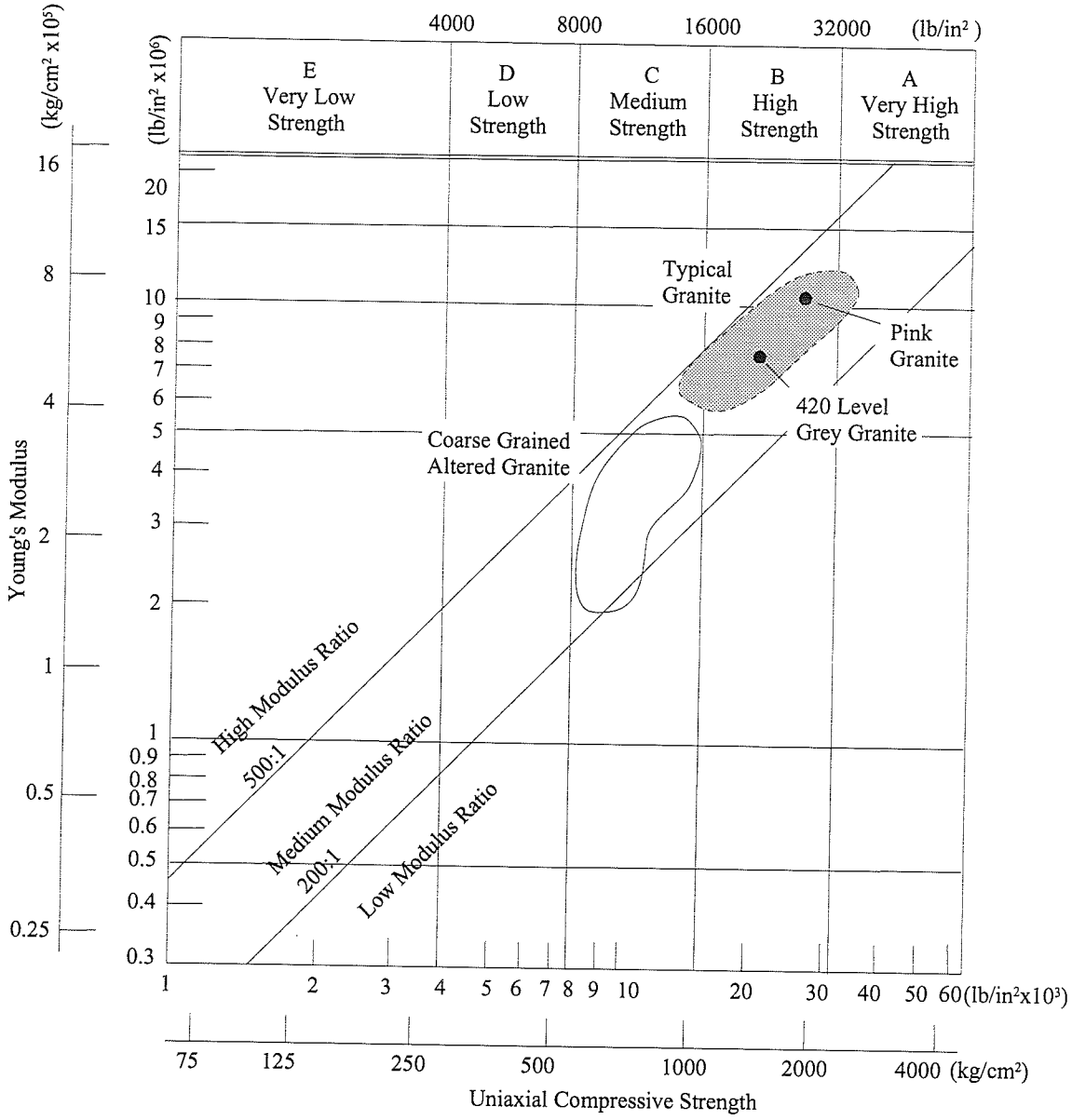

FIGURE 3.1: Classification of Lac du Bonnet Granite Using Deere's Classification System. Pink and grey granite are compared separately to sixteen worldwide locations from Deere (1980).

3.1 Basic Rock Properties

Table 3.1 provides a brief summary of some of the laboratory rock properties. The properties are divided by rock type and location.

TABLE 3.1

ROCK PROPERTIES FROM COLD SPRING QUARRY AND THE UNDERGROUND RESEARCH LABORATORY

Rock Type	Unconfined Compressive Strength MPa	Tangent Modulus E at 50%	Poisson's Ratio ν	Brazilian Tensile Strength (Dry) MPa
Cold Spring Quarry (Pink)				
Mean	228	71	0.25	13.5
Std. Dev.	15	4.7	0.04	1.2
n	62	15	15	43
URL Pink (0-200 m)				
Mean	200	69	0.26	9.3
Std. Dev.	22	5.8	0.04	1.3
n	81	81	81	39
420 Level (grey)				
Mean	154	53	0.30	9.2
Std. Dev.	25	7.2	0.06	0.9
n	110	109	103	13

Note: Grey granite data comes from within 40 m of the 420 Level
Data for all values averaged from a variety of CANMET, AECL and University of Manitoba sources.

The unconfined compressive strength (UCS) of the samples tested shows some spatial variation between the pink granite from the Cold Spring quarries and the URL. However, the UCS of the grey granite from near the 420 Level falls well below that of either set of pink granite samples. Geologists at the URL have found no geological evidence to suggest there should be any difference in the mechanical properties of the near surface

granite and granite at depth (Martin, 1992). The tangent modulus, which is measured from the stress-strain curves at 50% of the total load, shows a similar variation. The pink granite samples both show similar moduli whereas the grey granite shows a much lower modulus. The Poisson's ratios of the three sets of the granites are similar. The Brazilian Tensile Strength of the Cold Spring pink granite is slightly (about 4 MPa) higher than the samples at the URL.

3.2 Sample Damage

With increasing depth, there is visible core discing and stress relief microcracking in rock samples. This phenomenon is referred to as sample damage at the URL. Core retrieved from shallow depths shows no damage, while those from intermediate depths show some damage and those from greater depths show heavier damage and core discing (Figure 3.2). Cold Spring Quarry samples (surficial/shallow) have little or no damage visible prior to testing. While some damage is apparent in samples from the 240 Level (intermediate), samples from the 420 Level of the URL show the existence of heavier damage. Cores drilled in the vertical direction on the 420 Level, ranging in size from 54 to 1240-mm-diameter exhibit discing regardless of size. Cores, ranging in size from 18 to 300-mm-diameter, in other orientations on the 420 Level show discing as well, but generally not as severe.

Stress relief or excavation damage related microcracks can be differentiated from naturally occurring microcracks by their physical appearance. Natural microcracks have irregular or rough walls and often have infillings. On the other hand, stress relief microcracks have smooth walls and lack infilling material (Brace et al. 1972, Chernis 1984).

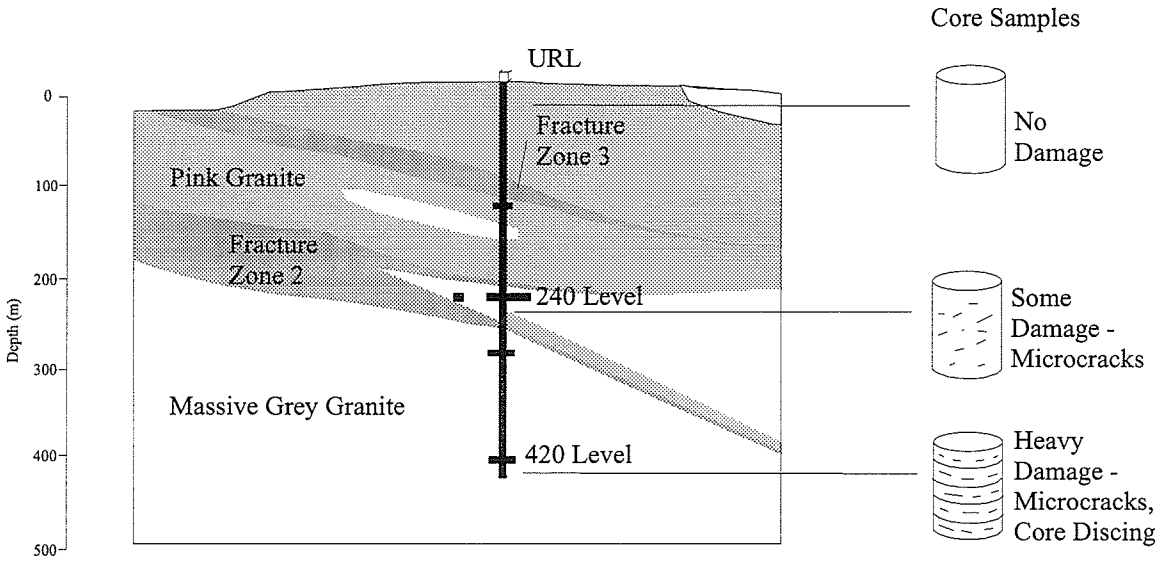

FIGURE 3.2: Sample Damage Versus Depth and Location at the URL

Samples taken from the 240 Level show the visible, stress-relief microcracks aligning with the sub-vertical joints (Martin and Chandler 1993). This is likely the dominant microcrack orientation above Fracture Zone 2 (Chernis Pers. Comm. 1994). Since microcrack alignments in the test blocks would influence the formation of the laboratory fractures, their orientation is of prime importance. Joints do exist at the quarry, but the pink granite is relatively homogeneous between the joints with the exception of a weak foliation which strikes 075° and dips steeply to the northwest (Svab and Lajtai 1981). However, the grey granite samples are visibly microfractured in several directions. In order to characterize the grey granite of the block tests, biaxial tension tests were conducted to reveal the orientations of the microcracks. Earlier biaxial tension tests for pink granite indicated only slight tensile strength variation with orientation (Svab and Lajtai 1981).

The biaxial tension test involves the bending of a circular disk of rock supported around the edges and point loaded at the centre of the disk. Because of the central symmetry cracks may propagate in any direction parallel with the load. The failure plane should

form in the plane where the tensile strength is the lowest. The plane of lowest tensile strength should also be the plane where the microcracks are the most numerous (Lajtai, Pers. Comm. 1994).

The process of testing involved drilling 32-mm-diameter core from an oriented block of grey granite taken from the sample site. Core was diamond-drilled in three orthogonal directions (Figure 3.3), into the 350x350 mm face of the block (Suite 1) in one side (Suite 2) and into the top (Suite 3) using a manually operated Milwaukee Dymo-Rig portable drill press with a diamond drill bit. By testing in the three orthogonal directions any preferential microcrack alignment should be detected. A series of lines with arrows indicating direction was marked on each face of the block to be drilled to ensure the orientation of the core after drilling could be determined. After drilling the orientation and the drilling direction was marked on each segment of core to ensure the direction of crack development was measured in the same direction (clockwise from the top) for each sample. The cores were cut into disks approximately 6-mm-thick using a manually-fed rock saw. Any rough spots on the disks were smoothed using a grinding wheel.

To test the disks a cylindrical, two-piece testing assembly, with a ring in one piece and a small bearing in the inner top-centre of the second piece (Figure 3.4) were used with a 30,000 lb. Baldwin loading frame. The ring acts as a support for the outer edge of the disk while the bearing on the second piece loads the centre of the disk. All tests were done at laboratory room humidity and temperature (~20°C).

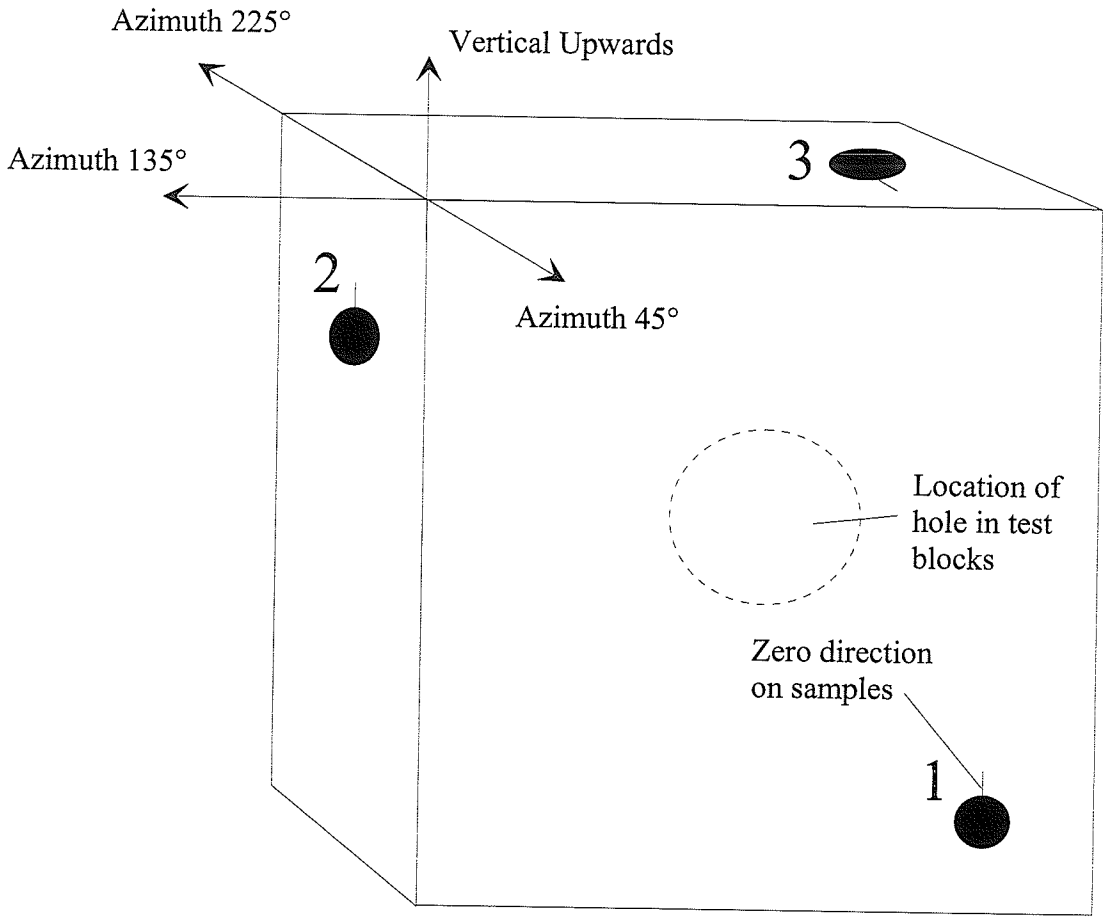

FIGURE 3.3: Grey Granite Block Showing Directions of Drilling for Biaxial Tension Test Samples. Suite 1 was drilled along Azimuth 225°, dipping 0°, Suite 2 was drilled along azimuth 315°, dipping 0° and Suite 3 was drilled vertically downwards (90° dip) with its "top" at 45° azimuth.

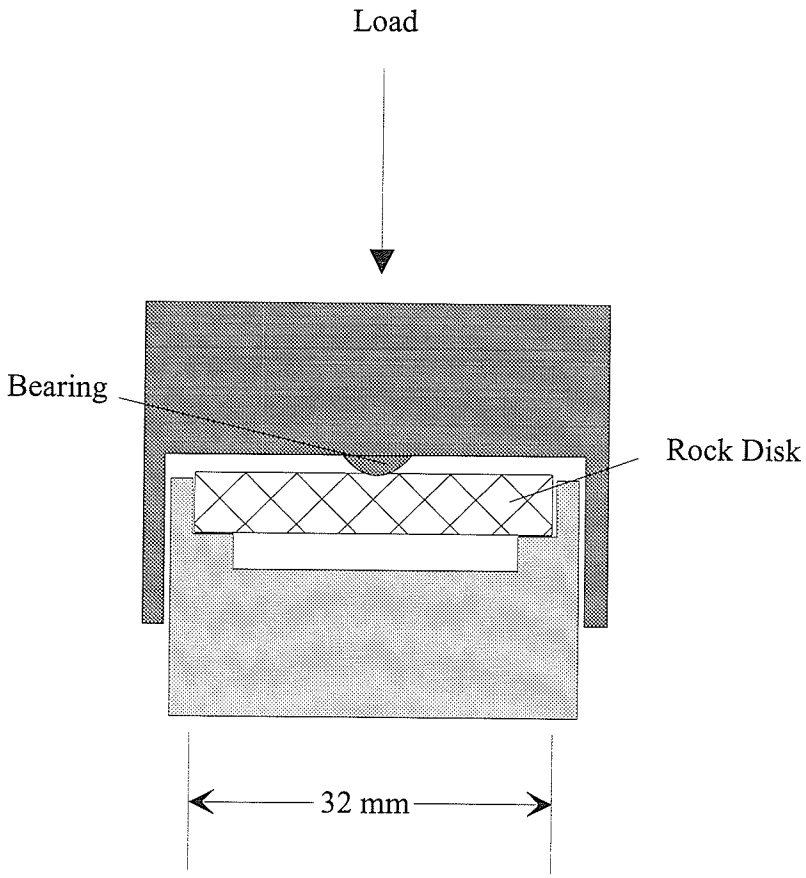

FIGURE 3.4: Biaxial Tension Test Assembly. Bearing in the top piece applies a point load to the rock disk, allowing cracking in any direction perpendicular to the loading axis.

Appendix A, Tables A-1 to A-3 provide the test results for Suites 1 to 3 respectively. The orientation of the cracks are given along with the specimen size. Figure 3.5 provides rose diagrams of the results and shows the locations and orientations of the cores.

Two of the samples which were loaded to failure using the biaxial tension test assembly are shown in Figure 3.6. On the left is Sample 32 from Suite 1, on the right is Sample 8 from Suite 1. In both samples the zero position (top of the block) is towards the top of the photograph. In Sample 32, one distinct crack formed, Sample 8 showed the formation of a triple center of cracks where two of the cracks formed a dominant crack pair. The

formation of a dominant pair was common for samples displaying a triple center. In the case of Sample 8 the horizontal cracks formed a dominant pair.

Clearly there are preferential orientations for microcrack development at the sample site. One subvertical set strikes 25° azimuth, dipping 85° northeast, a second subvertical set strikes 065°, dipping about 80° southeast and a sub horizontal set dips approximately 5° northwest.

The increase in sample damage seen in cores and the physical models is not found in situ, away from openings. A cross hole geophysics survey was conducted at the 420 Level in the area of the sample site prior to excavation. The P and S-wave velocities measured at the 420 Level show no variation (Hayles et al. 1994) and these values are very close to those seen at other depths at the URL (Martin 1993). This would indicate that microcrack density does not increase with depth (as an increase in microcrack density would act to slow seismic waves). However, variation in seismic wave velocity is seen after excavation, with a decrease in velocity in locations where damage is known to exist. The variation in rock properties can then be attributed to the sample damage related to extraction and stress relief.

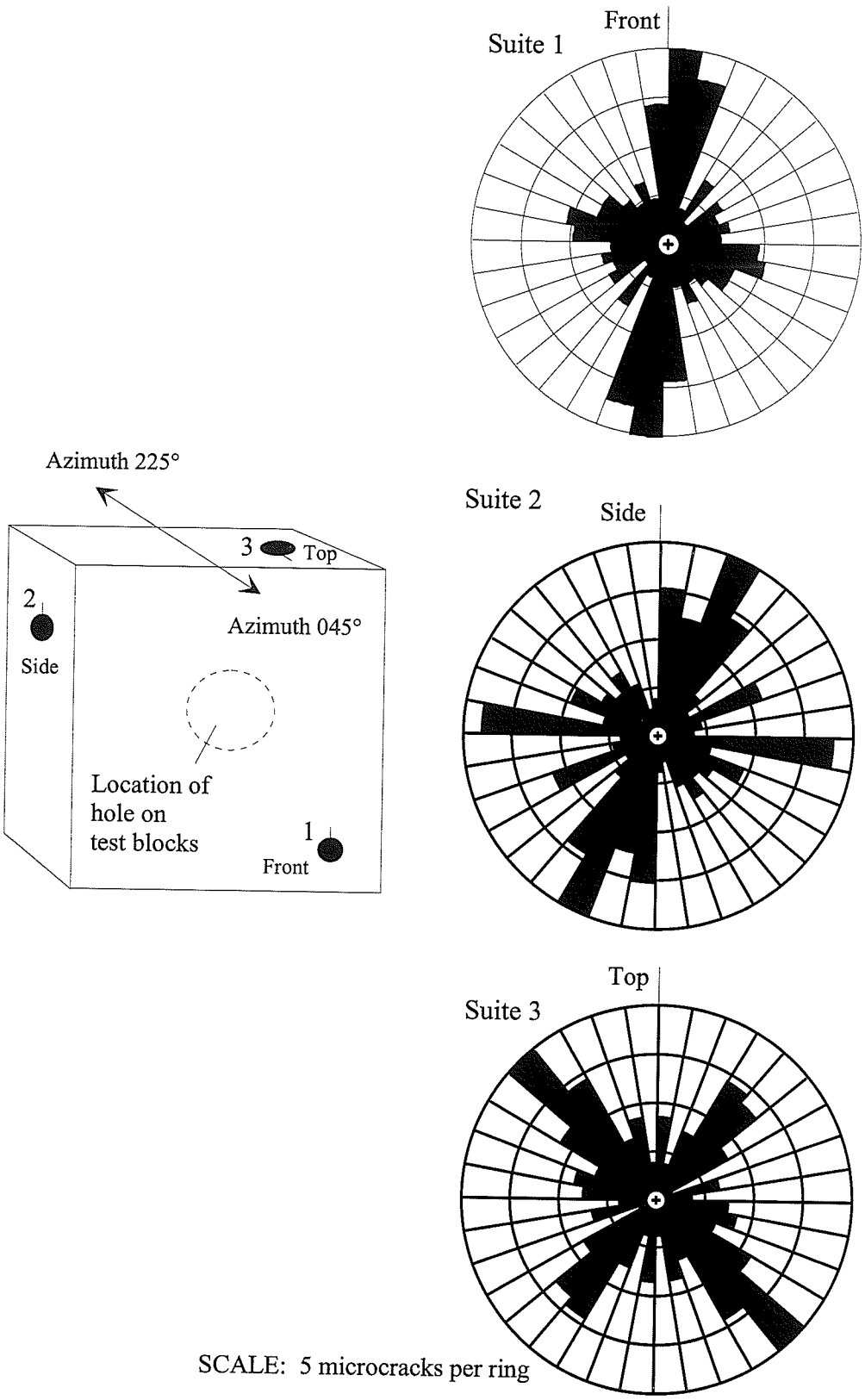

FIGURE 3.5: Rose Diagrams Showing Orientations of Crack Directions

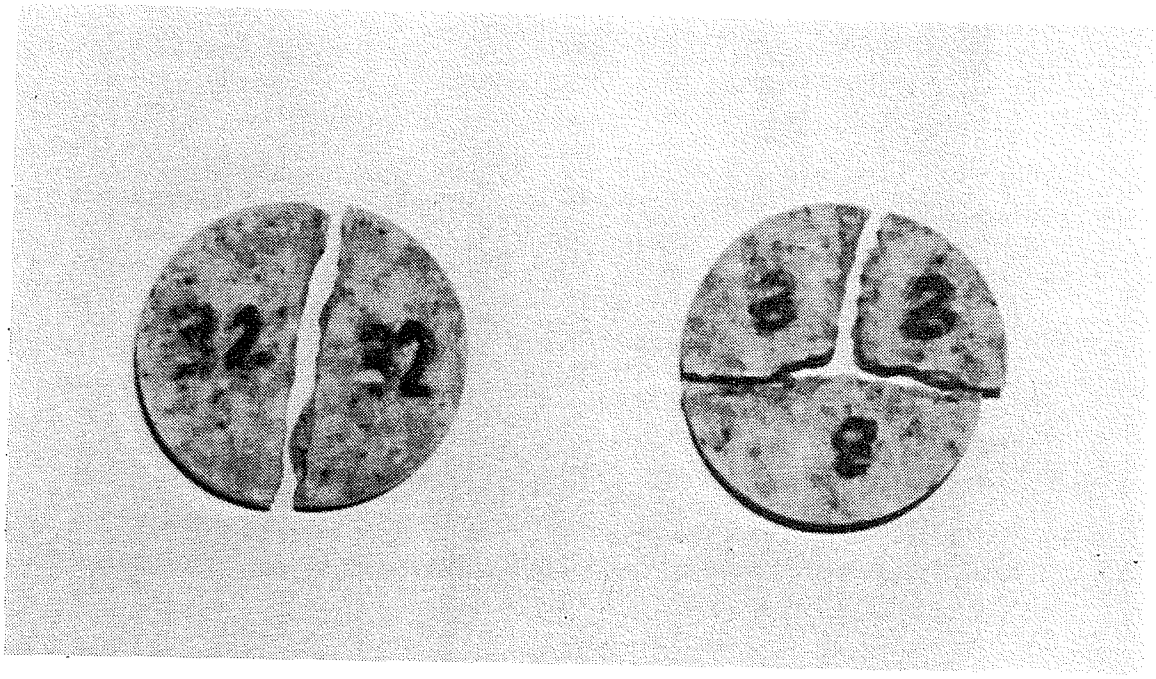

FIGURE 3.6: Photograph of Samples 32 and 8 of Suite 1. Grey granite rock disks were loaded to tensile failure using biaxial tension. Sample 32 developed a single distinct crack. Sample 8 developed a triple center of cracks with the horizontal pair forming a dominant crack. The vertical crack was split apart to better show its existence.

3.3 Crack Development

When a load applied to a material exceeds the material strength, bonds break and separate and a fracture or crack is formed with an attendant release of strain energy. For brittle rocks, under tensile conditions, the initiation of cracking coincides with failure. However, under compressive loading, crack initiation occurs well before failure. In this section, the stages of crack development in brittle solids are discussed.

The behaviour of brittle materials during loading and the stages of crack growth have been studied by many researchers; Cook (1965), Hoek and Bieniawski (1965), Bieniawski (1967), Scholz (1968), Wawersik and Fairhurst (1969), Wawersik and Brace (1970), Bombolakis (1973) Tapponnier and Brace (1976), and Lajtai et al. (1990, 1991). As loading, be it uniaxial, biaxial or triaxial, is increased cracks develop in the material and if loading is increased to sufficiently high levels, failure occurs. Much work has gone into identifying the stages of crack development. Bieniawski (1967) identified five main stages of crack development in brittle rocks. An idealized view of these stages is presented in Figure 3.7. The first stage is crack closure. Hoek and Bieniawski (1965) recognized that grain boundaries act as or contain microcracks, these cracks are generally considered to be barely visible to the naked eye, about 10 μm in length. Microcracks can also exist within mineral grains especially if stress-relief or previous loading has occurred. The first stage of loading involves the closure of the microcracks which are not parallel to the applied stress. This has the effect of increasing the modulus of elasticity of the rock and produces a non-linear stress-strain curve.

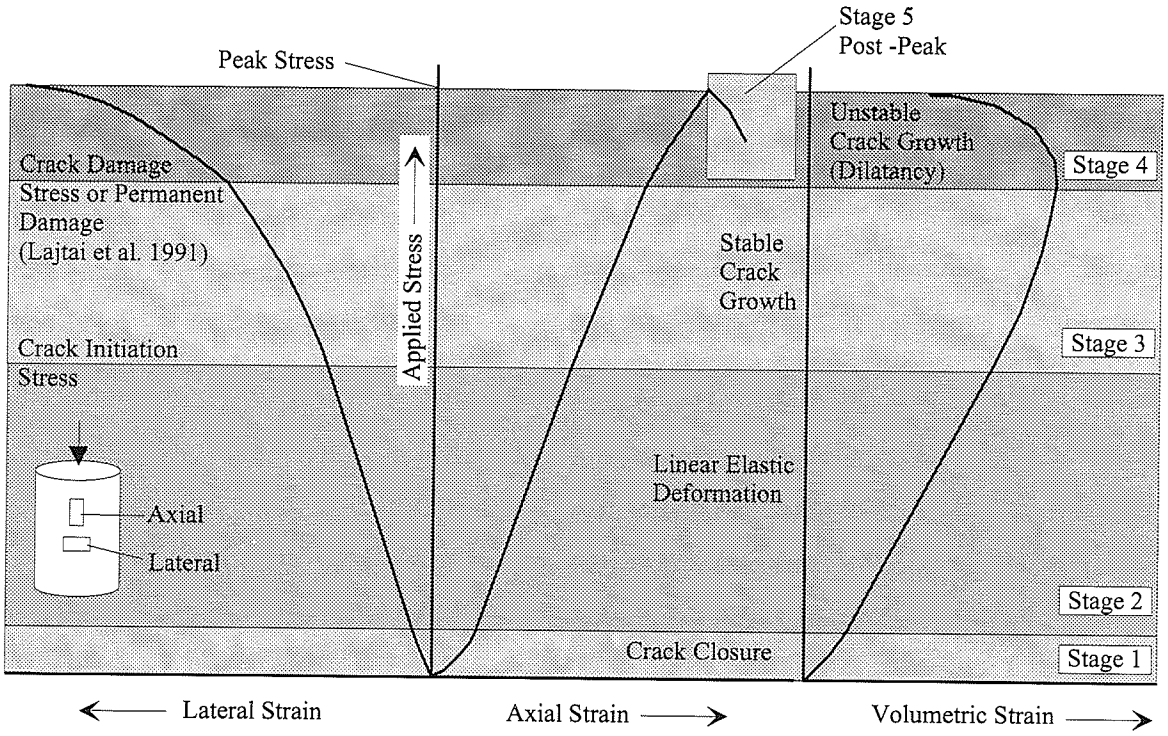

FIGURE 3.7: Strain Response to Uniaxial Loading of a Cylinder of Brittle Rock (after Bieniawski 1970). The five major stages are identified.

Once the cracks are closed, elastic deformation occurs, denoted by a straight-line section of the stress-strain curve. This stage is followed by the stage of stable crack propagation. The dividing point between the two stages in referred to as the crack initiation point. This occurs when the applied load increases stress concentrations in the rock past local strength. As a result, existing cracks can extend and new cracks can nucleate. Because the cracks develop parallel to the major principal stress, the strain gauges oriented along the specimen axis still produce a linear response while those oriented laterally produce a non-linear response.

The volumetric strain (3.1):

$$\frac{\Delta V}{V} = \frac{1-2\upsilon}{E}(\sigma_1 - \sigma_3) \approx \varepsilon_{axial} + 2\varepsilon_{lateral} \qquad (3.1)$$

which includes the contribution of the laterally oriented gauges, also becomes non-linear during this stage. Although the point of crack initiation may vary depending on rock type, strength and structure, a range of from 40% (Martin 1993) to 50% (Scholz 1968) peak strength for brittle rock is common.

A relatively sudden change in the pattern of propagating cracks is detected at a stress level of about 80% (Bieniawski 1967, Martin 1993) to 95% (Scholz 1968) of the peak strength of the sample. This stage is heralded by a reversal in volumetric strain and a rapid increase in volume. Permanent damage occurs in this stage and the term, crack damage stress has been coined by Lajtai et al. (1991) to describe the stress level at which permanent damage begins to occur. Specimens that have been loaded past the crack damage stress will show permanent lateral (circumferential) and volumetric strain when unloaded.

Continued loading results in the peak stress being achieved and permits strength failure to occur. This is easily noted by a decrease in axial strain on the stress-strain curve. The final stage is the post-peak stage. This stage is denoted by decreasing stress (Wawersik and Brace 1970).

Two samples of Lac du Bonnet granite, one Cold Spring pink, the other 420 Level grey, have been loaded to illustrate these stages. Note the differences between the two mineralogically similar granites, which have stress-relief microcracking (in the grey granite) as their physical difference. Figure 3.8 shows the response of a pink granite cylindrical sample to uniaxial loading conditions and Figure 3.9 shows the same for grey

granite. The sample in Figure 3.8 shows crack initiation beginning at 40% of peak strength and unstable growth beginning at 83% of peak strength.

The grey granite sample shows a much larger strain response to loading. This is because of the sample damage discussed in Section 3.2. The grey granite also has a lower peak strength. It is interesting to note that despite these differences the samples undergo crack initiation and unstable growth at roughly the same percentage of peak strength. However, the crack closure stress is much higher for the grey granite and truly elastic conditions exist over only a narrow stress range.

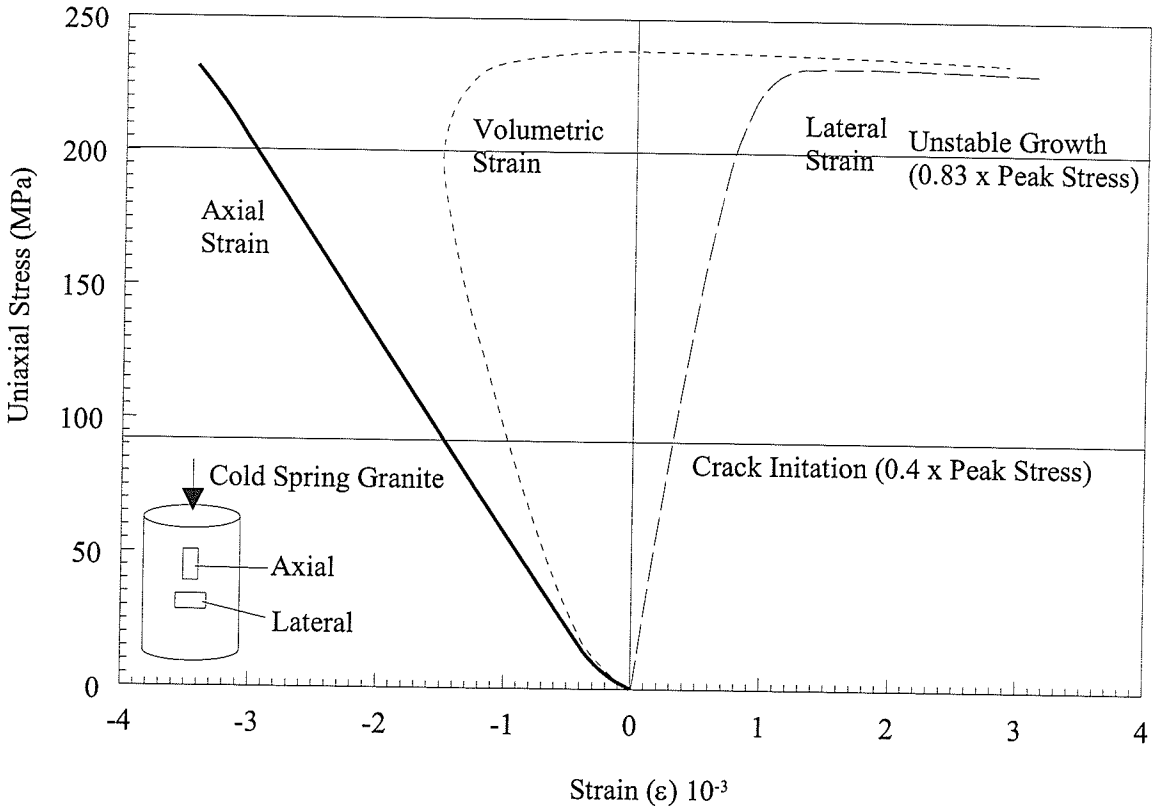

FIGURE 3.8: Stress-Strain Response of a Uniaxially Loaded Cold Spring Pink Granite Sample. Axial and lateral gauge responses and calculated volumetric strain are shown with estimates of crack initiation and unstable crack growth.

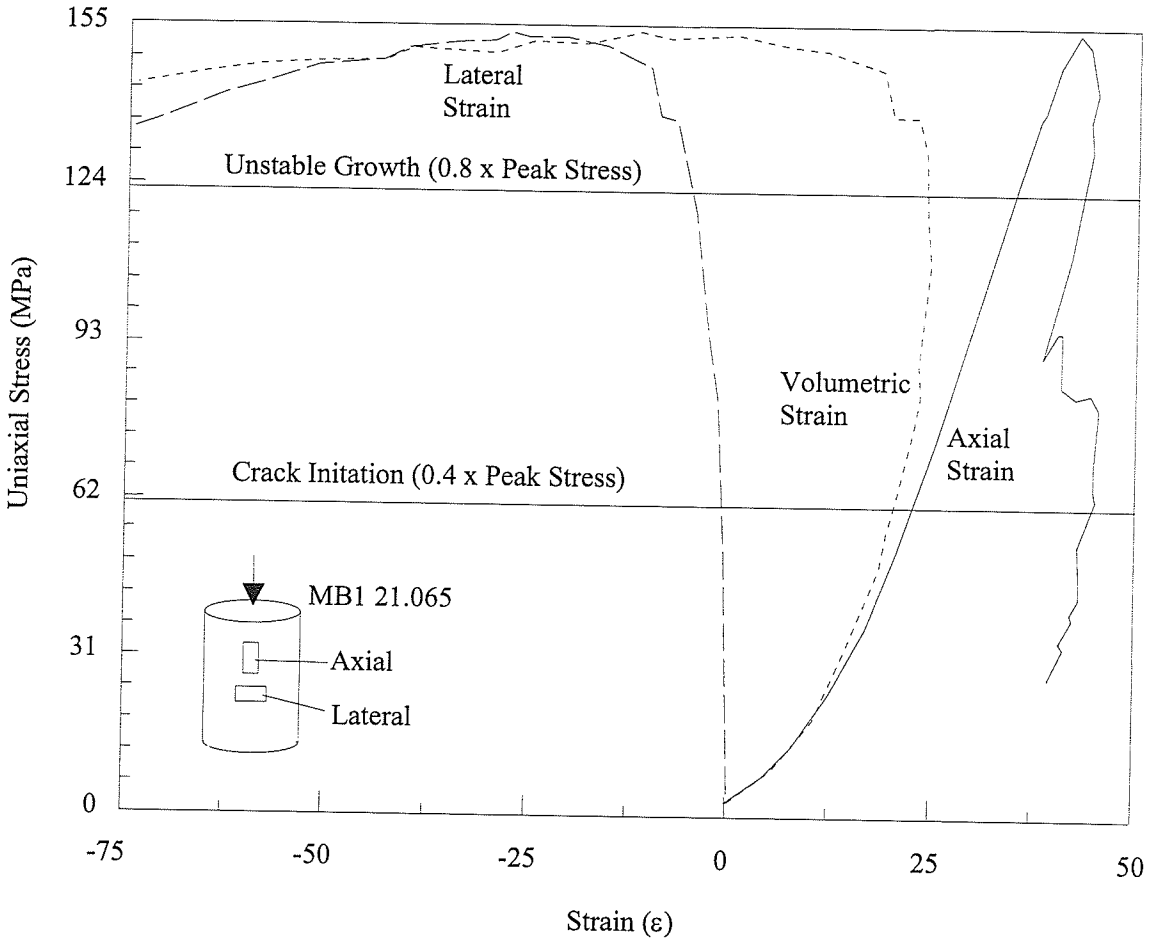

FIGURE 3.9: Stress-Strain Response of an Uniaxially Loaded 420 Level Granite Sample. Axial and lateral gauge responses and calculated volumetric strain are shown with crack initiation and unstable crack growth points (after Lau and Gorski 1991).

CHAPTER 4

PHYSICAL MODEL TESTING

Blocks of grey and pink granite with holes drilled through their centres were loaded under uniaxial and biaxial conditions. Tests on the influence of holes on the strength and fracture characteristics of rock blocks has been previously carried out by Hoek (Hoek and Brown 1980), Carter (1988, 1992) and Haimson and Herrick (1989) among others. This section describes the testing procedures and presents the results of the tests.

4.1 Testing Procedures

The block testing was the primary focus of the experimental work done for this thesis. In brief, blocks of pink and grey Lac du Bonnet batholith granite were cut to the desired size, had a hole drilled through the centre of each block, and were instrumented and loaded. The load level at which cracks developed was recorded, and the patterns and types of fractures were observed.

Two suites of block testing were carried out, Grey Granite (GGHOLE) tests 1 to 6 and Pink Granite (PGHOLE) tests 1 to 5. Both suites of samples were cut to their final sizes (350 x 350 x 105 mm) and polished at Cold Spring Quarries. The pink granite blocks were bought unoriented from Cold Spring Quarries.

The blocks were transported to the University of Manitoba and 61-mm-diameter holes were diamond drilled in each block using a manually operated Milwaukee Dymo-Rig. Holes were drilled in the center of the 350x350 face of the blocks. The hole diameter was

less than a fifth of the block width which should minimize edge effects. The holes in the grey granite blocks were drilled parallel to the Mine-by Experiment tunnel. Water was used as the cooling lubricant. The sides of the blocks to be loaded received final grinding and polishing to ensure the sides were parallel so that the stress from loading would be evenly distributed in the block.

Cracking was observed visually and with the strain gauge instrumentation. Gauge patterns (Appendix B, Figures B-1 to B-10) were chosen strategically, to maximize recording of crack formation. A typical pattern is shown in Figure 4.1. Gauge placement was based on previous tests on granite blocks, Babulic (1985), Carter (1988) and Carter et al. (1991). The strain gauges were glued to the front face of the blocks as well as inside the drilled holes, thus permitting the circumferential strain right at the hole perimeter to be recorded. The standard gauge type used was a Micro-Measurements, Measurements Group Inc. CEA-06-250UW-350. Coloured ribbon wires were soldered to the strain gauges and were connected to the data acquisition system which in turn was controlled by a computer. A Measurements System Data Scan 7000 datalogger was used in conjunction with a MTS 810 Materials Test System control unit and a MTS 1200 kip loading frame working in stress-control mode (Figure 4.2). The strain gauge data were collected by the logging computer and transferred to floppy disk. The data were translated into ASCII format for importation into spreadsheets for data manipulation and plotting.

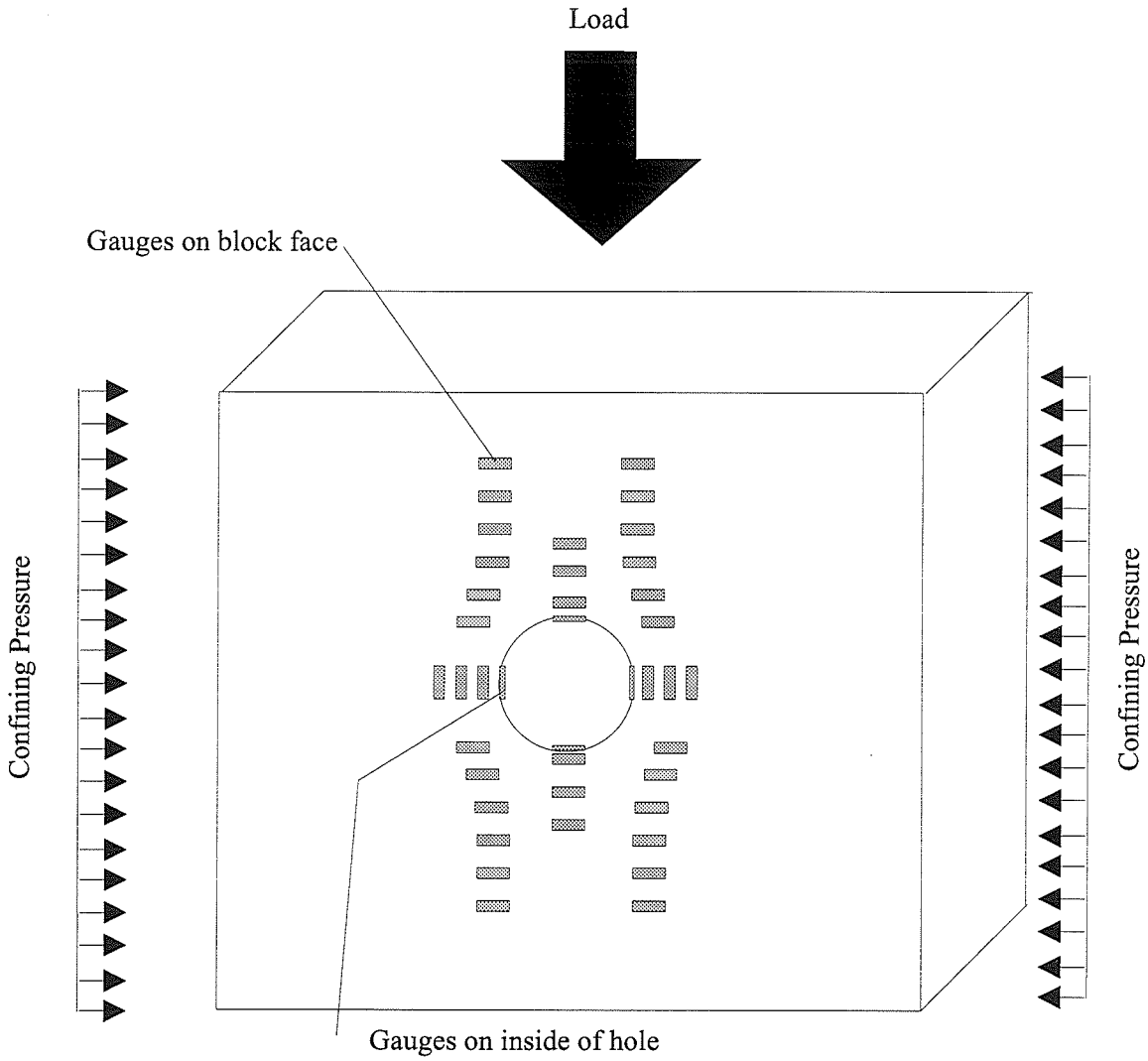

FIGURE 4.1 Typical Gauge Pattern

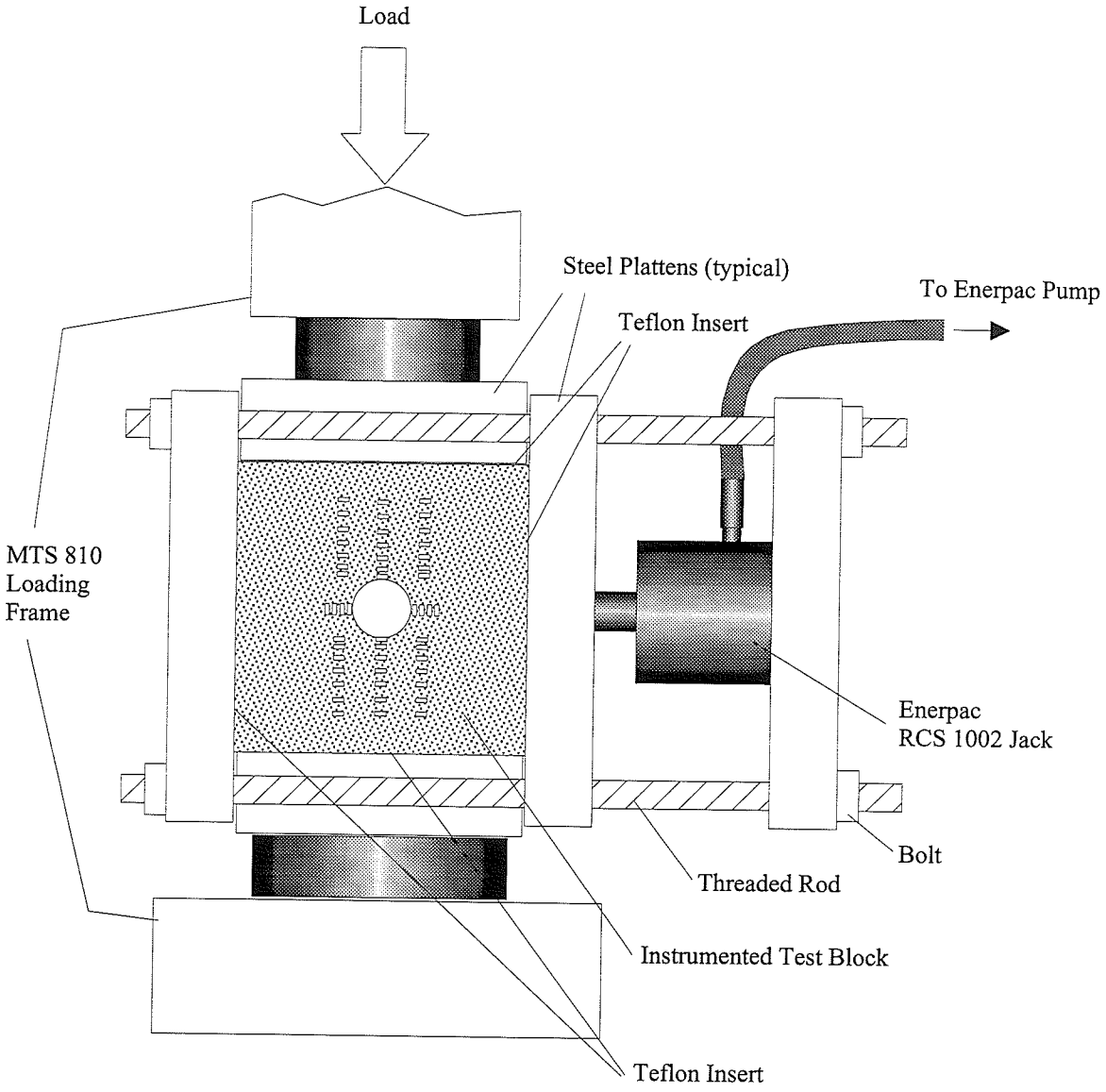

FIGURE 4.2: Set-up used for Block Testing. Set-up shown is for a biaxial test. Confining pressure is provided by an Enerpac pump and jack pressing against steel platens.

4.2 Results

The blocks were loaded axially from zero load under stress control. When confining pressure was used it was set to the specified load before the axial load was applied. Tests were done on both the pink and grey granite in either uniaxial or 2.5, 5, 10 and 15 MPa biaxial confining pressures conditions. Under increasing compression at a relatively low confining pressure, primary cracks form first, followed by remote cracks and finally hole-wall slabbing occurs (Figure 4.3). Primary tension fractures form outwards from the tunnel wall in response to predictable tensile stress. Remote cracks form from stress concentrations remote from the tunnel wall which develop when the primary crack locally changes the stress field. Slabbing along the hole wall forms in response to compressive stress concentrations and develops into breakout notches.

The gauge results from the block testing are located in Appendix C, Tables C-1 to C-10. All three types of cracks (Figure 4.3) were seen as the axial load was increased. A general description of the cracks on the instrumented face of each block are given in Appendix C, Table C-11. Cracks paths and spalling locations are given on the gauge location figures in Appendix B.

Although fracture could occasionally be seen on the block faces, or inside the hole, crack initiation was usually interpreted from the output of the strain gauges. Primary crack initiation (Figures 4.4 and 4.5) was set at the point where the strain curve first showed deflection. The first deflection point is roughly equivalent to the point of crack initiation seen in axially loaded, cylindrical samples (Section 3.3).

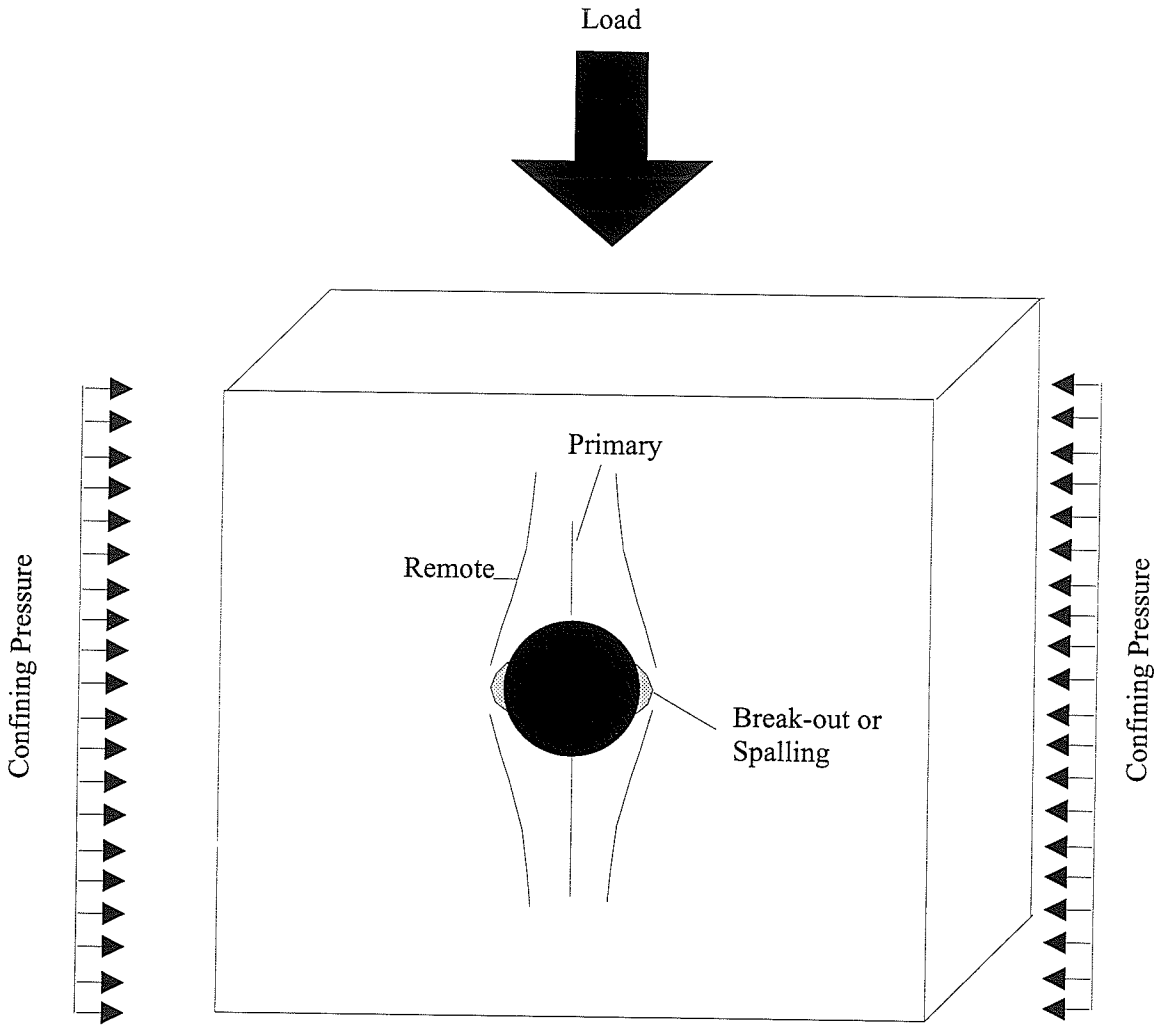

FIGURE 4.3: Crack Types Seen During Loading of Granite Blocks. The primary(ies) forms first, followed by the remote(s) and finally the side-wall slabbing.

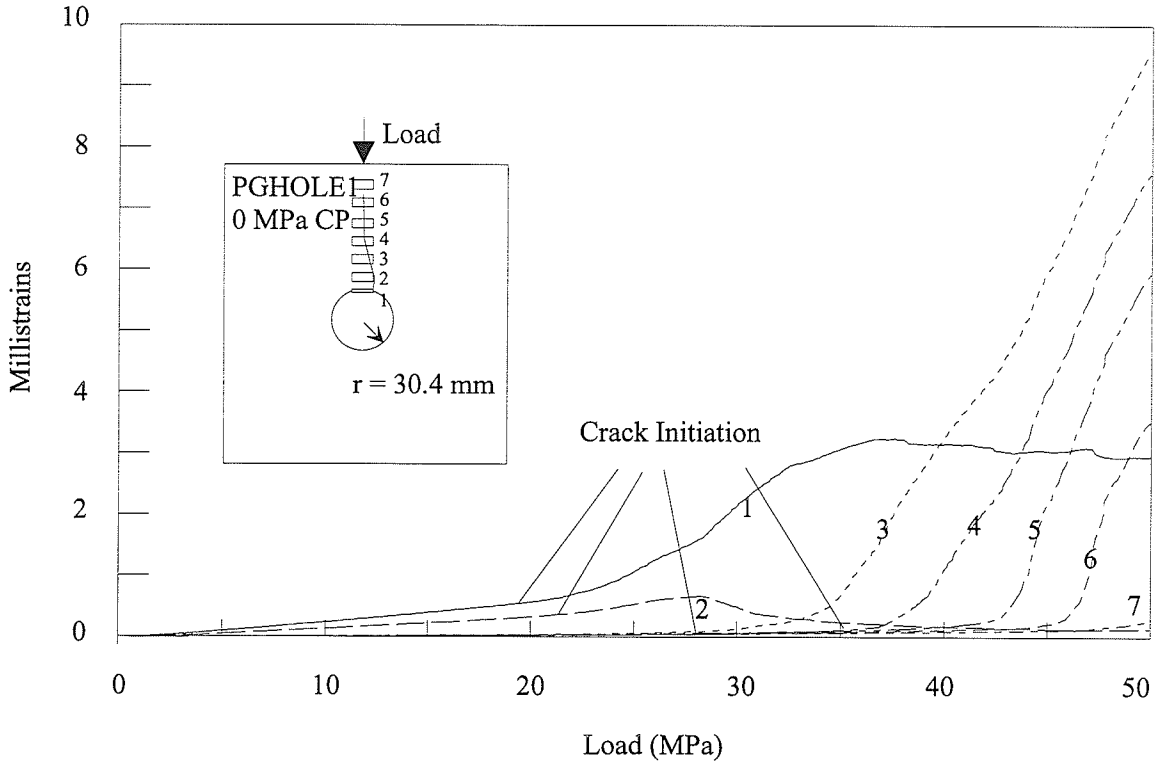

FIGURE 4.4: Primary Crack Gauge Responses for PGHOLE1 Upper Primary. The crack passes under the edge of Gauge 1, misses Gauge 2, passes under Gauges 3, 4, 5 and 6 and does not quite reach Gauge 7.

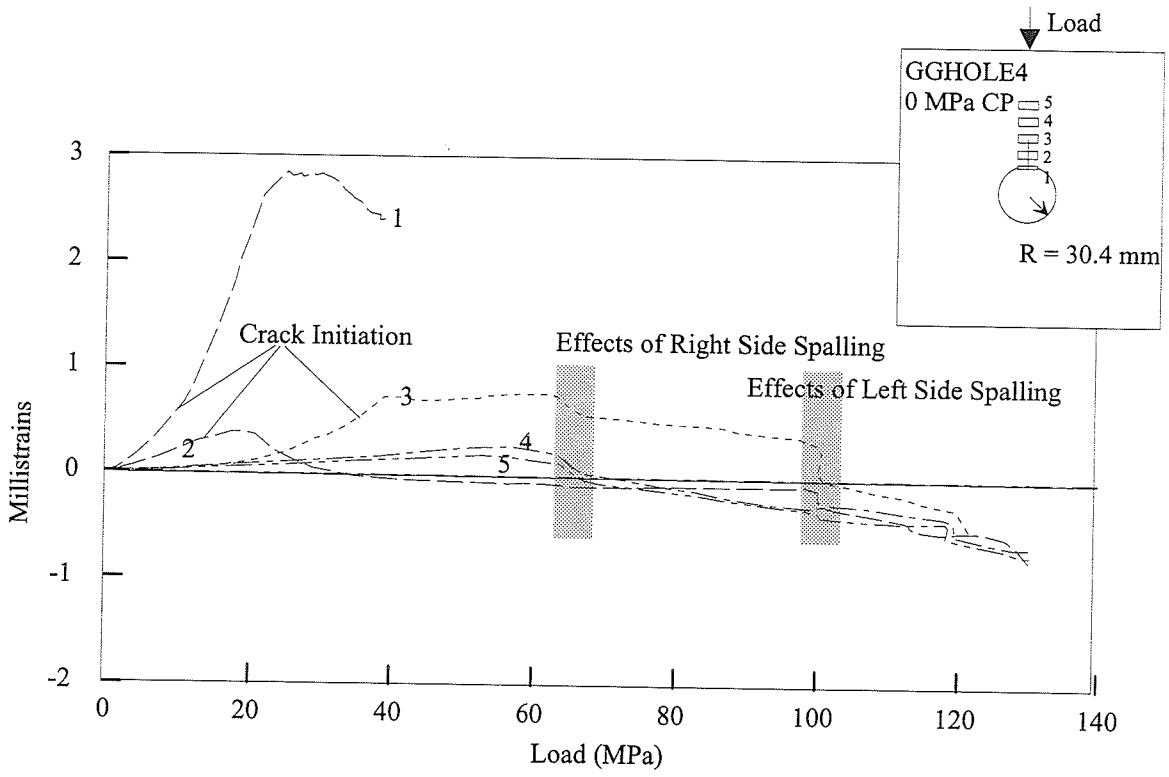

FIGURE 4.5: Primary Crack Gauge Responses for GGHOLE4 Upper Primary. The crack passes under gauges 1 to 3.

The upper primary strain gauge results for sample PGHOLE1 (Figure 4.4) are described to give a better understanding of the strain gauge responses. Gauge 1 was glued on the inside surface of the hole. The crack developed directly under Gauge 1 and passed by the edge of Gauge 2, near the hole edge. The strain increase was noticeably less and dropped off as the crack propagated past the gauge. Gauges 3 to 6 showed increased strain as the crack neared their locations on the block. A rapid increase in strain levels was measured by Gauges 3 to 6 when permanent damage occurred. In physical terms this was when the crack became more strongly developed or widened. The crack did not reach Gauge 7. When the crack development did not cause gauge debonding the gauge was capable of recording the development of later cracks in the block. Figure 4.5 illustrates this for block GGHOLE4 where spalling was detected by the gauges used to record the upper primary

crack development. When either type of sample was loaded with a confining pressure, the confining pressure tended to retard development of the primary crack, although the crack did form even at the highest (15 MPa) confining pressure.

Remote cracks nucleated away from the hole boundary and first propagated outwards from the hole, developing along the maximum principal stress trajectory. They also propagated back towards the hole, but generally at a slower rate. The first remote to form generally propagated rapidly, often faster than could be followed visually. Remote crack initiation was more difficult to select from the strain curves as gauges placed to pick up the remote crack formation often reflected the primary crack development as well. This meant the first deflection seen by the remote crack gauges may not have been the crack initiation and had to be checked versus the primary crack response.

A feature seen with the remote cracks and to a lesser extent, the primary cracks, were frequent step-outs (Figure 4.6). Step-outs or en echelon cracks (Lajtai et al. 1994) form when a developing crack is unable to overcome the material strength at its tip but the local strain increase causes a parallel crack to form nearby. The grey samples showed slightly more step-outs than did the pink samples. There were approximately 4-5 step-outs per 100 mm of remote crack path in the grey samples as compared to 3-4 step-outs per 100 mm in the pink samples.

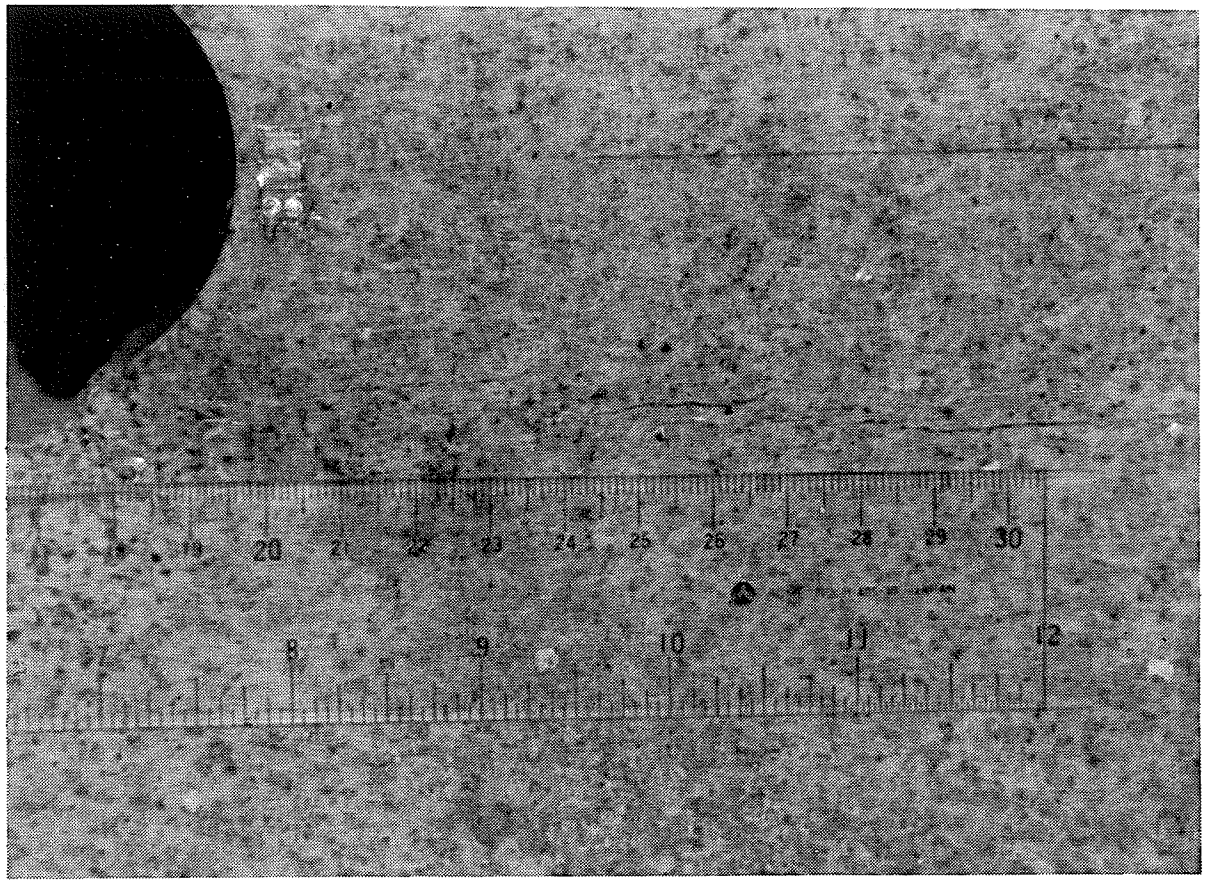

FIGURE 4.6: Photograph showing the en-echelon arrangement of this remote crack caused by a succession of step-outs.

Unlike the primary cracks, the growth in length of the remote cracks was generally not retarded by an increase in confining pressure. However, as confining pressure increased, the gauge responses to the formation of the remote cracks did show less deflection , the crack paths showed more wander and the cracks appeared to have smaller apertures. Figures 4.7 and 4.8 illustrate the difference in gauge responses to remote crack formation

for an unconfined state and 15 MPa confining pressure state. In general, the crack initiation points were less difficult to detect in the unconfined tests.

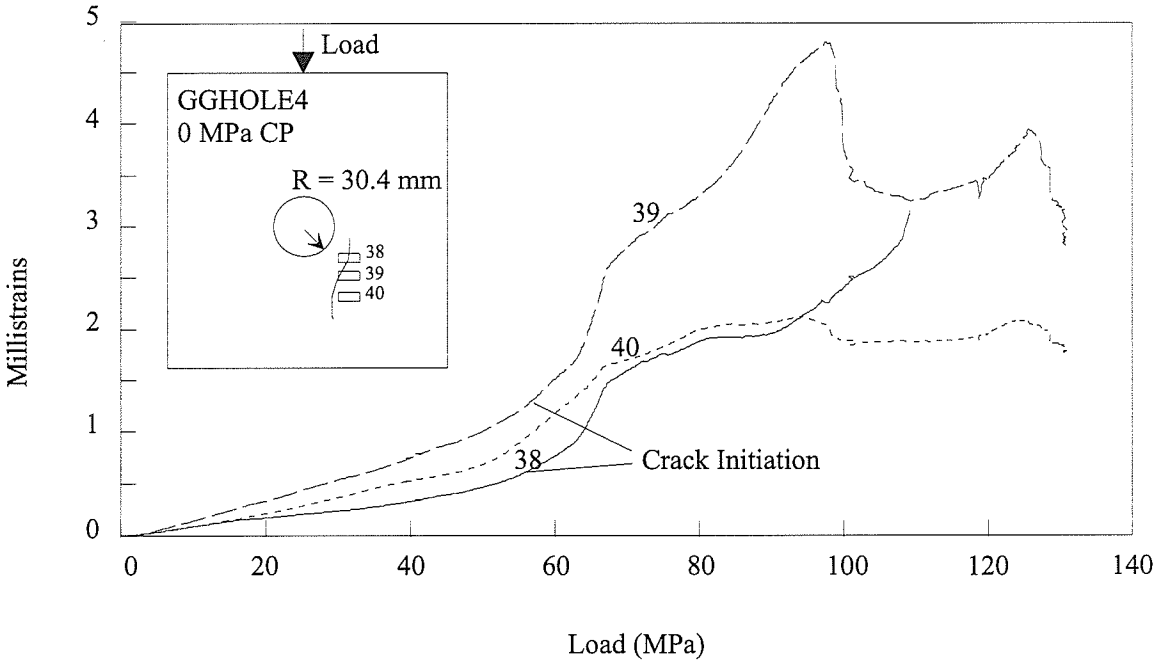

FIGURE 4.7: Gauge Response for a Remote Crack in GGHOLE4 with no confining pressure. Compare with response shown in Figure 4.8.

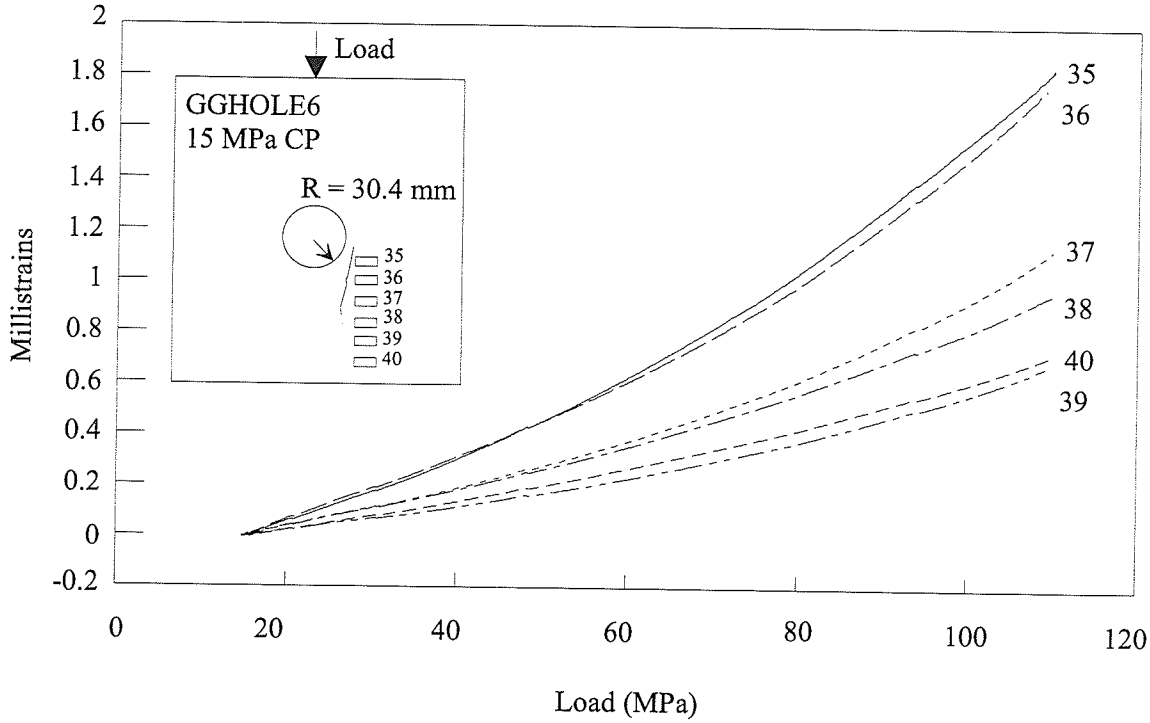

FIGURE 4.8: Gauge Response for a Remote Crack in GGHOLE6 with 15 MPa Confining Pressure. Compare to gauge response in Figure 4.7. It was very difficult to identify the initiation points on the strain curves for the microfractured rock as the curves were non-linear from the beginning

The last form of cracking to develop in the block samples was sidewall failure, occurring where the compressive stresses are concentrated at the hole edge. As loading increased the sidewall began to develop a whitish, discoloured hue and pieces of rock were seen to literally peel away from the sidewall (Figure 4.9). Similar whitish, discolouration was seen in experiments by Gay (1976). The process accelerated as the load climbed higher and rock slabs shot out from the sidewall, obscuring the hole from view during the remainder of the spalling process. The sidewall slabbing process lead to the development of breakout notches on either side of the hole. Spalling also occurred on the faces of the blocks before and during this process. Eventually the rate of spalling decreased, loading was stopped at this point because previous testing (Hoek in Hoek and Brown 1980) had

shown no further cracks formed prior to sample collapse and/or the limits of the testing machine was reached.

Figure 4.10 and 4.11 show gauge responses for sidewall slabbing in pink and grey granite. It is important to note the spalling failures on the face of the blocks often caused gauges near the sidewall slabbing locations to peel away and had a tendency to mask the sidewall slabbing responses. Gauges near the sidewall slabbing locations could show deflections from the formation of previous cracks, just like the remote crack gauges, so the first deflection on the strain curve from these gauges did not always indicate crack initiation. The pink and the grey granite showed essentially the same gauge response to breakout notch and face slabbing development.

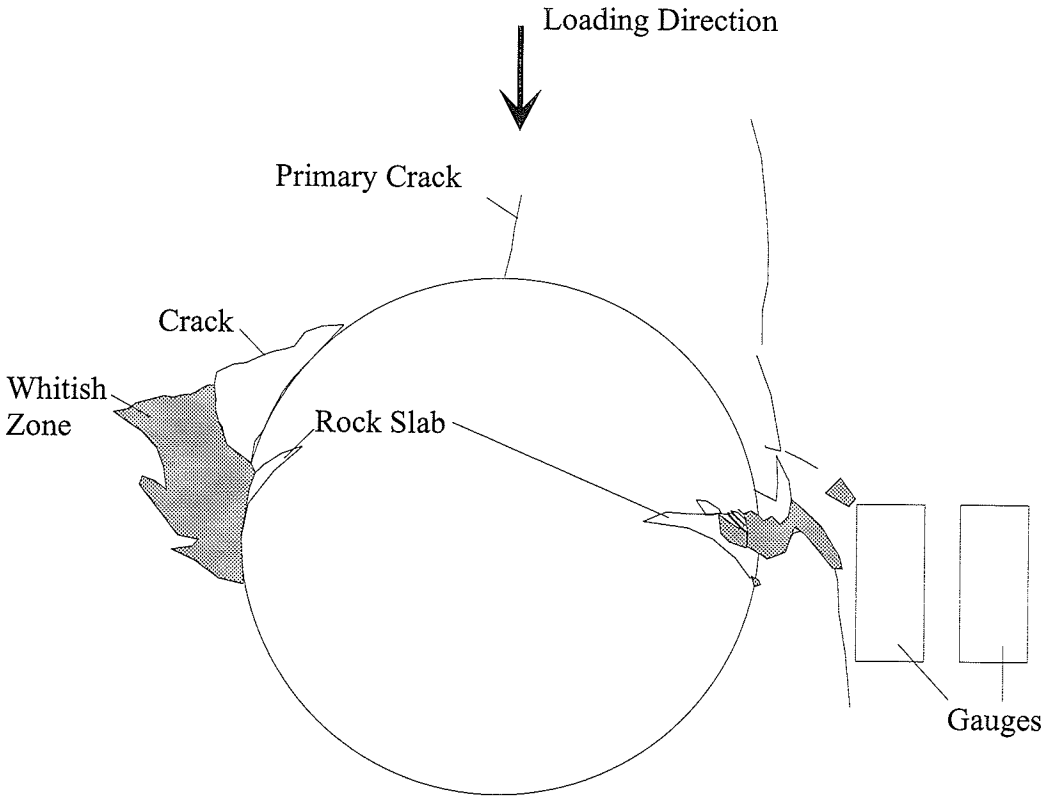

FIGURE 4.9: Sketch of Rock Slab Peeling Away from Hole Wall. The slabs were seen to peel away once sidewall slabbing had initiated. A whitish coloured, damaged zone was evident at the base of the slabs. As successive slabs peeled away breakout notches were formed.

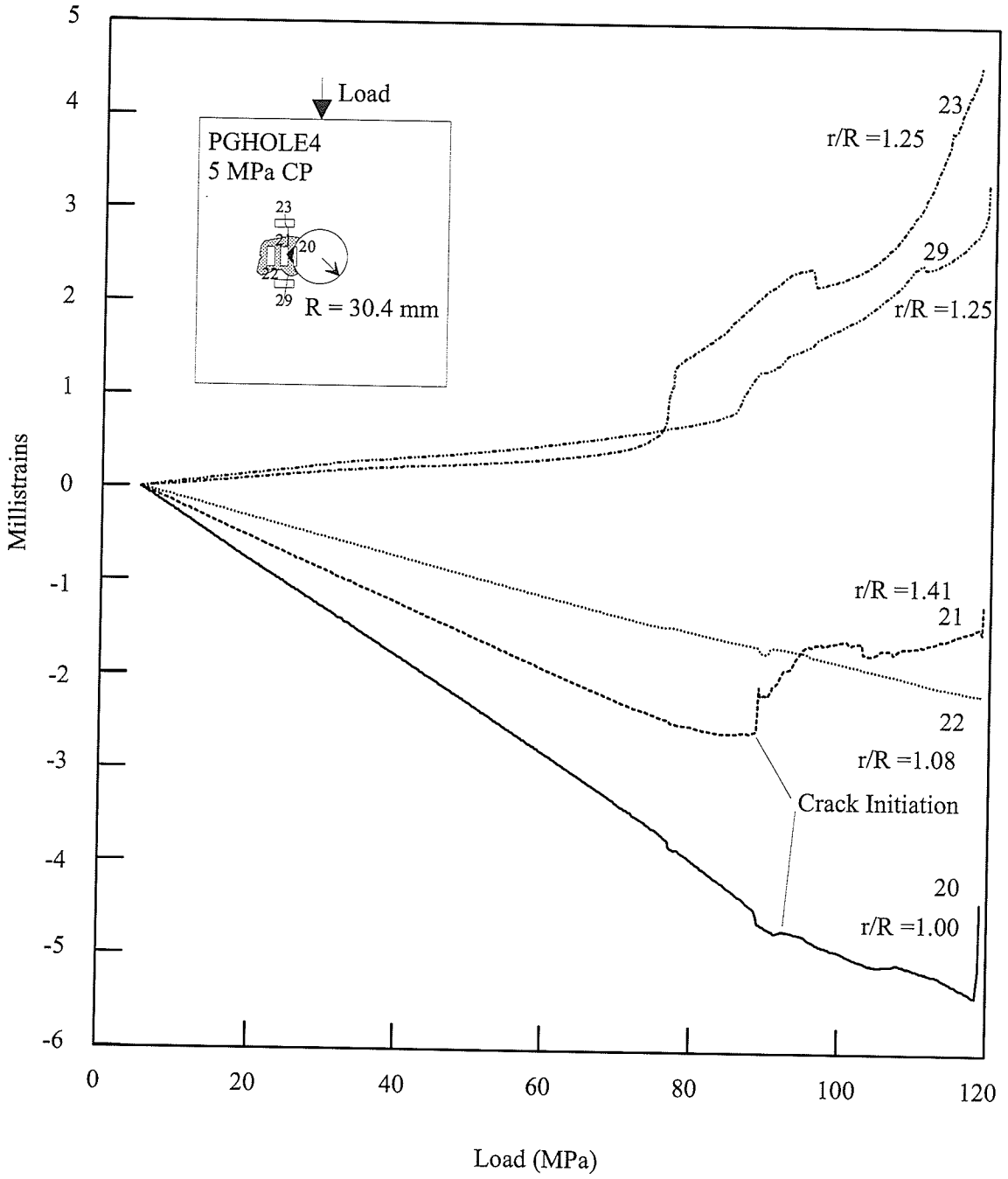

FIGURE 4.10: Gauge Response to Formation of Sidewall Spalling, Breakout Notch and Face Slabbing in Pink Granite. Some face slabbing occurred prior to development of the sidewall slabbing leading to deflections in the strain curve prior to sidewall slabbing crack initiation. Gauges 23 and 29 show responses to development of the remote cracks. The r/R ratio refers to the radial distance (from the hole center) of the gauge location (r) over the hole radius (R).

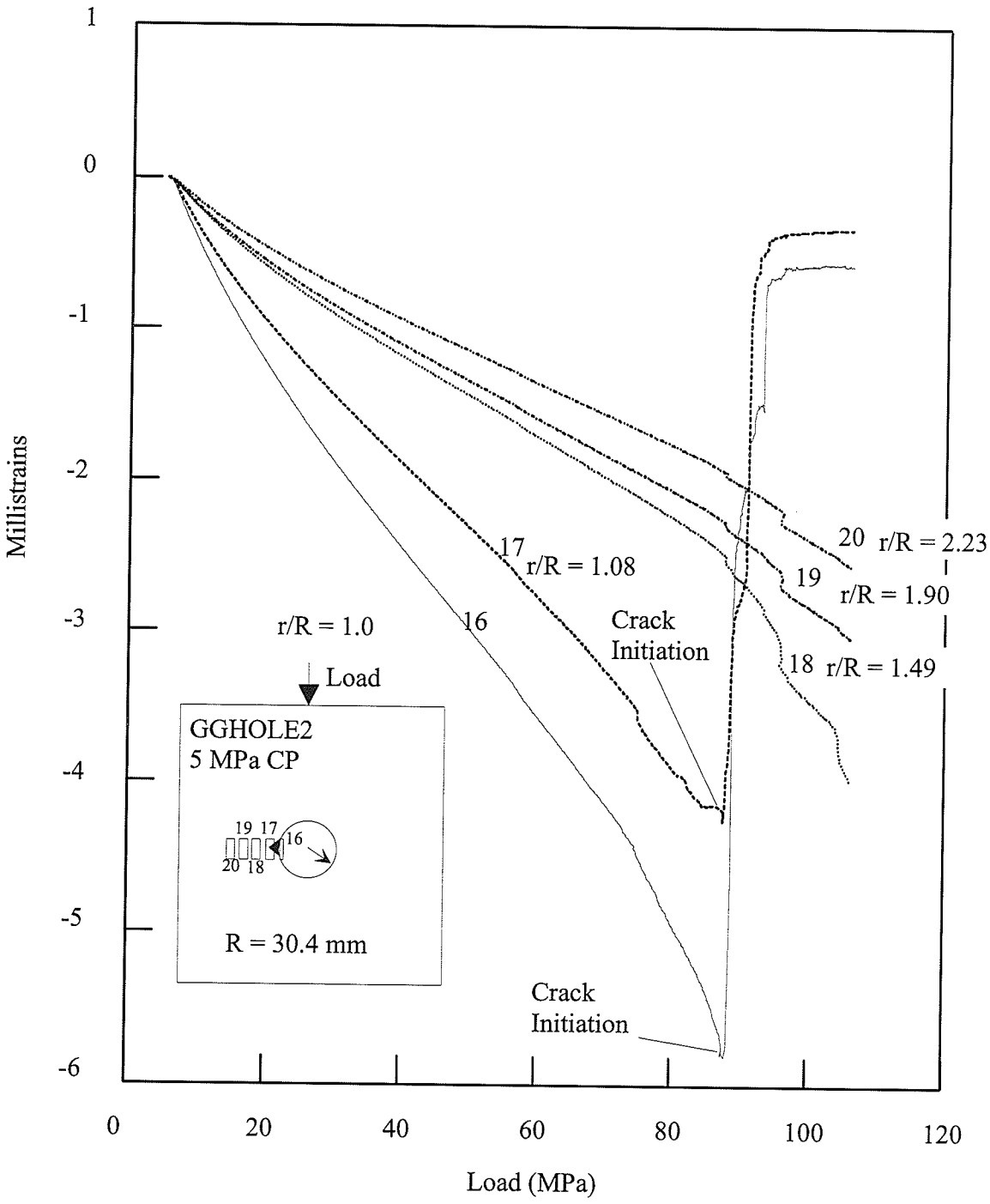

FIGURE 4.11: Gauge Response to Formation of Sidewall Spalling, Breakout Notch and Block Face Slabbing in Grey Granite. Gauges 16 and 17 shows the effects of block face slabbing occurring prior to initiation of the sidewall slabbing. The r/R ratio refers to the radial distance (from the hole center) of the gauge location (r) over the hole radius (R).

CHAPTER 5
DISCUSSION

The pink and grey granite samples had the same mineralogical composition (Kelly et al. 1993 and Tammemagi et al. 1980). The deep (grey) granite samples, however, exhibited sample damage due to stress relief accompanying their removal from their natural in situ stress conditions. The shallow or pink granite existed in a region where stress had been relieved by thrusting and joint formation and significant excavation related microcrack formation was not expected or seen. Therefore, the only visible differences were colour and stress-relief microcracking. Biaxial tension testing had shown there were preferential planes of weakness in the grey samples. The planes of weakness (microcracking) at the sample site had three orientations; a subvertical (dipping 85° NE) plane ran through the front of the blocks striking 025° azimuth, a second subvertical (dipping 80° SE) plane ran through the side off the block striking at 065° azimuth, and a less prominent sub horizontal plane dipped approximately 5° NW (Figure 5.1). The subvertical planes were the most prominent and were visible on the samples as oriented microcracks. These planes of microcracking are not parallel to the regional stress fields. The pink granite showed no evidence of significant strength variations with orientation based on earlier biaxial tension tests (Svab and Lajtai 1981). The orientations of the microcracks in the grey granite were likely related to the proximity of the sample site to the sidewall of Room 415. The access chamber to Room 415 (Room 414, see Figure 2.3) was excavated using drill and blast methods and damage was apparent in the roof of the room. As Room 415 was developed breakout notches formed in upper southeast and lower northwest quadrants as the excavation advanced. The tunnel runs along azimuth 225° and the

sample site is about one metre from the wall. Three dimensional modeling (Figure 5.2) suggests excavation damage to be responsible for the subvertical microcracking. The most prominent subvertical set (azimuth 025°) closely follows the stress trajectories found using Examine3D[1]. Excavation damage occurred ahead of the excavation face and is known to exist around Room 415 from acoustic emission/microseismic surveys (Martino et al 1993). Similar damage would have resulted ahead of Room 414 which could have contributed to the other microcrack set orientations.

The blocks were tested in either uniaxial or biaxial compression. In the latter case, a constant confining pressure was added to the sides of the block. In these tests the front of the block was always stress free (plane stress conditions). In the Mine-by tunnel conditions are somewhat different since the stress parallel with the tunnel axis is not zero, but 48 MPa. Since both the primary and remote cracks strike parallel with the tunnel axis they should not be affected by the axis parallel stress. The case is somewhat different for slabbing. In the Mine-by tunnel the minimum principal stress lies in the plane of the cross section. In the laboratory experiments, the minimum principal stress is perpendicular to the plane of the cross section (along the tunnel axis). This may have some effect on the way the breakout notch forms.

[1] Examine3D is a three dimensional boundary element modelling program

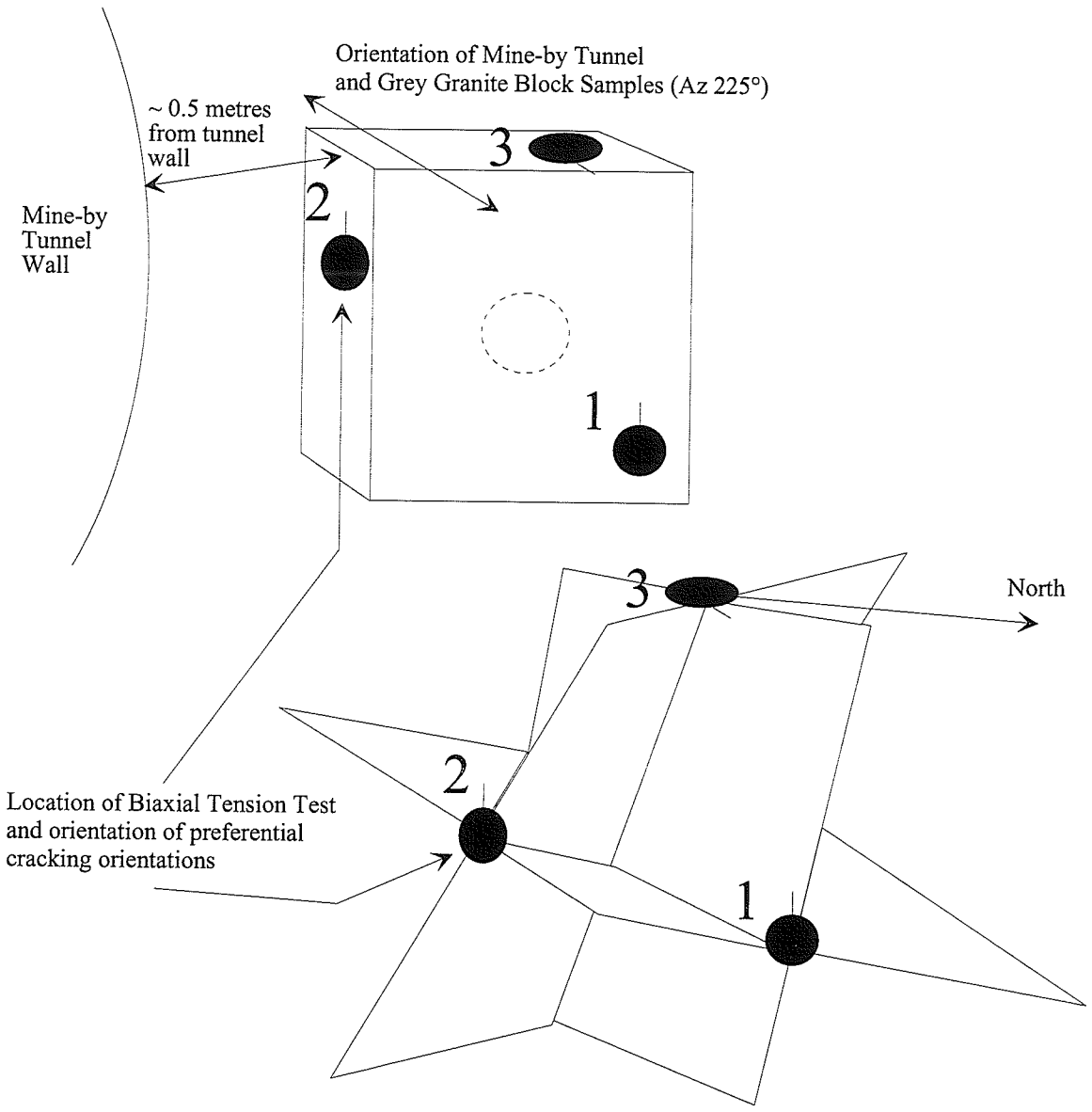

FIGURE 5.1: Planes of Weakness in the Grey Granite Samples. Orientation of planes from biaxial tension testing of oriented rock disks.

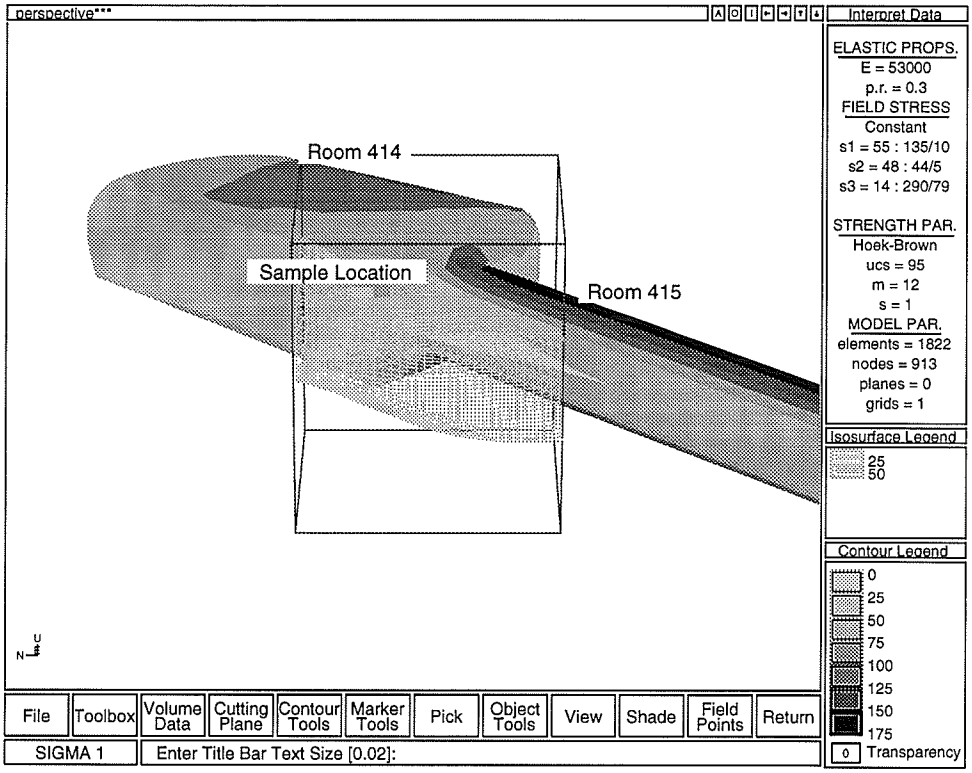

FIGURE 5.2: Model of Stresses in the Grey Granite Sample Area Using Examine3D. The shading on the tunnels represents the stress level (MPa) at the tunnel wall. The darkest shading shows the highest stresses, at the top and bottom of the tunnel, where the breakout notches formed. The sample location was near the corners of the two rooms. Isosurface shading shows the stress level in the rock around the sample area. The stress contours tended to follow a path close to azimuth 025° at the sample location.

5.1 PHYSICAL COMPARISON

The same types of cracks (primaries, remotes and spalling) formed under similar loading conditions in the pink and grey granite but had somewhat different appearances. The number of step-outs in the grey granite was 4-5/100 mm which was slightly greater than the number of step-outs observed in the pink (3-4/100 mm). The remote crack path wandered more in the grey granite as well which is to be expected. Svab and Lajtai (1981), showed that cracks take advantage of structural weaknesses in the rock as they

propagate and because the grey granite contains more microcracks more variation in the path is expected. Other potential fracture nucleation sites or weakness, such as feldspar or biotite cleavages and grain boundaries are relatively similar between the two rocks.

The final length of the primary crack was substantially shorter in the grey than in pink granite. Figure 5.3 shows that in the unconfined case for the pink granite, the primary cracks (upper and lower) developed to about 125 mm or four times the hole radius (a = 30.4 mm), which is almost to the edges of the block (approximately 140 mm). Uniaxial loading of the grey granite sample produced primary cracks of only 40 mm in length or about 1.3 times the radius. This holds true for higher confining pressures as well, with the length of the grey primary cracks ranging from one-half to one-third the length of the pink primary cracks. Crack length decreased to about 0.8a in the pink and 0.3a in the grey at 15 MPa confining pressure. At each confining pressure, the final load reached on the grey block was roughly equal to the load on the pink block. Therefore, a difference in applied loads did not play a role in the crack lengths. It is probable that the almost vertical alignment of microcracks (perpendicular to the confining pressure) in the grey samples may have caused the reduction in length by relieving the tensile stress in the primary fracture zone.

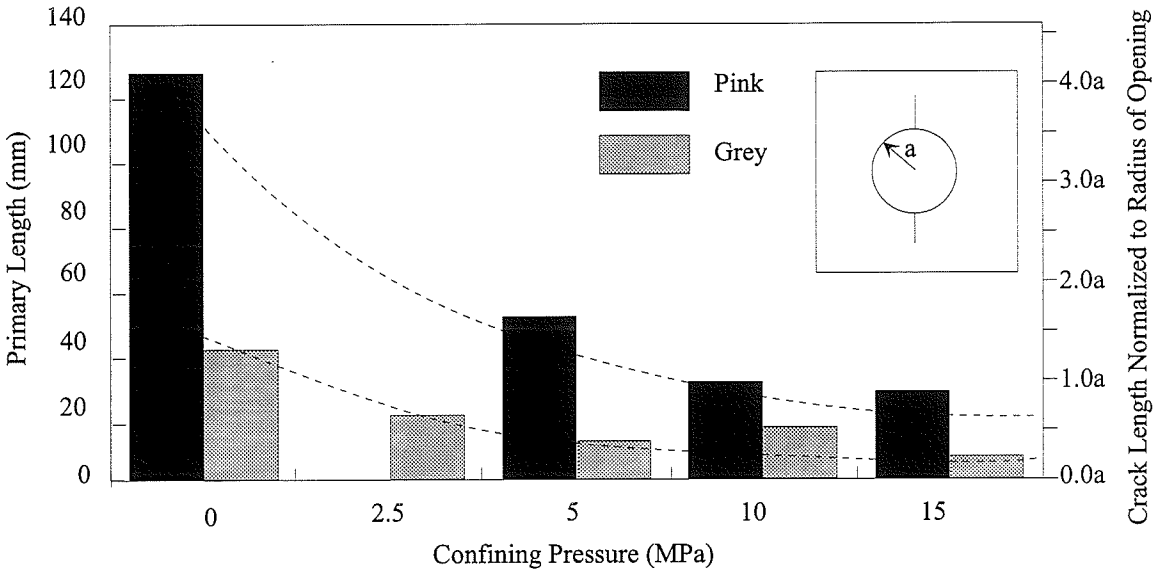

FIGURE 5.3: Average of Upper and Lower Primary Crack Lengths in Pink and Grey Granite for Confining Pressures of 0 to 15 MPa. Final loads on pink and grey blocks were similar (~122 MPa).

Plotting the applied load versus the crack length for primary cracks in the pink and grey uniaxially loaded blocks further illustrates the difference in growth. The crack length is given for specific loads, which can easily be determined by the load at which a gauge first shows a response. The distance of the gauge was then plotted from the first gauge detecting the crack formation (Figure 5.4). The values for this plot are from sample blocks PGHOLE1 (pink granite) and GGHOLE4 (grey granite) and the data are in Appendix D. This method only determined the linear crack growth and did not account for path wander between gauges which might increase the crack length. Primary cracks in both rock types grew relatively smoothly, but the pink granite showed a more rapid increase in primary crack length.

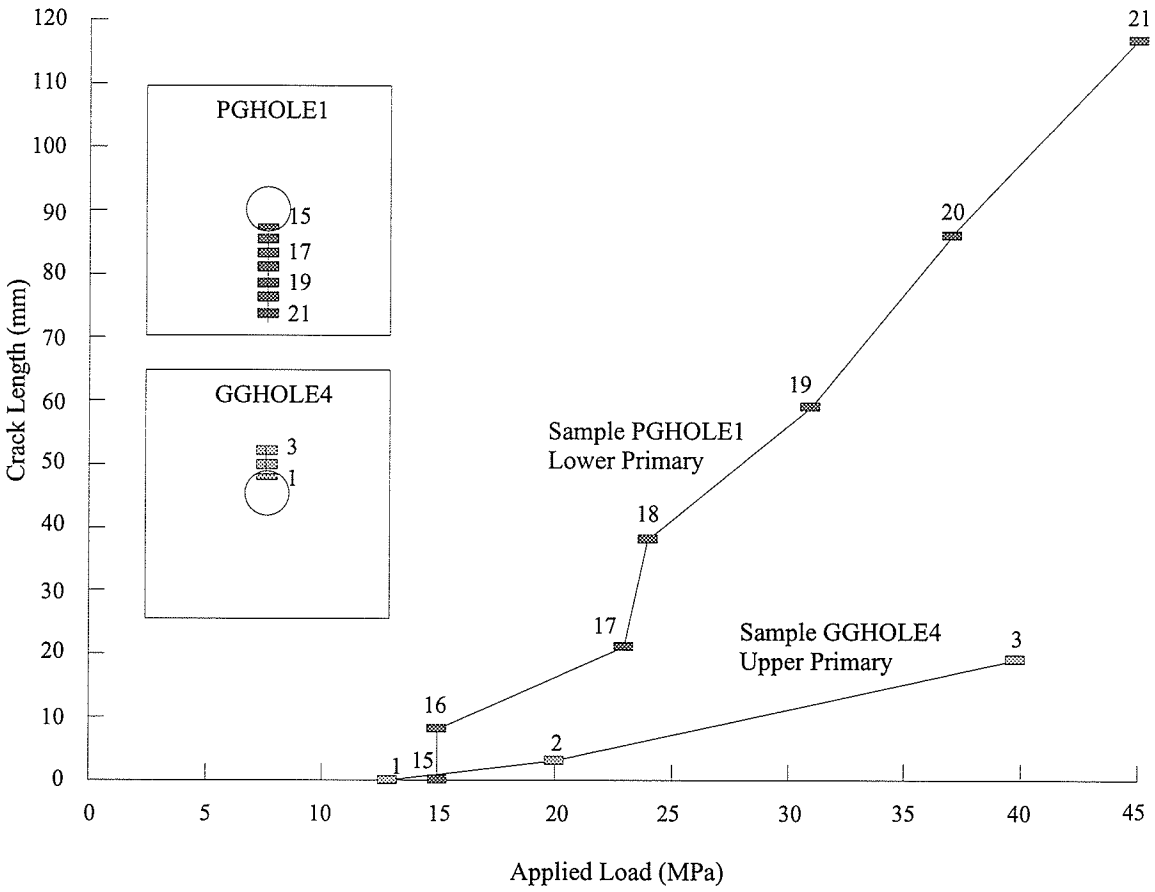

FIGURE 5.4: A Comparison of Primary Crack Growth Versus Applied Load in the Uniaxial State for GGHOLE4 and PGHOLE1. Crack length is measured from the edge of the first gauge detecting crack formation. Crack length at a specific load is represented by the rectangular gauge symbol, the small block figures show the position of the gauges relative to each other on their respective sample blocks. The pink granite showed a more rapid increase in length than the grey granite.

The development of the primary cracks was followed by the nucleation of remote cracks. Earlier numerical modeling showed that the position of remote nucleation varied with confining pressure (Carter 1988). The point of nucleation of the remote cracks was difficult to discern, as most observations had to made after the completion of loading. Spalling had obscured the locations in some cases and propagation of the cracks back towards the hole obscured the locations in other cases. The remote cracks did not show a

marked difference in length between the pink and grey granite. The confining pressure did not seem to have a limiting effect on the length of the remote cracks and in nearly every case, except for the grey granite at 15 MPa confining pressure, one or more remotes were seen to have propagated to the end of the block. In the case of the remotes in the grey granite at 15 MPa the maximum growth was approximately 2a in length. Since the remote cracks are driven mainly by compressive stress and since the pre-existing microcracks do not provide an additional mechanism for relief of compressive stresses, the similarity in the length of the remote cracks between pink and grey granite is not surprising.

There were differences in the physical appearance of the remote cracks. The remote cracks in the pink granite displayed straighter paths with less wander or step-outs than the grey granite. The grey granite also showed the formation of many more parallel splays and in some cases, bands of microcracks instead of an individual fracture. Figure 5.5 shows that remote cracks in both the pink and grey granite grew at roughly the same rate during loading, although in the grey granite they tended to develop at lower loads. Crack development at lower confining pressures (Figure 5.6) displayed similar characteristics. It is interesting to note that the lower left remote crack (named for its location on the block face to the left and below the hole) in the grey granite (Sample GGHOLE2) begins to develop earlier than the upper right remote crack in the pink granite (Sample PGHOLE4) but then slows down. The same PGHOLE4 upper right remote pink granite crack shows evidence of stalling. This was a common characteristic of remote crack growth in the block samples tested, where crack growth slows or stops until the load is raised sufficiently to cause increased growth. Lajtai (1981) discusses crack growth in compression and states minerals such as biotite may act to stop crack advance. The values for Figures 5.5 and 5.6 are in Appendix D.

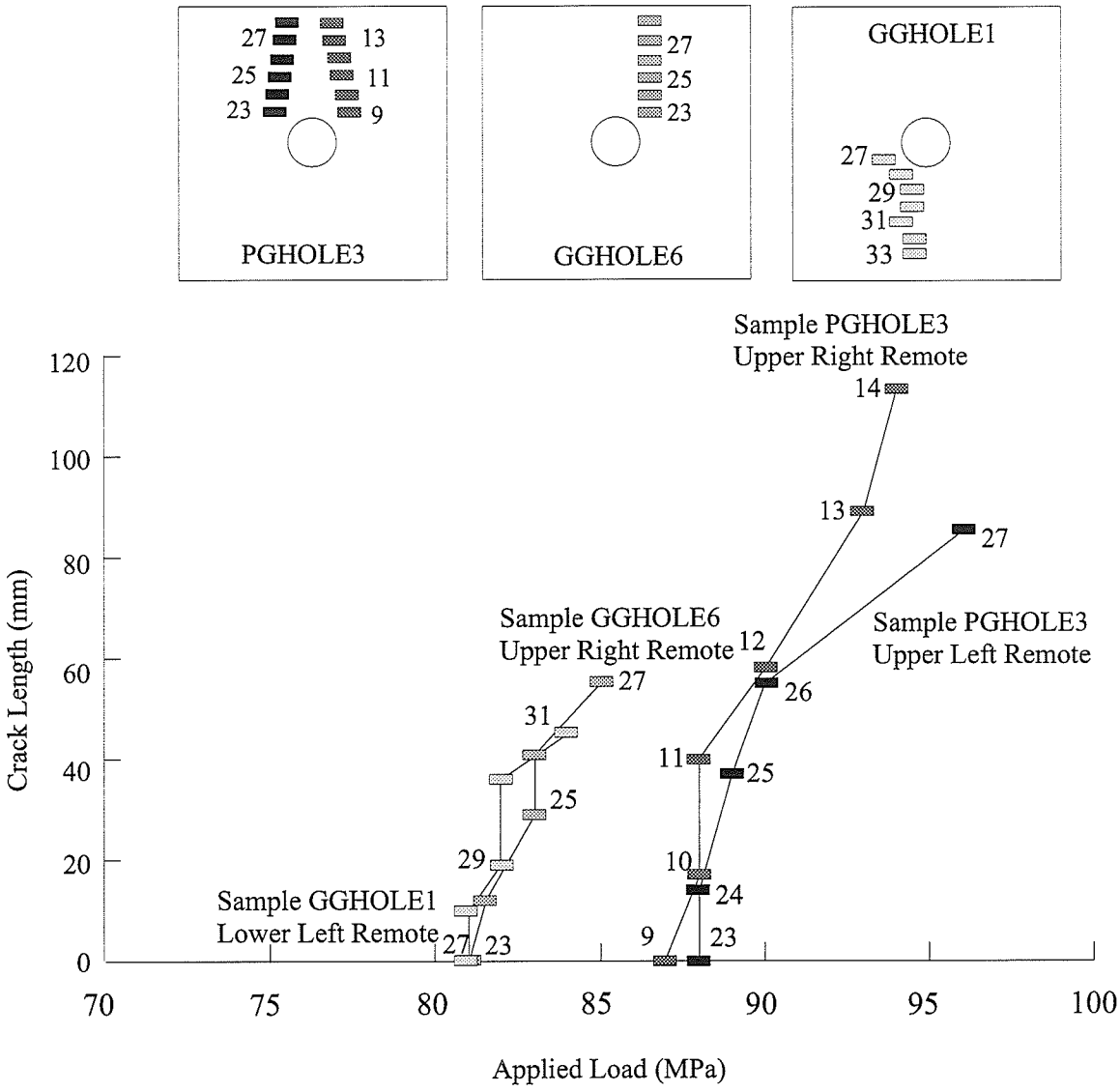

FIGURE 5.5: A Comparison of Remote Crack Growth Versus Applied Stress with a Confining Pressure of 15 MPa for Samples GGHOLE1, GGHOLE6 and PGHOLE3. Crack length is measured from the edge of the first gauge detecting crack formation. Crack length at a specific load is represented by the rectangular gauge symbol, the small block figures show the position of the gauges relative to each other on their respective sample blocks. Remote cracks in the pink and grey granites develop at roughly the same rate although the grey granite remotes tended to initiate sooner than the pink granite remotes. The remote cracks in the grey granite did not grow beyond the last point indicated with no further propagation occurring in the 85-120 MPa stress range.

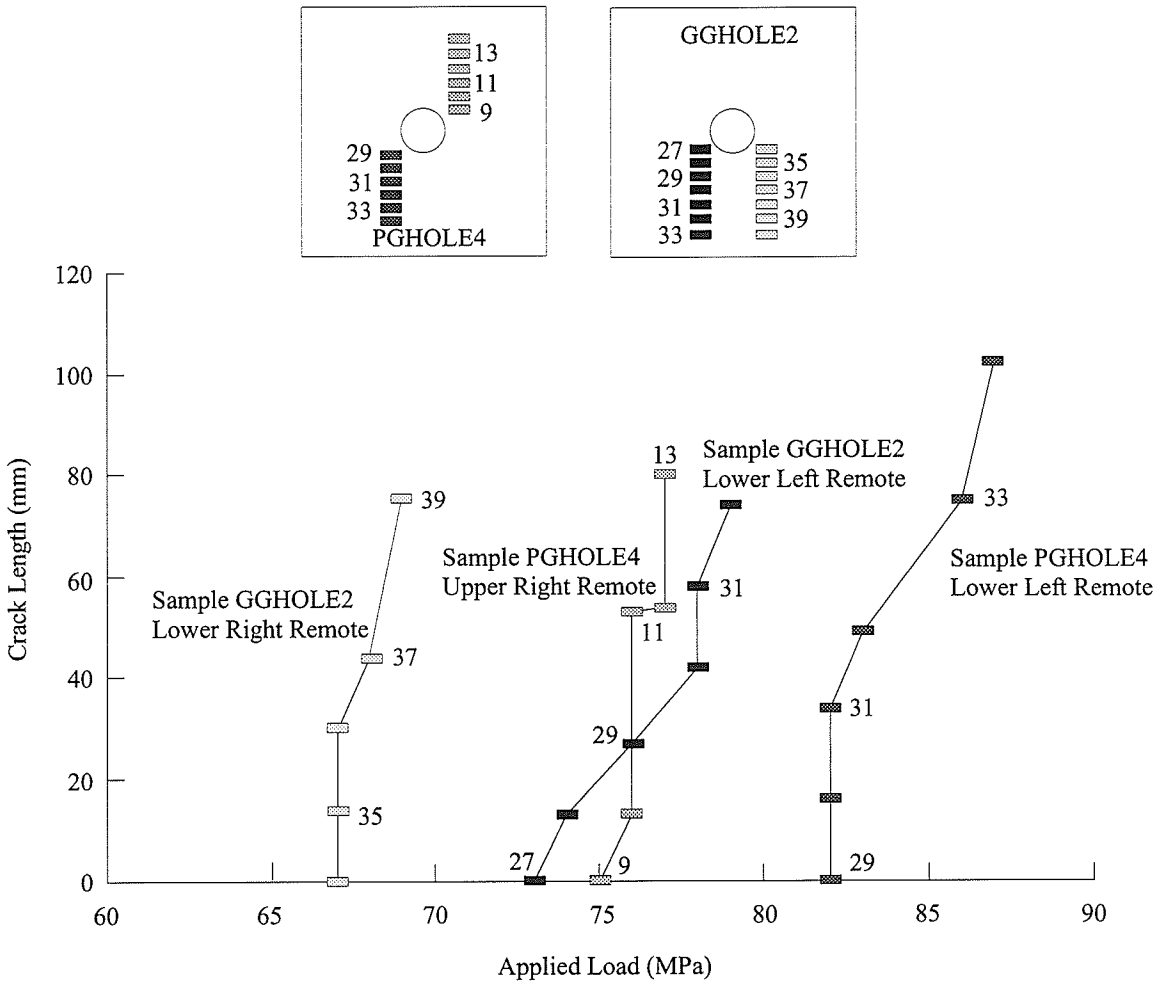

FIGURE 5.6: A Comparison of Remote Crack Growth Versus Applied Stress with a Confining Pressure of 5 MPa for Samples GGHOLE2 and PGHOLE4. Crack length is measured from the edge of the first gauge detecting crack formation. Crack length at a specific load is represented by the rectangular gauge symbol, the small block figures show the position of the gauges relative to each other on their respective sample blocks. Crack development on remotes sometimes stalled, producing a decrease or flattening in development rate as is seen in the upper right remote crack of PGHOLE4.

The final stage of fracturing observed in the blocks was spalling. The breakout notches produced by the spalling in the holes were slightly larger in the grey granite than in the pink and the grey granite displayed more face spalling around the hole. As seen by Haimson and Herrick (1985) the notches developed diametrically opposite to one another

in the direction of the minimum applied stress. Figure 5.7 shows a laboratory block sample and Figure 5.8 shows in situ breakout.

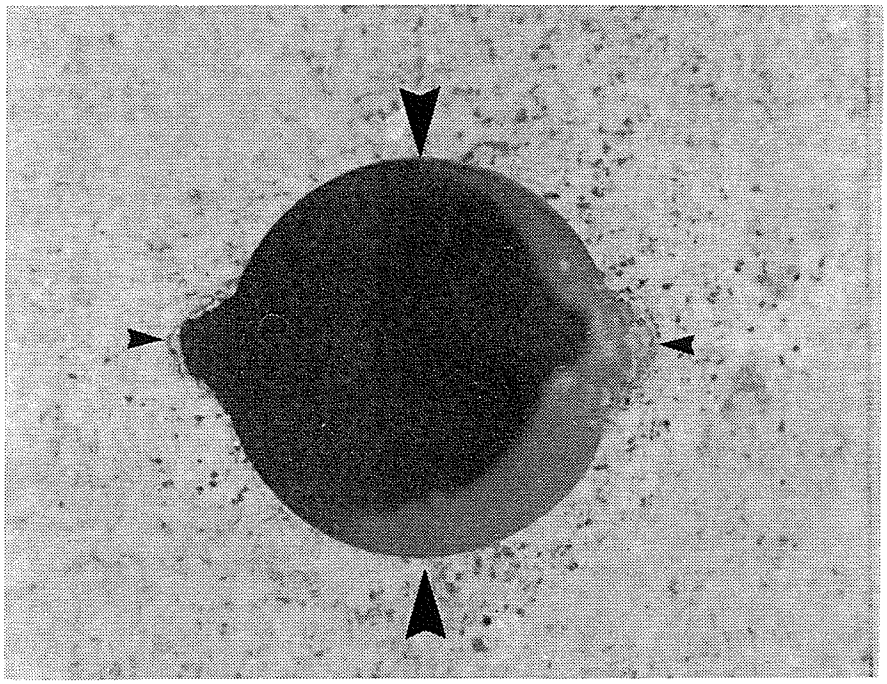

FIGURE 5.7: Breakout Notch Development in a Laboratory Block Samples. Breakout develops towards the minimum principal stress which is marked by the smaller arrows. Larger arrows indicate the loading direction. Compare with Figure 5.8.

FIGURE 5.8: Breakout Notch Development In Situ in the Mine-by Tunnel. The breakout develops towards the minimum principal stress which is marked by the smaller arrows. Larger arrows indicate the maximum principal stress direction. Compare with Figure 5.7.

The depth of the notches cannot be directly compared between in situ and laboratory samples because the loading history is quite different (Martin et al. 1994). However, the process of formation, the successive spalling of slabs leading to development of a breakout notch, is the same. Figure 5.9 illustrates the depth of notch development in the block samples. The lower plot shows the radial notch development (depth, r) normalized over the radius of the hole (a). The notch development ratios range from 1.12 to 1.24. The grey granite notches tend to be slightly larger (an average of 5 mm depth for the grey

granite as opposed to 4 mm for the pink granite) with the exception of the 2.5 MPa confining pressure case. The upper plot illustrates the final loads were similar, within ± 0.15%, so there is no influence on the notch depths from test to test differences in the maximum applied load.

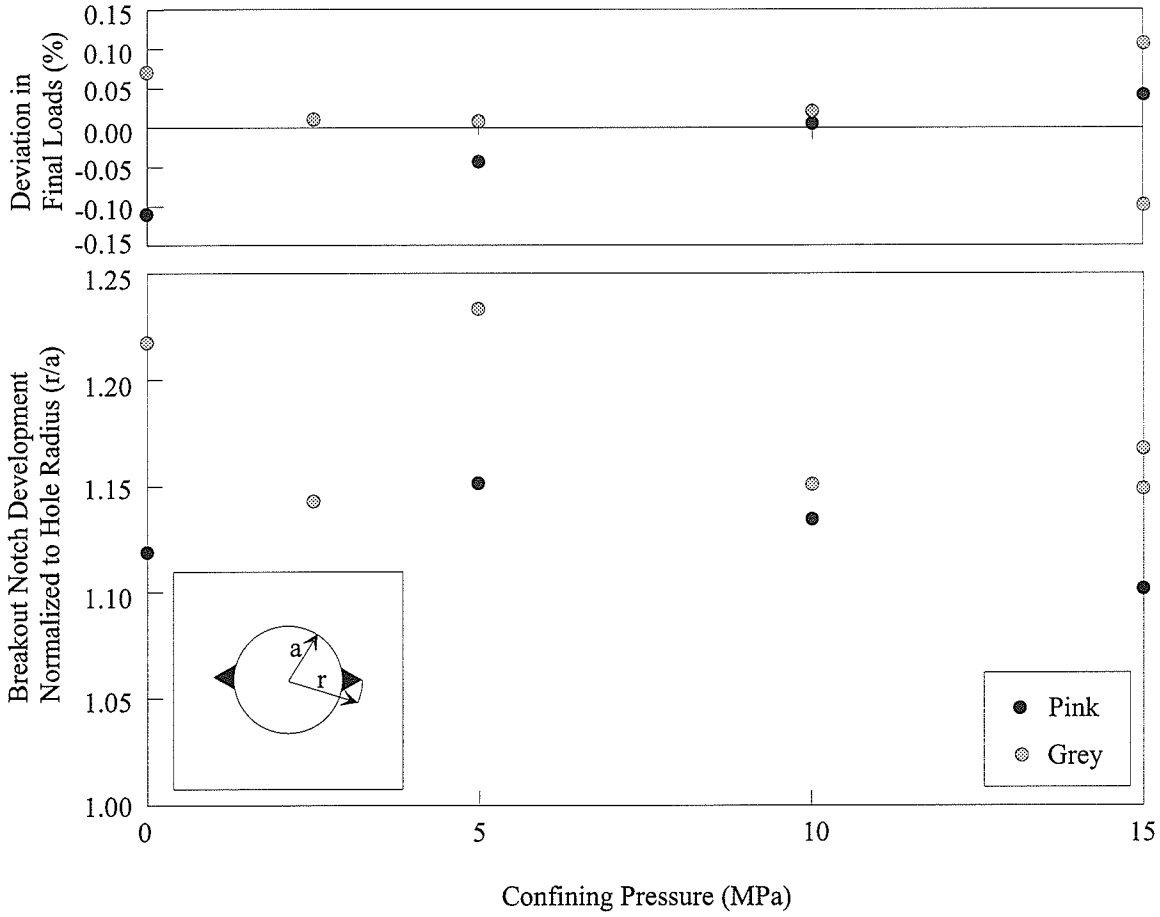

FIGURE 5.9: Notch Depth Normalized by Hole Size Versus Confining Pressure. Final loads in each case were similar and no significant difference in final notch depth and confining pressure is noticeable.

No change in notch depth was seen with an increase in confining pressure. This differed from the findings of Haimson and Herrick (1989), where they found the notch depth to increase linearly with an increase in the minor applied stress perpendicular to the hole in limestone. This difference can be understood by the fact that the confining pressure used

on the granite blocks were relatively small in comparison with the unconfined compressive strength (UCS) of the rock (0 to 0.1 UCS), while the confining pressure used on Haimson and Herrick's limestone blocks was higher in comparison to the UCS, (0.15 to 1.2 UCS) (Figure 5.10). Therefore the confining pressure effect may have been lost in statistical scatter. Scale effects may also play a role in the difference. The holes in the limestone were 20-mm-diameter, while the blocks in this study had 61-mm-diameter holes. Martin (1993) has shown (Figure 5.11) that scale effects are present for holes less than 75-mm-diameter.

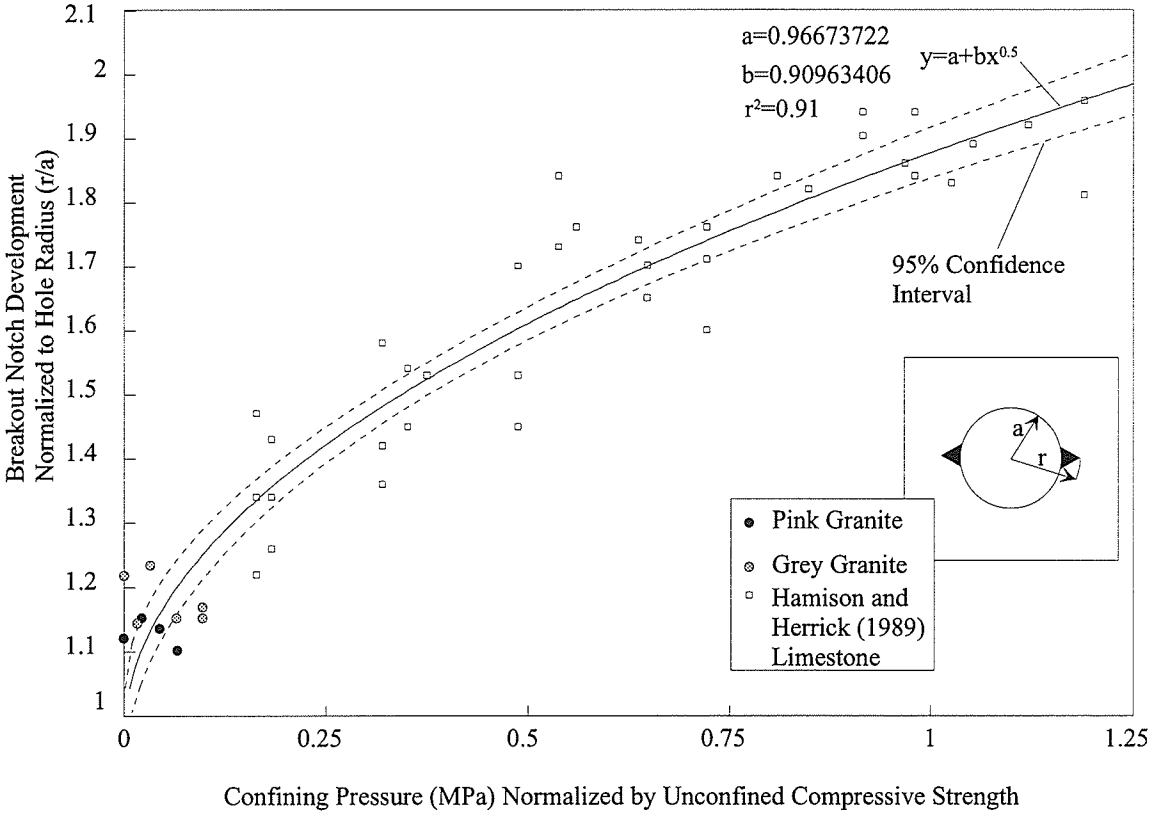

FIGURE 5.10: Breakout Depth Compared to Normalized Minimum Stress. The size of the confining pressure relative to the unconfined compressive strength of granite is small in comparison with the relative magnitude of the confining pressures used by Haimson and Herrick (1989). This may explain why there is little difference in the breakout notch depths of the granite. The curve fitting was done using TableCurve[2] both the limestone and granite results were curve-fitted.

[2] TableCurve is a commercially available curve fitting program from Jandel Scientific

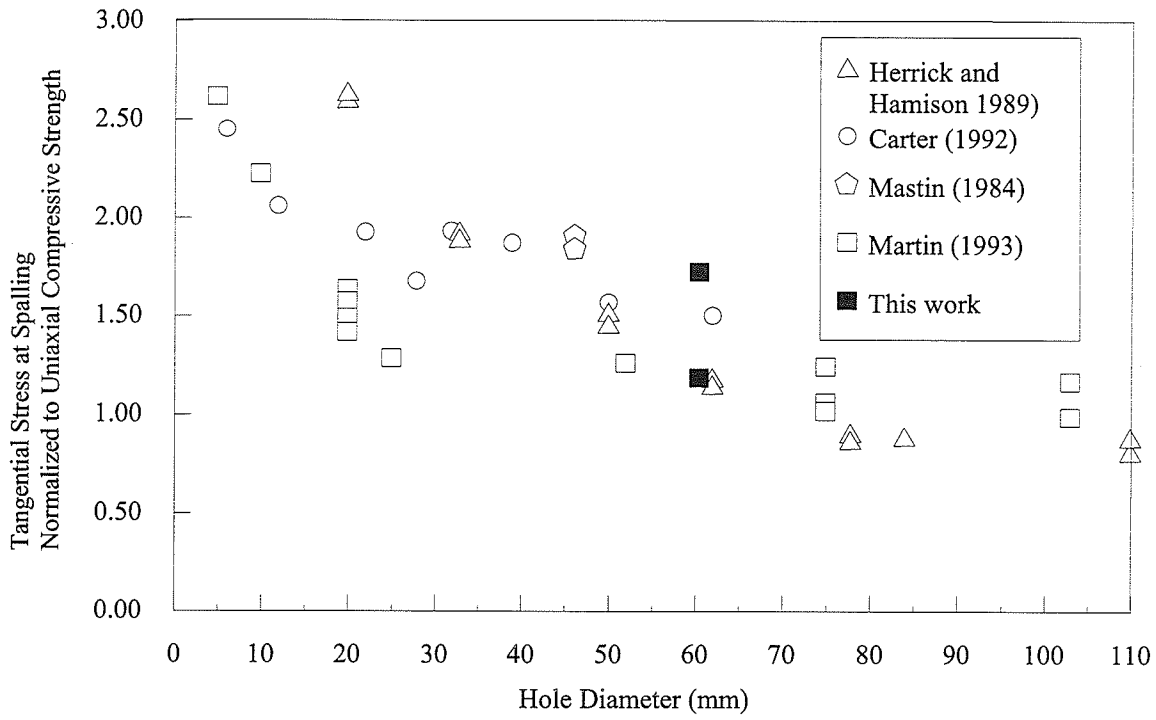

FIGURE 5.11: Normalized Tangential Stress at Failure as a Function of Hole Size

5.2 NUMERICAL COMPARISONS

Previous researchers (Babulic 1985, Carter 1988 and Petuhkov in Carter 1988) have all carried out uniaxial loading tests of Cold Spring Quarries pink granite blocks. Their results are similar to the uniaxial results from this study (Table 5.1), although it must be remembered the blocks in those studies used smaller diameter holes (38-mm-diameter).

TABLE 5.1

A COMPARISON OF CRACK INITIATION VALUES FOR LABORATORY GRANITE TESTS

Researcher	Crack Type		
	Primary	Remote	Spall
Petuhkov (*)	16	100	115
Babulic (1985)	15	78	92
Carter (1988)	16	126	157
This Work (Pink)	17	76	90
(Grey)	12	65	88

* In Carter (1988)

All crack initiation values in MPa

The primary crack initiation results all show values which are close to the uniaxial tensile strength of Cold Spring Quarry pink granite (13.5 MPa). This is expected since the tensile stress concentration at the primary crack nucleation point is theoretically equal to the tensile strength. The similar uniaxial test for the grey granite shows the initiation of the primary is close to the uniaxial tensile strength of grey granite (9.2 MPa). The uniaxial case shows cracks in the grey granite form at lower loads than in the pink granite; the primary crack in the grey granite begins to form at roughly 70% of the load of the pink (from this work) while remote crack develops at approximately 85% the load of the pink granite. Since the solid rock in both the pink and grey granite is mineralogically identical, it must be microcracks that are responsible for lowering the fracture loads. Figure 5.12, 5.13 and 5.14 compare the crack initiation points for the pink and grey granite at all confining pressures for the primary, remote and spalling cracks respectively. In general, the pattern seen for uniaxial conditions is repeated with cracks in grey granite developing

sooner than those in the pink granite. The applied load required for crack initiation increased with higher confining pressure. The data are fitted reasonably well by a linear curve, as was modeled by Carter (1988). The slope of the primary crack curve for the grey granite however is quite low when compared with that of the pink granite. It is suspected that microcracks create stress shadowing in the blocks, thus reducing the effects of the confining pressure. A stress shadow is created when the confining pressure does not completely close the microcracks and therefore does not transmit the confining pressure energy to the inner parts of the block.

The grey granite crack initiation values for the 10 MPa confining pressure case are lower than expected based on results at the 5 and 15 MPa confining pressures. This is most noticeable when looking at crack initiation results for the remote cracks and the spalling. Best fit lines were added to the grey and pink granite data, except in the case of the grey granite spalling because the scatter in the results was too great to define a single curve.

Numerical models have become an important part of understanding the loads and loading conditions at which fractures initiate around openings. Closed-form solutions (the Kirsch Equations) exist for primary crack initiation (Bray 1987). The same closed-form solutions are invalid for later forms of fracturing because the existence of the primary fracture changes the stress distribution. However, a plethora of numerical models exist which can be applied towards investigating remote and sidewall spalling. Two programs are being developed at the University of Manitoba to model discrete fracture propagation in rocks, EZELOP[3] and INSIGHT2D©[4].

---

[3]EZELOP was developed by Dr. E.Z. Lajtai, University of Manitoba, it requires a high resolution monitor (1280x1024) and is available at no charge from the author's institution.
[4]INSIGHT2D was developed by E.J. Dzik, AECL Research and University of Manitoba.

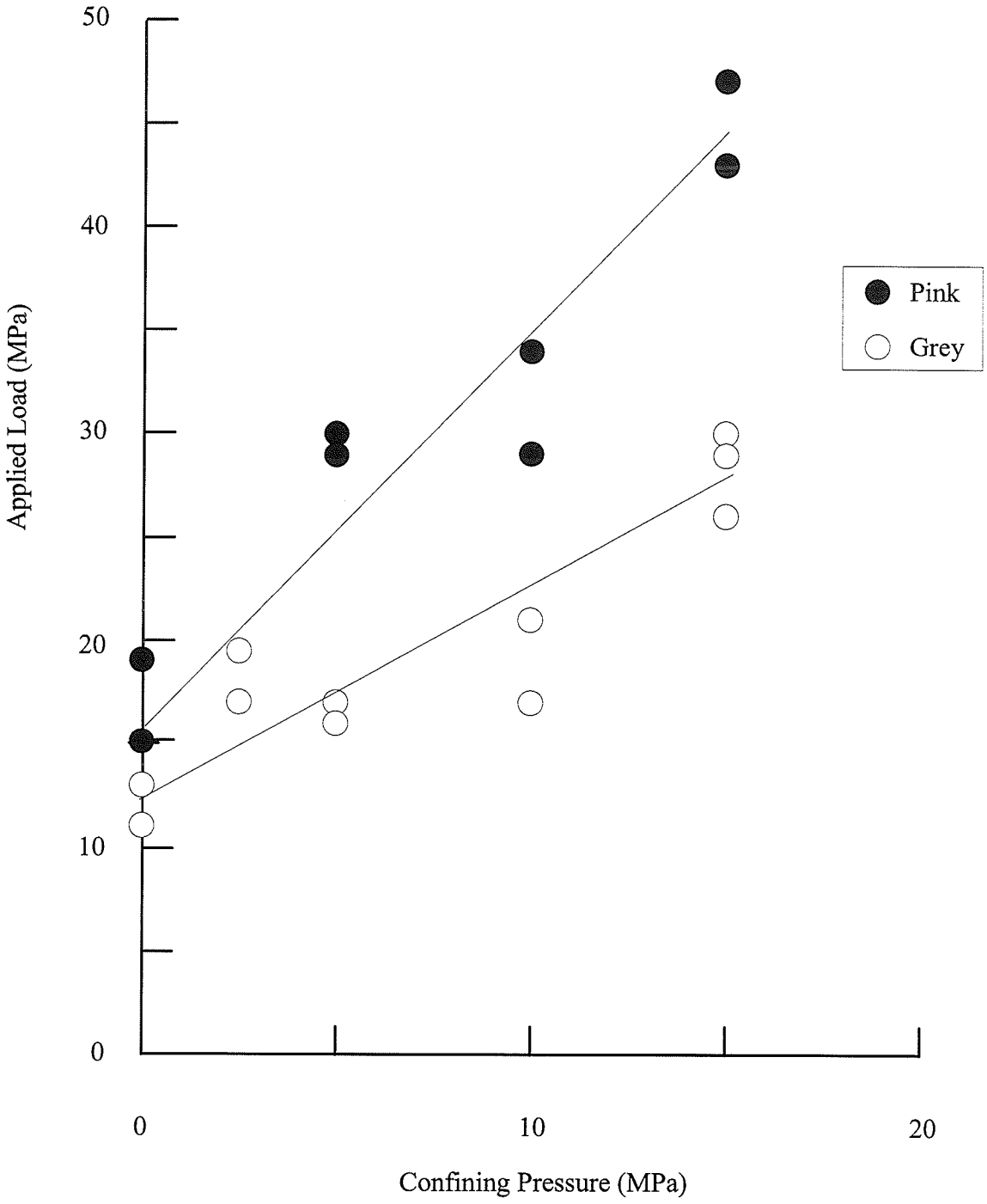

FIGURE 5.12: Crack Initiation Points for Primary Cracks in the Physical Models. There is a very high scatter in the grey granite results.

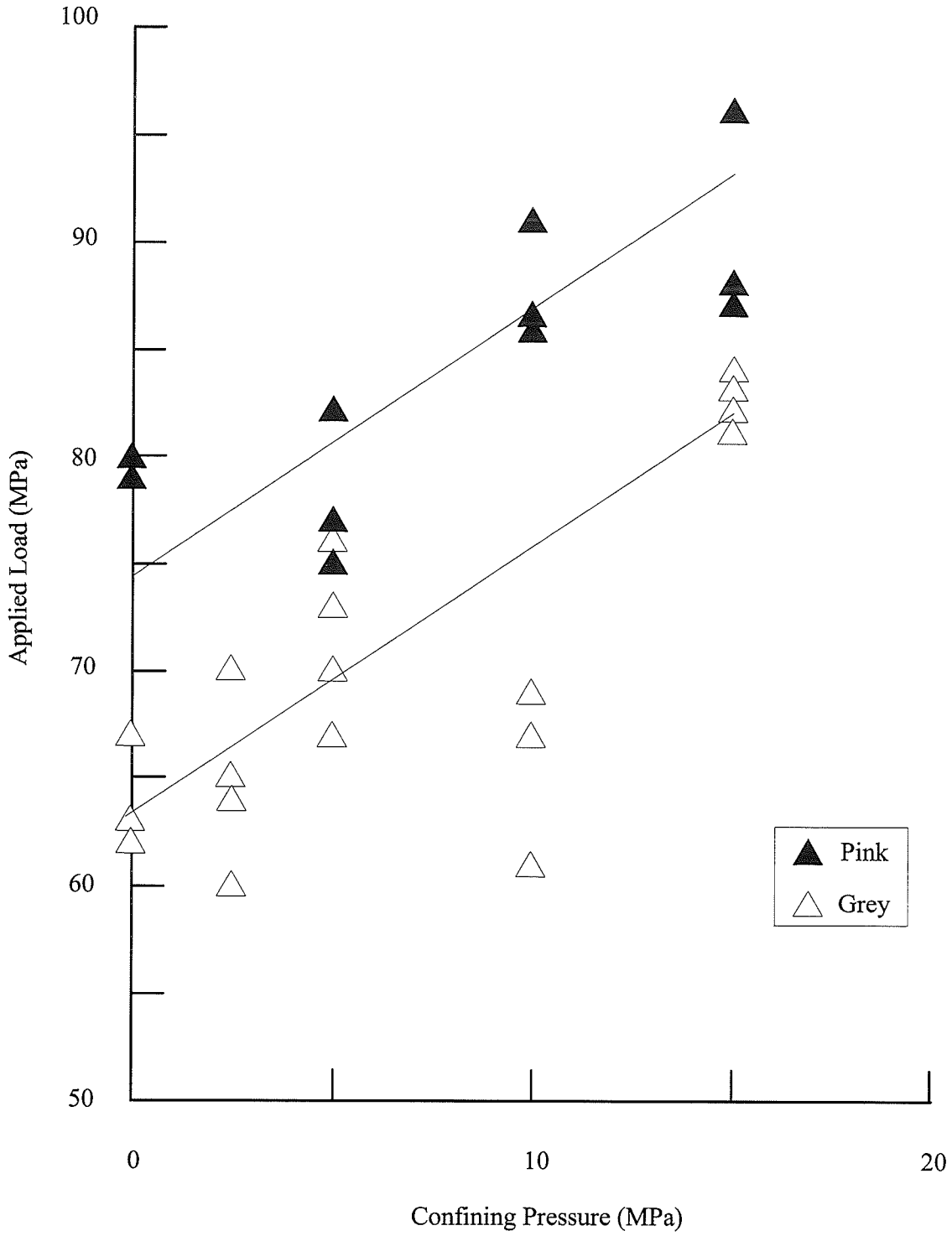

FIGURE 5.13: Crack Initiation Points for Remote Cracks in the Physical Models. The linear fit for the grey granite omits the 10 MPa confining pressure case because it is suspected the confining pressure was not fully applied for that sample.

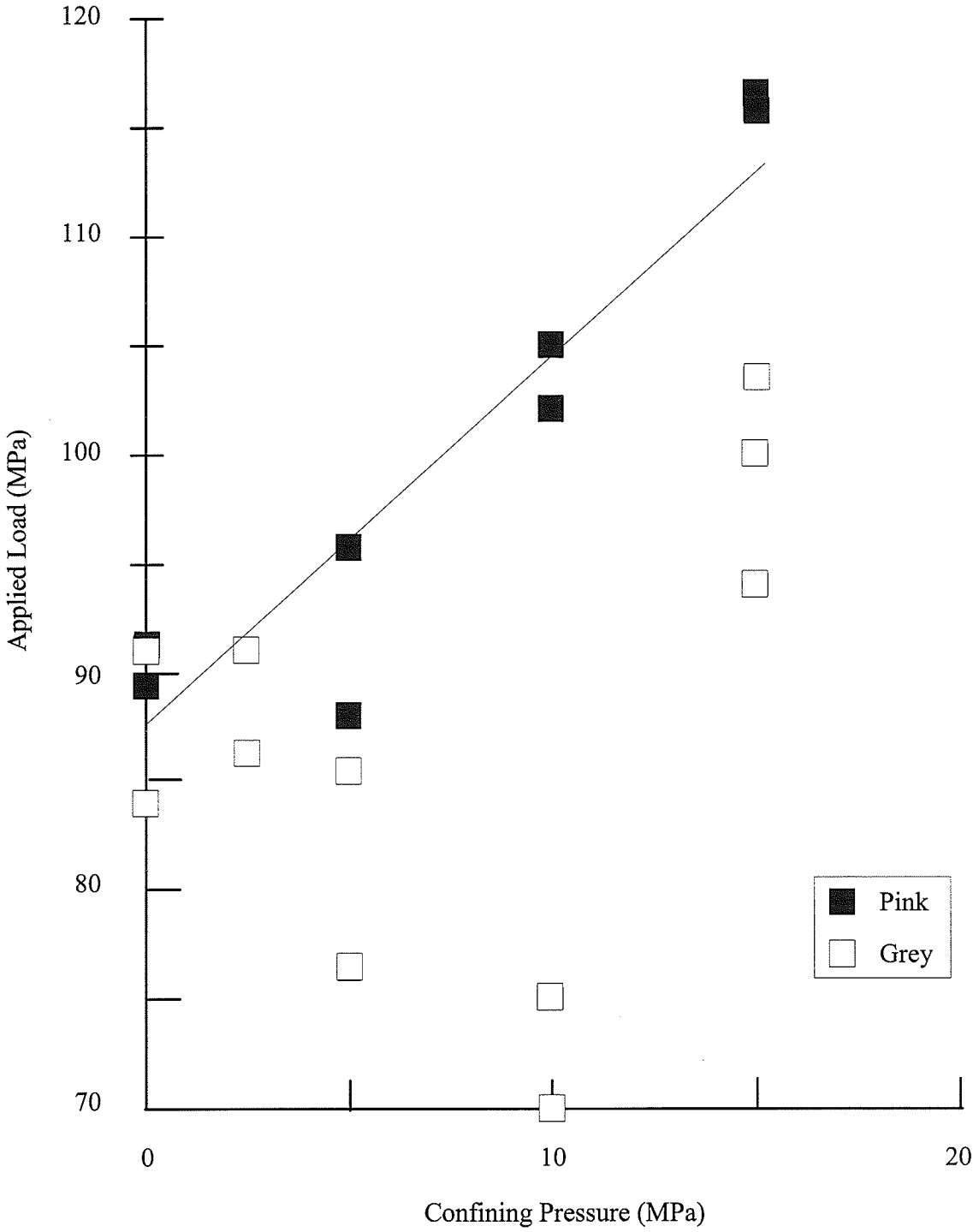

FIGURE 5.14: Crack Initiation Points for Spalling in the Physical Models. The grey granite results showed too much scatter to define a single curve.

EZELOP is a Windows™[5] application which allows a graphical display of the spatial distribution of the safety factor around a two-dimensional, elliptical opening of arbitrary orientation. The computations are based on the closed-form solution for an elliptical cavity (Bray 1987). The program also outputs the principal stresses and safety factors to a table format. EZELOP was used to solve for the primary crack initiation. INSIGHT2D© is a two-dimensional, linear elastic, finite element modeling program using isoparametric linear triangular elements (Dzik et al. 1994). It allows the user to draw or enter the desired excavation shape or add cracks via a mouse-driven user interface. The density of the grid can be controlled around the opening by increasing the number of line segments (finer grid) which make up the opening. Both programs make use of the Rocker strength function and Rocker USR or unconfined strength ratio (Lajtai et al. 1991) to develop the failure criteria.

Both the analytical (EZELOP) and the numerical (INSIGHT2D©) procedure implemented the finite-width crack and the stress-averaging technique. The zero-width mathematical crack of engineering fracture mechanics is ill-suited to the compressive stress environment because a zero-width crack is insensitive to the normal stress along its plane. This is because in a typical rock mechanics application, where substantial compressive stress exist, a zero-width crack cannot be propagated in response to a compressive stress alone. Tension must exist perpendicular to the plane of the crack for propagation to occur. For the problem on hand tension did exist around the cylindrical cavity, and a zero-width crack would propagate, but not in the unstable manner observed in the relatively large-diameter granite tests of this work. The finite-width crack model seemed to overcome these difficulties (Carter et al. 1991, Yuan et al. 1993).

---

[5]Windows is the registered trademark of Microsoft Corp.

The effect of coaxial compression was introduced into EZELOP and INSIGHT2D© by selecting fracture criteria that include both the maximum and minimum principal stress. The functional form for this is known as the USR (Lajtai et al. 1991). The USR is simply a form of the safety factor; the condition of fracture is represented by USR = 1 condition. Values less than unity represent unsafe values and values greater than unity, safe conditions. USR is actually the measure of the distance between the state of stress (σ_1 and σ_3) and the failure criterion. For the failure criterion the Rocker strength function (Lajtai et al. 1991) is used:

$$\sigma_{1f} = C_o\left(1-\frac{\sigma_3}{T_o}\right)^R \tag{5.1}$$

σ_{1f} is the maximum principal stress at failure and is a measure of the strength at confining pressure σ_3.

The function anchors the failure criteria at two points, the uniaxial tensile (T_o), and uniaxial compressive strength(C_o). A good fit is important in these regions because the majority of cracking near openings takes place under the effect of low tensile stress and low confining pressure. A third parameter, R, is used to shape the curve. When the exponent of the Rocker function (R) is 0.5, the value of USR for a given state of stress (σ_1 and σ_3) can be expressed in closed-form:

$$USR = \frac{T_o}{\frac{\sigma_3}{2}-\left[\left(\frac{\sigma_3}{2}\right)^2+\left(\frac{\sigma_1 T_o}{C_o}\right)^2\right]^{0.5}} \tag{5.2}$$

Using at-the-point stress components (σ_1 and σ_3) in the USR would result in erroneous results in situations where large stress gradients are present, as in this case. To overcome this problem, at-the-point stresses are replaced by the "averaged stresses", where averaging is implemented over a constant area (Carter et al. 1991). The averaging distance (diameter) is considered to be a material property (Lajtai 1972). The models require the physical properties of the rock to be entered. These include the averaging distance and the crack width. The crack width is simply the crack aperture. EZELOP is designed to average at all points of the model. The version of INSIGHT2D© used carried out stress averaging only at the crack tip.

Sample output from EZELOP is given in Figure 5.15 which shows initiation of the primary crack at the top and bottom of the hole, where the USR < 1. A sample grid from INSIGHT2D© showing a primary crack above and below the hole is given in Figure 5.16. In the case of the primary crack, the crack was propagated in 10 cm increments, by redrawing and re-running the model with the longer crack length, until crack development (USR < 1) moved off the crack tip and into the remote region. Eventually a match of primary crack length and applied load was found for remote crack formation at each confining pressure. The crack length and load were varied to achieve this match, while the other material properties were kept constant. In Figure 5.17, crack development has moved off the tip to the remote crack position. Crack development was taken further in one case where the remote crack was manually propagated from this starting position. Manual propagation of the remote crack was done in only one case because of the large model size and amount of computer run-time required. The path of propagation followed the stress trajectories in the modeled block. Propagation in this case was done in three steps rather than every 10 cm. The grid from the second step is shown in Figure 5.18.

Figure 5.19 shows the effect of the remote crack and primary crack together. Stress distribution becomes irregular and the model indicates failure occurring on both ends of the remote crack. This can be tied to the propagation of the remote cracks in the physical models where the crack works its way back towards the hole (Section 4.2) as well as towards the end of the block.

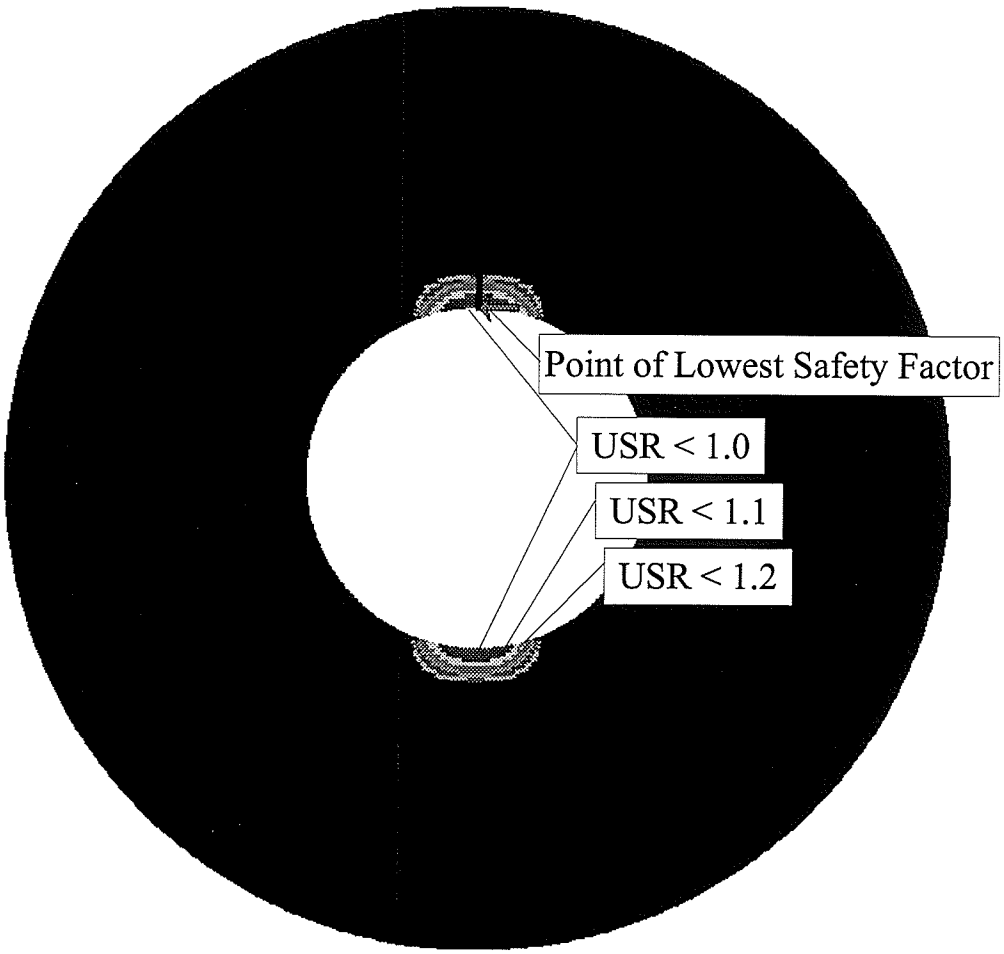

FIGURE 5.15: Crack Development Around a Circular Opening. In terms of the physical models, this would be the initiation of the primary. Crack development occurred where the USR was below 1 at the top and bottom of the hole.

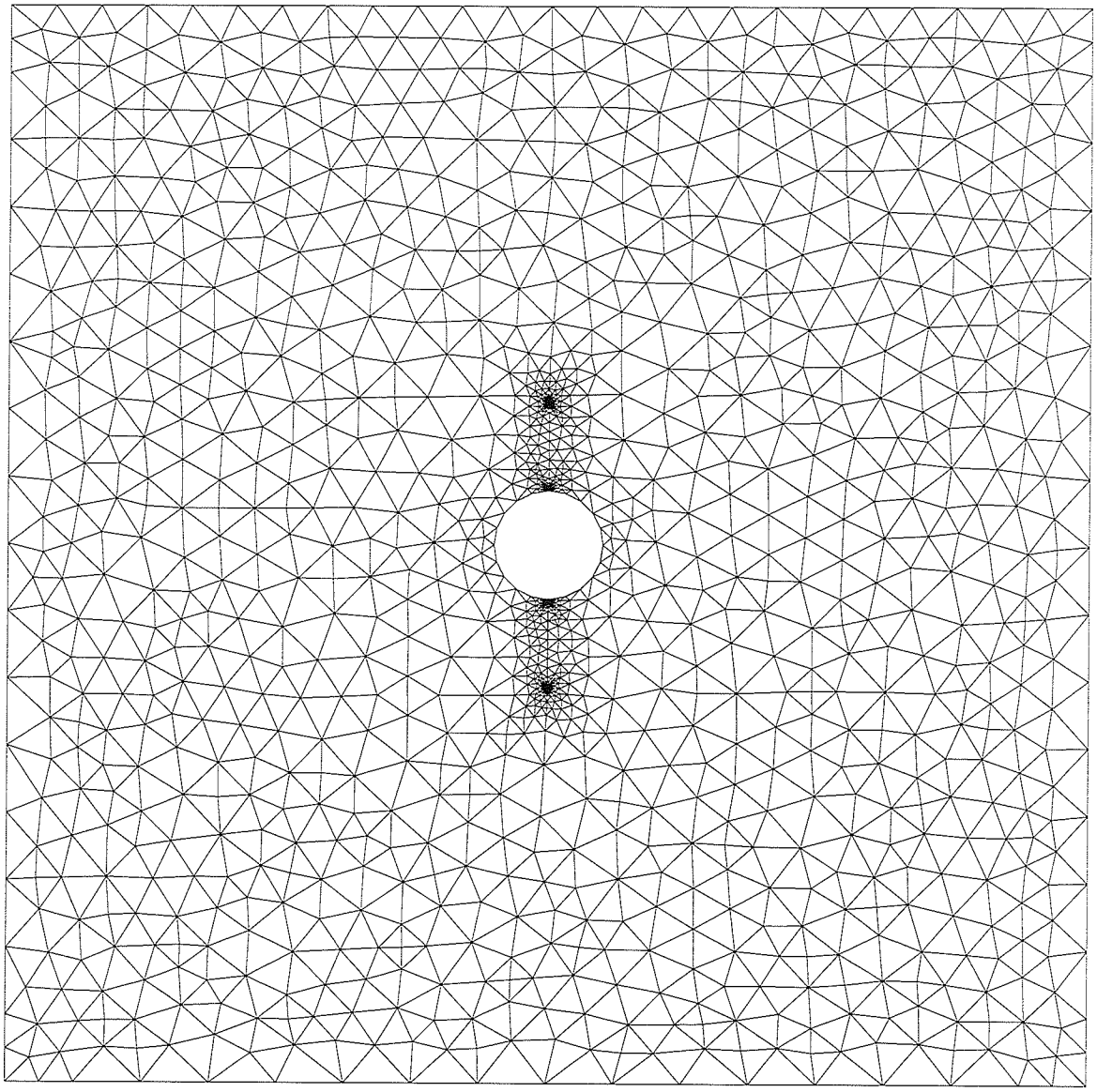

FIGURE 5.16: Typical Grid from INSIGHT2D©. The denser mesh above and below the opening shows the locations of the crack tips.

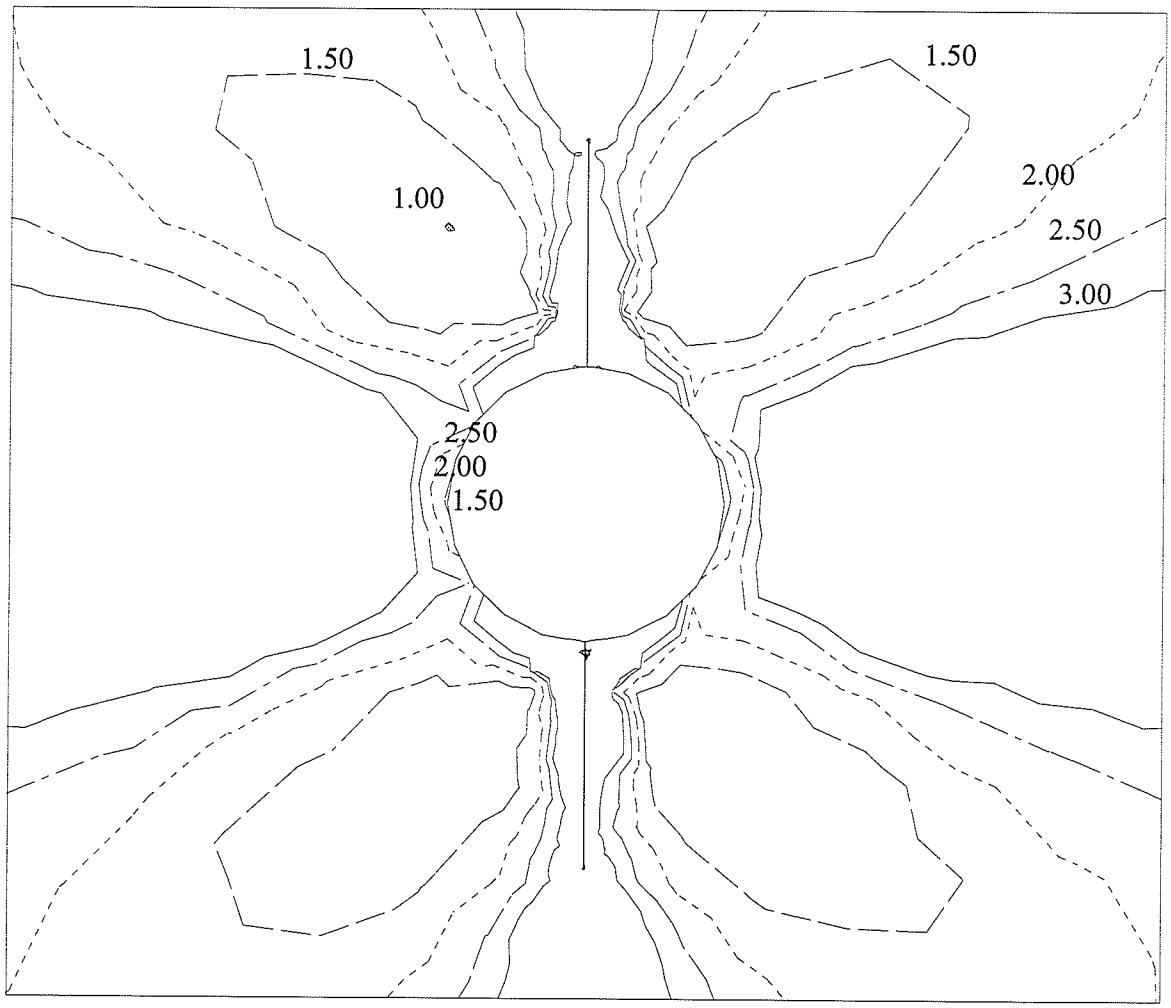

INPUT FILE: P5RC
NODES = 1527
ELEMENTS = 2824
FACTOR OF SAFETY
CONTOUR INTERVAL = 0.5
CONTOURS X 10**0

PLANE STRESS CONDITIONS
--- FIELD STRESS ---
SIGMA1 = 120 MPa
SIGMA3 = 5 MPa
THETA = 90 DEGREES

--- MATERIAL 0 ---
YOUNG'S MODULUS = 71000 MPa
POISSON'S RATIO = 0.25
USR (ROCKER) YIELD CRITERIA
COMPRESSIVE STRENGTH = 228 MPa
TENSILE STRENGTH = -13.5 MPa
ROCKER EXPONENT = 0.5

FIGURE 5.17: Development of Failure in the Remote Region. Primary crack length was increased with increased load until the crack development (USR < 1) moved off the tip and into the remote crack position.

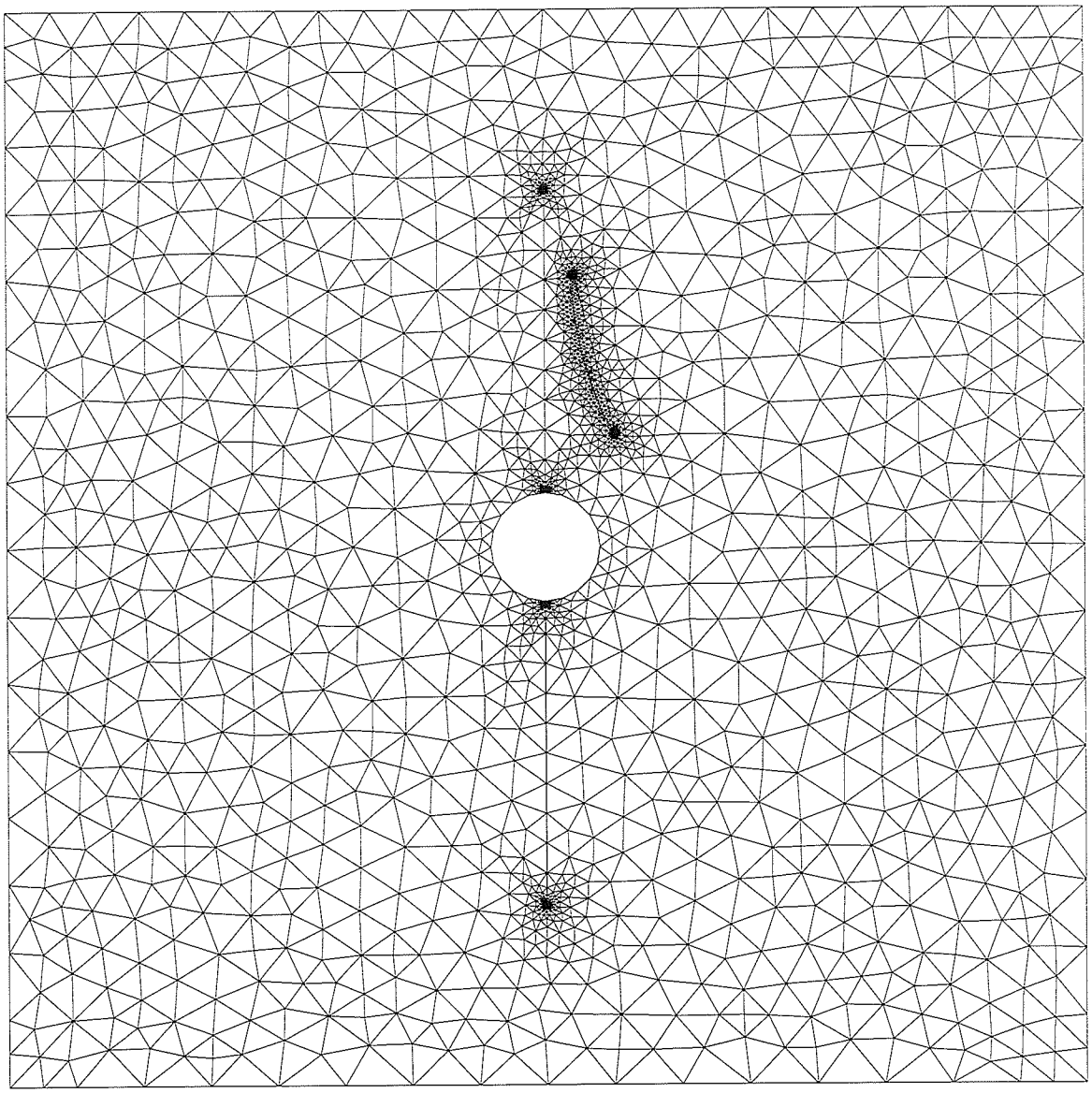

FIGURE 5.18: INSIGHT2D© Grid Showing a Remote Crack Manually Propagated Along Principal Stress Trajectories. Primary crack(s) can be seen by the denser grid at the tips, the remote crack has a denser grid along its entire length.

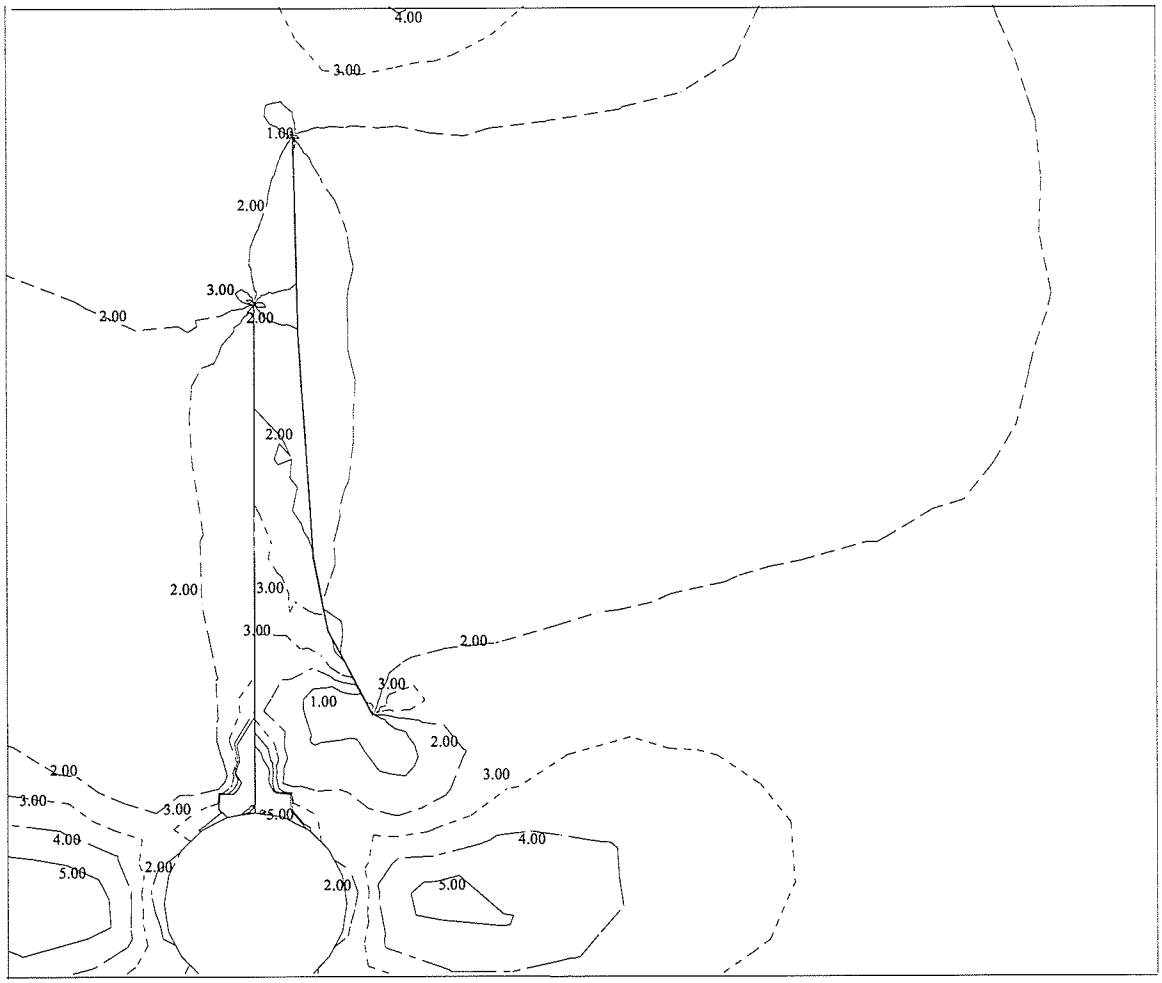

FIGURE 5.19: Contours of USR when a Remote Crack is Propagated

Modeling of the spalling was done using both EZELOP and INSIGHT2D©. When using INSIGHT2D© the primary was left at the length to which it was propagated for the development of the remote. The remote crack was not added for modeling of the spalling initiation because the models became too large when using INSIGHT2D©. EZELOP

does not have the option of adding a remote crack. Before considering the comparison of the modeled crack initiation to the physical model response it must be remembered that these models assume homogeneous conditions. This is perhaps acceptable for the pink granite but is not truly correct for the grey granite because of the existence of the microcracking which causes heterogeneous conditions. When plotting the modeled primary initiation versus the physical response (Figure 5.20) it was immediately obvious that a poor fit was obtained with data above 5 MPa in the pink granite and above 2.5 MPa in the grey granite. The effect of changing the averaging distance, d, in the model is illustrated in Figures 5.20 and 5.21. When plotting the modeled results for spalling versus the block sample results the physical model results were higher than the model predicted (Figure 5.21).

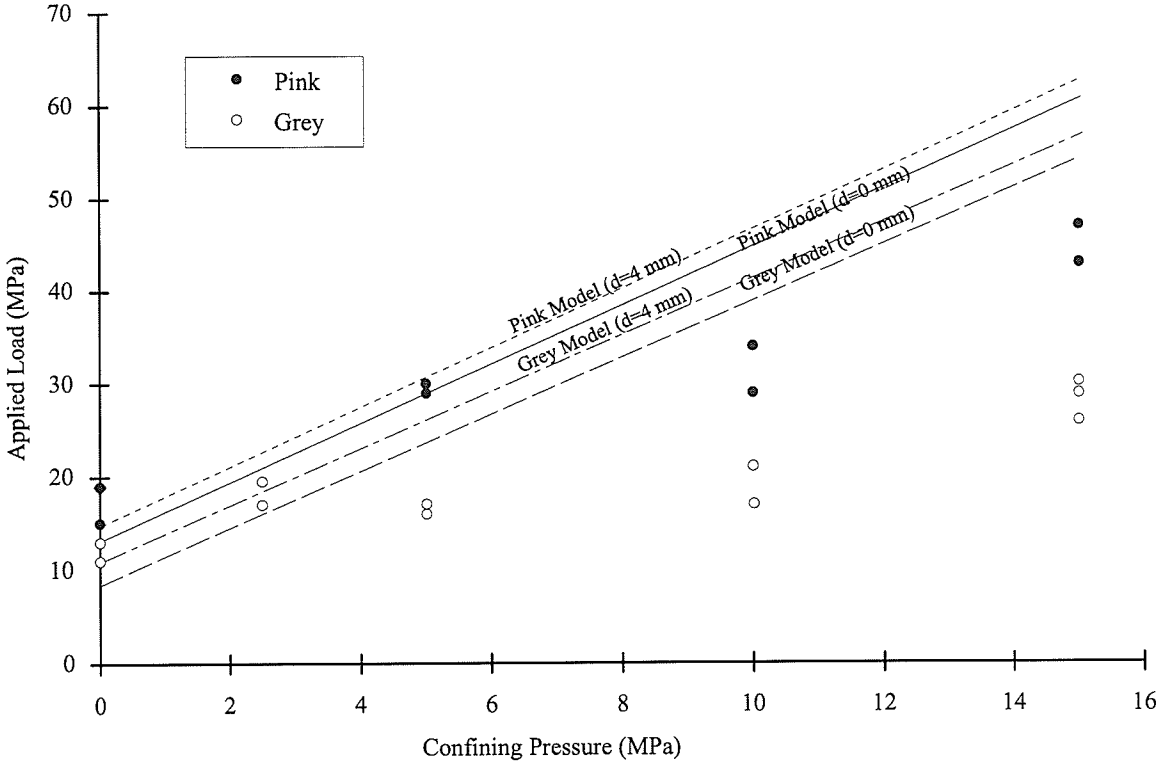

FIGURE 5.20: Comparison of the Physical Model Results to Computer Modeled Crack Initiation Points for the Primary Cracks. The averaging distance, d, has been varied for both the pink and grey granite models.

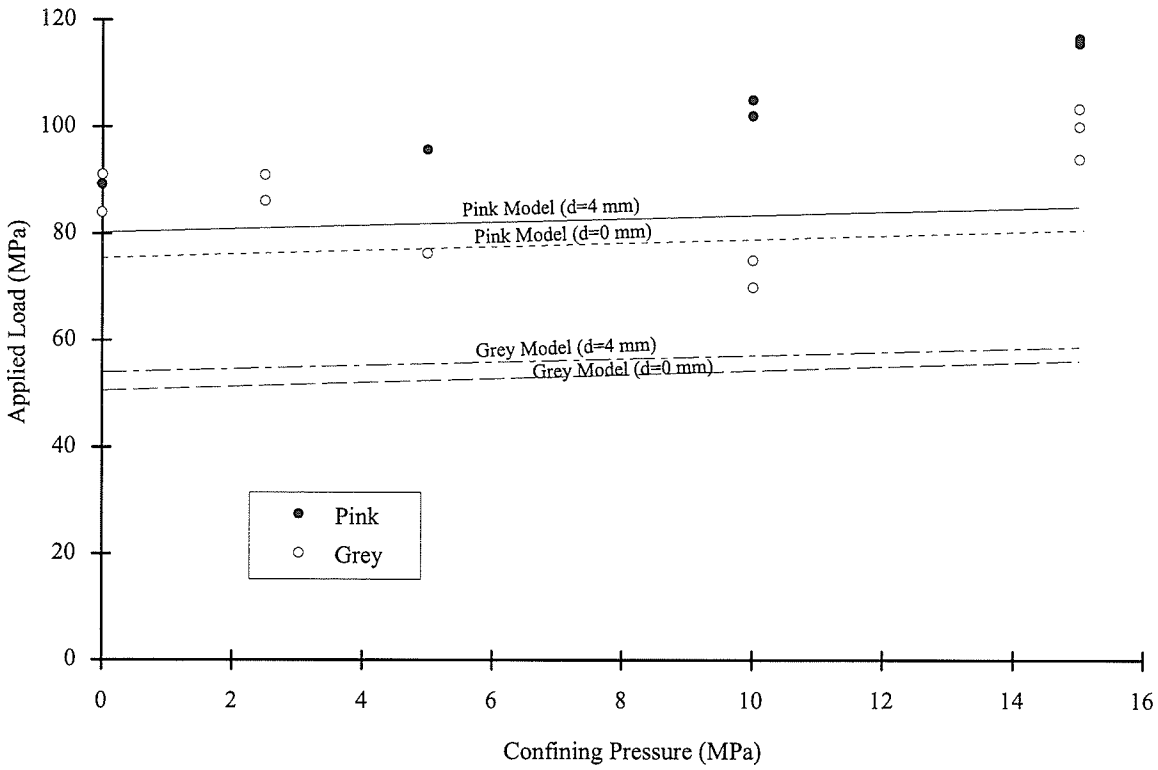

FIGURE 5.21: Comparison of the Physical Model Results to Computer Modeled Crack Initiation Points for the Spalling. The averaging distance, d, has been varied for both the pink and grey granite models.

As mentioned, the numerical model results for the primary cracks provide a reasonable fit for the unconfined cases and the 2.5 MPa grey and 5 MPa pink confining pressure cases. Above these confining pressures the responses of the physical model were less than that of the numerical models. This may indicate the effective confining pressure was lower than thought, not only from stress shadowing (from the microcracks in the grey granite) but also in the application of the load.

The numerical model fit for the spalling showed less of an increase with confining pressure and was much lower overall for the grey granite case. In this case, the numerical models

did not have remote cracks as did the physical models which may have changed the values at which crack initiation occurs.

When considering the loading response and crack formation of the laboratory samples it is important to remember the physical models did have fracture features in common with the in situ Mine-by tunnel. The most obvious feature was the spalling and the formation of breakout notches, although the depth of notches are not comparable because of the difference in loading histories (Martin et al. 1994). It is also obvious that the in situ maximum principal stress of 55 MPa is much lower than the values from the grey or the pink laboratory samples which show values of 95 and 115 MPa respectively. Part of this difference likely results from size effects (Martin 1993); the in situ tunnel is 3.5 m in diameter, the laboratory sample holes are only 0.061 m in diameter.

The decrease in primary fracture length with increased confining pressure in the physical models is similar to the in situ conditions, however, in situ, no tensile (primary) crack is visible. Since it is suspected the laboratory confining pressures were not fully applied, the in situ case may have somewhat higher confining pressure, which in turn is preventing the tensile crack formation. The remote cracks do not appear in situ around the Mine-by tunnel, perhaps because the tensile (primary) crack has not developed and therefore the necessary compressional stress concentration for remote crack nucleation has not developed.

CHAPTER 6
CONCLUSIONS

Six grey and five pink granite blocks were loaded in uniaxial or biaxial compression to compare the crack development around circular holes drilled through their centres. The pink granite was intact and showed no change in strength with orientation. The grey granite, carried three sets of microcracks. One subvertical set strikes north-south, a second subvertical set strikes 085°, dipping about 10° southeast and a sub horizontal set dips approximately 5-10° northwest. The two subvertical sets were in a position to effect the development of the induced fractures of the laboratory block testing. Because of the presence of the pre-existing microcracks, fractures that developed in the grey granite had several features that distinguished them from those in the intact, pink granite.

Contrasting with the relatively regular, straight cracks in the pink granite, the cracks in the grey granite are less regular: they wander more and often appear discontinuous by forming more frequent step-outs (four to five per 100 mm opposed to three to four in the pink granite).

The microcracked medium has the greatest effect on the primary fracture. In the uniaxial compression tests, the primary fractures in the pink granite would normally propagate to a distance of 125 mm or four times the radius of the cavity. In the grey granite, crack extension is much shorter, about 40 mm, only 1.3 times the radius. Interestingly, the remote fractures of the two rock types showed no significant difference in length. Considering the primary fracture is driven largely by tensile stresses and the remote fractures by compressive stresses, the indication is that the tensile stresses can be relieved

by the pre-existing microcracks. Obviously, no such relief is possible for the compressive stresses.

Confining pressure had the expected effect of limiting primary fracture propagation. There was again a difference in the total primary crack length. The final length of the primary fractures in the grey granite was one half to one third of those in the pink granite blocks. The range of confining pressures used in the experiment was quite modest, 0 to 15 MPa, which may explain why the depths of the breakout notches did not vary greatly. The various fracture nucleation points for the pink granite showed the expected linear variation with confining pressure, although not as much as expected from theoretical studies. For the grey granite, the confining pressure effect was not clear because of statistical scatter. The cause may lie in the stress-shadowing effect of the micro-fractures.

Numerical modelling of the fracture development was carried out. The numerical models match the uniaxial primary fracture case and the smaller confining pressure cases but as the confining pressure increased, the physical model results indicated the primary fracture formed at lower loads than suggested by the numerical models. This may show the higher confining pressure cases (10 and 15 MPa) were not fully achieved by the confining pressure assembly. Numerical modelling of the remote crack showed that development was occurring at both ends of a manually propagated remote crack, which agrees with physical model results. The spalling results showed the numerical model results to be lower than those of the physical models, perhaps because the presence of the remote cracks in the physical models effects the crack initiation values.

When comparing physical model fracturing to the in situ Mine-by tunnel, spalling was seen in both. The load at which the spalling began was lower for the in situ case, likely because of size effects. The decrease of primary fracture length with confining pressure in the

physical models is similar to the in situ case, where no tensile crack is visible. Because no tensile fracture forms, a compressional stress concentration remote from the tunnel wall would not take place, this may be why the remote cracks did not form in situ.

REFERENCES

ANSYS PC/ED (1985) Engineering analysis system user's manual, Issued Sept. 1, by R.W. Gorman for ANSYS, rev. 4.2, Swanson Analysis systems Inc., Houston, PA.

Babulic, P. J.. 1985. Fracture propagation around a circular opening in granite, Unpublished B.Sc. Thesis, Department of Geological Engineering, University of Manitoba.

Bieniawski, Z.T. 1967. Mechanism of brittle fracture of rock, Parts I, II and III. *Int. J. of Rock Mech. and Min. Sci.*, Vol. 4, pp. 395-430.

Bombolakis, E.G. 1973. Study of the brittle fracture process under uniaxial compression. *Tectonophysics*, Vol. 18 pp. 231-248.

Brace, W.F., E. Silver, K. Hadley and C. Goetze. 1972. Cracks and pores: a closer look. *Science*, 178, pp. 162-164.

Bray, J.W. 1987. *Some applications of the elastic theory.* In Analytical and Computational Methods in Engineering Rock Mechanics. E.T. Brown, ed., Allen and Unwin Publishers, London.

Brown, A., N. M. Soonawala, R. A. Everitt and D. C. Kamineni. 1989. Geology and geophysics of the Underground Research Laboratory site, Lac du Bonnet Batholith, Manitoba. *Canadian Journal of Earth Sciences*, Volume 26, pp. 404-425.

Carter, B. J.. 1988. Remote fracturing around underground openings. M.Sc. Thesis, Department of Civil Engineering, University of Manitoba.

Carter, B. J., E. Z. Lajtai and A. Petukhov. 1991. Primary and remote fracture around underground cavities. *International Journal for Numerical and Analytical Methods in Geomechanics,* Volume 15, pp. 21-40

Carter, B.J. 1992. Size and stress gradient effects on fracture around cavities. *Rock Mechanics and Rock Engineering*. Vol. 25 No. 3, pp. 167-186.

Carter, B.J., E.Z. Lajtai and Y. Yuan. 1992. Tensile fracture from circular cavities loaded in compression. *International Journal of Fracture*, Vol. 57, pp. 221-236.

Chernis, P. J.. 1984. Comparison of the pore-microcrack structure of shallow and deep samples of the Lac du Bonnet Granite. Atomic Energy of Canada Limited Technical Record TR-233.

Cook, N.G.W. 1965. The failure of rock. *Int. J. Rock Mech. & Min. Sci.*, Vol. 2, pp 389-403.

Deere, D. U.. 1980. Geological Considerations. In K. G. Stagg and O. C. Zienkiewicz, editors, *Rock Mechanics in Engineering Practice*, pages 1-20. John Wiley & Sons, London.

Dzik, E.J., E.Z. Lajtai and C.D. Martin. 1994. Numerical modelling of discrete fractures in granite. *In Proceedings of the Eighth International Conference of the Association for Computer Methods and Advances in Geomechanics*, Morgantown, West Virginia, USA, May, 22-28.

Everitt, R. A., M. Gascoyne, C. C. Davison, A. Brown and C. D. Martin. 1990. Regional and local setting of the Underground Research Laboratory. In R. S. Sinai, editor, *Proc. Int. Symp. on Unique Underground Structures, Denver, Colorado*, volume 2, pp. 64:1-23 CSM Press, Denver.

Gay, N.C. 1976. Fracture growth around openings in large blocks of rock subjected to uniaxial and biaxial compression. *Int. J. of Rock Mech., Min. Sci. and Geomech. Abstr.*, Vol. 13, pp. 231-243.

Haimson, B.C. and C.G. Herrick. 1985. In situ stress evaluation from borehole breakouts - experimental studies. In Proceedings of the 26th US Symposium on Rock Mechanics, Rapid City, SD, June 26-28, pp 1207-1218.

Haimson, B.C. and C.G. Herrick. 1989. Borehole breakouts and in situ stress. In Proceedings of the 12th Annual Energy Sources Technology Conference and Exhibition, Drilling Symposium, pp 17-22, ASME, New York

Hayles, J.G., M.H. Serzu, G. Lodha, P.J. Street and D.T. Stedner. 1994. Seismic velocity studies for the Mine-by Experiment. Atomic Energy of Canada Limited Technical Report.

Herget, G. 1980. Regional stresses in the Canadian Shield. *CIM Special Volume 22*, Thirteenth Canadian Rock Mechanics Symposium, Toronto, Ontario, May 28-29.

Hoek, E. and Z.T. Bieniawski. 1965. Brittle fracture propagation in rock under compression. *Journal of Fracture Mechanics*, Vol. 1 No. 3 pp. 137-155.

Hoek, E. and E. T. Brown. 1980. *Underground Excavations in Rock.* Institution of Mining and Metallurgy, London, England.

Kelly, D., D. C. Peck and R. S. James. 1993. Petrography of granitic rock samples from the 420 Level of the Underground Research Laboratory, Pinawa, Manitoba. Department of Geology, Laurentian University, Sudbury, Ontario.

Lajtai, E.Z.. 1972. Effect of tensile stress gradient on brittle fracture initiation. *Int. J. Rock Mech. & Min. Sci.* 9, pp. 569-578.

Lajtai, E.Z. 1981. Creep and crack growth in Lac du Bonnet granite due to compressive stress. In Proceedings of the 5th Canadian Fracture Conference, Winnipeg, Manitoba, Sept. 3-4.

Lajtai, E.Z. 1982. The fracture of Lac du Bonnet granite. Contract Report by the University of Manitoba. TR-M-0007.

Lajtai, E.Z, B.J. Carter and M.L. Ayari. 1990. Criteria for brittle fracture in compression. *Engineering Fracture Mechanics*, Vol. 37, No. 1, pp. 59-74.

Lajtai, E.Z., B.J. Carter and E.J.S. Duncan. 1991. Mapping the state of fracture around cavities. *Engineering Geology*, Vol. 31, pp. 277-289.

Lajtai, E.Z., B.J. Carter and E.J.S. Duncan. 1994. En echelon crack-arrays in potash salt rock. *Rock Mech. Rock Engng.*, Vol. 25 No. 3, pp. 167-186.

Lau, J.S.O. and B. Gorski. 1991. The post-failure behavior of the Lac du Bonnet grey granite. Mining Research Laboratories Divisional Report MRL 91-079(TR). Canada Centre for Mineral and Energy Technology.

Martin, C. D.. 1993. The strength of massive Lac du Bonnet Granite around underground openings. Ph. D. Thesis, Department of Civil Engineering, University of Manitoba.

Martin, C.D. 1989. Characterizing in situ stress domains at AECL's Underground Research Laboratory. In proceedings of the 42nd Canadian Geotechnical Conference, Winnipeg, Manitoba, Oct. 23-25.

Martin, C.D. and R.S. Read. 1992. Strength of massive granite around underground openings. In P.K. Kaiser and D.R. McCreath editors, *Proc. of the Canadian Rock Mechanics Symposium*, Sudbury, Ontario.

Martin, C.D. and N.A. Chandler. 1993. Stress Heterogeneity and Geological Structures. *Int. J. Rock Mech., Min. Sci. & Geomech. Abstr.* Vol. 30, No. 7, pp. 993-999. Pergamon Press Ltd., Great Britain.

Martin, C.D., J.B. Martino and E.J. Dzik. 1994. Comparison of borehole breakouts from laboratory and field tests. In proceedings of EUROCK 94.

Martino, J.B., R.S. Read and D.S. Collins. Mine-by experiment data summary: Part 6 - Acoustic Emission/Microseismic Results. Atomic Energy of Canada Limited Technical Record, TR-597.

Read, R.S. and C.D. Martin. 1991. Mine-by experiment final design report. Atomic Energy of Canada Limited Report, AECL-10430.

Read, R.S.. 1994. Interpreting near-face displacements around a tunnel in highly stressed granite. Ph.D. thesis, Department of Civil and Geological Engineering, University of Manitoba, Winnipeg, Manitoba, Canada.

Scholz, C.H.. 1968. Experimental study of the fracturing process in brittle rock. *Journal of Geophysical Research*, Vol. 73, No. 4.

Svab, M. and E.Z. Lajtai. 1981. Microstructural control of crack growth in Lac du Bonnet Granite. In *Proceedings of the Fifth Canadian Fracture Conference*. Winnipeg, Canada, 3-4 September, Pergamon Press.

Tapponnier, P. and W.F. Brace. 1976. Development of stress-induced microcracks in Westerly Granite. *Int. J. of Rock Mech., Min. Sci. & Geomech. Abstr.*, Vol. 13, pp. 103-112.

Tammemagi, H.Y., P.S. Kerford, J.C. Requeima and C.A. Temple. 1980. A geological reconnaissance study of the Lac du Bonnet batholith. Atomic Energy of Canada Limited Report, AECL-6439.

Wawersik, W.R. and C. Fairhurst. 1969. A study of brittle rock fracture in laboratory compression experiments. *Int. J. Rock Mech. Min. Sci.*, Vol. 7, pp. 561-575.

Wawersik, W.R. and W.F. Brace. 1971. Post-failure behaviour of a granite and diabase. *Rock Mechanics*, 3, 61-85

Yuan, Y.G., E.Z. Lajtai and M.L. Ayari. 1993. Fracture nucleation from a compression-parallel, finite-width elliptical flaw. *Int. J. Rock Mech., Min. Sci. & Geomech. Abstr.*, Vol. 30, No. 7, pp. 873-876.

APPENDIX A

BIAXIAL TENSION TEST RESULTS

TABLE A-1

CRACK ORIENTATIONS FROM SUITE 1 BIAXIAL TENSION TEST SAMPLES

Sample Number	Maximum Load Lbs.	Diameter mm	Thickness mm	Orientation of Crack (° from top) 1	2	3	4	Comments
1	203	32	5.4	53	144	245		
2	145	32	7.55	132	222	359		
3	118	32	7.3	0	146	245		
4	203	32	8.3	129	303	359		#2 wandered at end
5	125?	32	7.7	175	355			
6	157	32	7.4	41	180	233	232	#1,2,3 off centre
7	103	32	7.55	75	196	280		#2 off centre
8	87	32	7.2	95	195	290		
9	160	32	7.5	0	110	257		two piece failure zone in centre
10	140	32	8.2	29	163	251		
11	163	32	8	7	140	278		#2 starts at 0°
12	146	32	7	0	145	212		#1 curves, 90° section in center
13	96	32	7.1	80	230	311		
14	123	32	6.8	74	180	282		#2 off center
15	77	32	6.82	127	196	309		#3 starts at 90°
16	92	32	7.03	20	155	283		#3 off center
17	135	32	7.65	0	110	177		#1 starts at 325°
18	65	32	6.2	0	152			
19	74	32	6.6	5	165			#1,2 off center
20	71	32	5.9	35	215			
21	76	32	5.9	17	197	263		
22	64	32	5.9	0	102	183	282	
23	89	32	5.65	10	156	312		#3 wanders
24	89	32	6.3	9	109	179	261	center runs 40-220°
25	67	32	6.1	184	355			
26	64	32	5.45	2	132	245		#2 off center
27	78	32	6.1	168	354			
28	77	32	5.9	18	95	204		
29	66	32	5.3	16	121	212		
30	110	32	7.4	64	219			#2 starts at 294°
31	41	32	5.2	51	151	259	335	
32	68	31.9	6.9	10	190			
33	67	32	6.35	180	355			
34	85	32	6.9	92	176	276	339	
35	77	32	6.3	130	197	340		
36	52	32	6	17	170	230	330	center runs 60-300°
37	76	32	6.4	35	127	275		
38	75	32	7.15	10	97	180	249	#2,4 off center
39	53	32	5.5	178	357			

continued ...

TABLE A-1 (concluded)

Sample Number	Maximum Load Lbs.	Diameter mm	Thickness mm	Orientation of Crack (° from top)				Comments
				1	2	3	4	
40	101	32	8.1	87	187	272	350	center runs 33-213°
41	100	32	8	6	100	186		
42	87	32	7.6	53	233	308		
43	81	32	6.8	104	203	305		
44	67	32	6.8	30	210	350		
45	79	32	6.85	0	195			
46	58	32	6.2	12	90	183	270	
47	120	32	7.85	10	73	226		
48	119	32	8	105	285			
49	89	32	7.5	112	293			
50	133	32	7.85	116	289			
51	147	32	7.77	11	117	196	312	#1,2,3,4 off center
52	63	32	5.9	85	260			
53	126	32	7.3	78	162	242	295	

All cracks from center unless otherwise noted
Orientation of crack is clockwise from top
At the time of loading there was some concern as to the calibration of the loading frame

TABLE A-2

CRACK ORIENTATIONS FROM SUITE 2 BIAXIAL TENSION TEST SAMPLES

Sample Number	Maximum Load Lbs.	Diameter mm	Thickness mm	Orientation of Crack (° from top) 1	2	3	4	Comments
1	181	32	5	15	72	186	273	
2	175	32	5.5	15	195	247		
3	222	32	6	16	166	242		
4	130	32	5	39	212	292		
5	100	32	4	24	184			Punch Through
6	145	32	5.5	10	162	276		
7	145	32	5.5	95	275			
8	148	32	6	0	131	210	322	Cracks off centre
9	123	32	4	68	196	277	344	
10	141	32	5	60	175	240	332	
11	183	32	6	100	185	324		
12	275	32	6.2	30	178	280		
13	183	32	6	190	353			Punch Through
14	92	32	4	37	184	241		Punch Through
15	104	32	5	97	204	325		Punch Through
16	178	32	6	27	142	204	310	
17	207	32	6	77	158	246	332	
18	168	32	6	127	210	323		Punch Through
19	219	32	6	23	116	200	320	
20	118	32	5	15	180	299		
21	199	32	6	5	94	274		Punch Through
22	124	32	4	20	88	190	278	Punch Through
23	147	32	6	85	182	275		#1,3 off centre
24	158	32	5	35	150	230	304	Punch Through
25	150	32	5	31	125	206	272	
26	306	32	7	118	205	350		
27	100	32	6	3	90	138	240	Punch Through
28	147	32	6	30	110	210	290	
29	132	32	5	60	98	180	274	punch through
30	254	32	6.25	29	108	209	282	punch through
31	200	32	6	5	145	222		#3 off centre
32	240	31.9	5.2	25	205			
33	240	32	6	84	226	304		
34	114	32	6.29	21	201			
35	152	32	6.45	50	221			
36	215	31.8	5.6	22	113	192	277	
37	403	32	6.6	29	117	210	295	
38	161	32	5.95	70	210	302		
39	155	32	5.26	60	130	200	270	

continued ...

TABLE A-2 (concluded)

Sample Number	Maximum Load Lbs.	Diameter mm	Thickness mm	Orientation of Crack (° from top) 1	2	3	4	Comments
40	194	32.2	5.21	46	190	274		
41	279	31.9	6.79	63	208	335		
42	121	32	4.8	51	192	258		
43	189	32	5.55	58	212			
44	173	31.8	5.3	22	77	180	293	
45	120	31.5	4.95	98	210	315		
46	128	32	4.45	93	180	300		
47	193	31.8	5.3	17	100	212	318	
48	164	31.8	5.07	21	180	249	336	
49	222	31.8	6.02	45	81	225	305	
50	165	31.8	5.35	0	106	187	320	#2 off centre

All cracks from center unless otherwise noted
Orientation of crack is clockwise from top
At the time of loading there was some concern as to the calibration of the loading frame

TABLE A-3

CRACK ORIENTATIONS FROM SUITE 3 BIAXIAL TENSION TEST SAMPLES

Sample Number	Maximum Load Lbs.	Diameter mm	Thickness mm	Orientation of Crack (° from top) 1	2	3	4	Comments
1	190	31.8	5.85	37	225	312		
2	293	31.8	7.1	70	165	250	320	
3	186	31.8	6.15	32	77	215	270	shattered
4	220	31.8	6.01	0	90	210		
5	254	31.8	7.1	130	310			dropped
6	250	31.8	6.35	120	293			#1 splay at end
7	186	31.78	5.3	47	111	180	270	
8	210	31.7	6.2	20	60	255		
9	254	31.8	6.675	45	145	220		
10	214	31.8	6.19	25	190	315		cracks off centre
11	260	31.8	6.95	70	217	301		
12	240	31.85	6.75	60	158	235		
13	232	31.8	6.35	15	82	195	306	
14	170	31.9	6.72	11	50	183		some punch through
15	211	31.8	6.71	20	100	250	305	cracks off centre
16	226	31.8	5.71	28	150	220	290	#4 curved crack path
17	234	31.72	6.9	30	210	325		
18	126	31.8	5.51	35	145	220	330	
19	140	31.8	4.88	128	220	325		
20	112	31.8	4.69	43	170	230		
21	160	31.8	5.6	157	260	337		
22	86	31.8	4.6	135	290	332		
23	120	31.75	5.02	15	145	325		
24	98	31.8	5.3	85	175	248	355	
25	148	31.8	5.6	132	255	355		
26	160	31.9	5.9	50	230			
27	172	31.8	5.1	44	130	217	315	
28	144	31.8	5.72	50	180	320		
29	136	31.9	5.82	35	101	184	290	
30	176	31.8	6.6	23	178	270		
31	217	31.8	5.45	79	211	323		
32	226	31.8	6.4	85	225	331		
33	299	31.8	6.05	102	160	275	324	
34	192	31.9	6.5	80	204	285		
35	292	31.8	6.8	130	220	344		
36	170	31.8	6.65	80	160	240		
37	252	32	6.1	75	162	260		
38	152	31.8	5.4	45	135	230		
39	160	31.8	5.85	57	136	221	321	

continued ...

TABLE A-3 (concluded)

Sample Number	Maximum Load Lbs.	Diameter mm	Thickness mm	Orientation of Crack (° from top) 1	2	3	4	Comments
40	122	31.8	5.5	50	238			
41	105	31.8	4.8	37	128	225	275	
42	230	31.8	6.1	66	146	275		
43	158	31.9	4.7	60	155	240	330	
44	178	31.85	6.1	51	178	240		
45	137	31.8	4.9	15	130	270		
46	123	31.8	4.7	15	135	180	315	
47	81	31.8	4.6	137	222	313		punch through
48	110	31.8	4.2	50	132	230	321	
49	114	31.8	4.95	35	125	200	287	
50	124	31.8	5.78	30	60	185		

All cracks from center unless otherwise noted
Orientation of crack is clockwise from top
At the time of loading there was some concern as to the calibration of the loading frame

APPENDIX B

PHYSICAL MODEL GAUGE PATTERNS

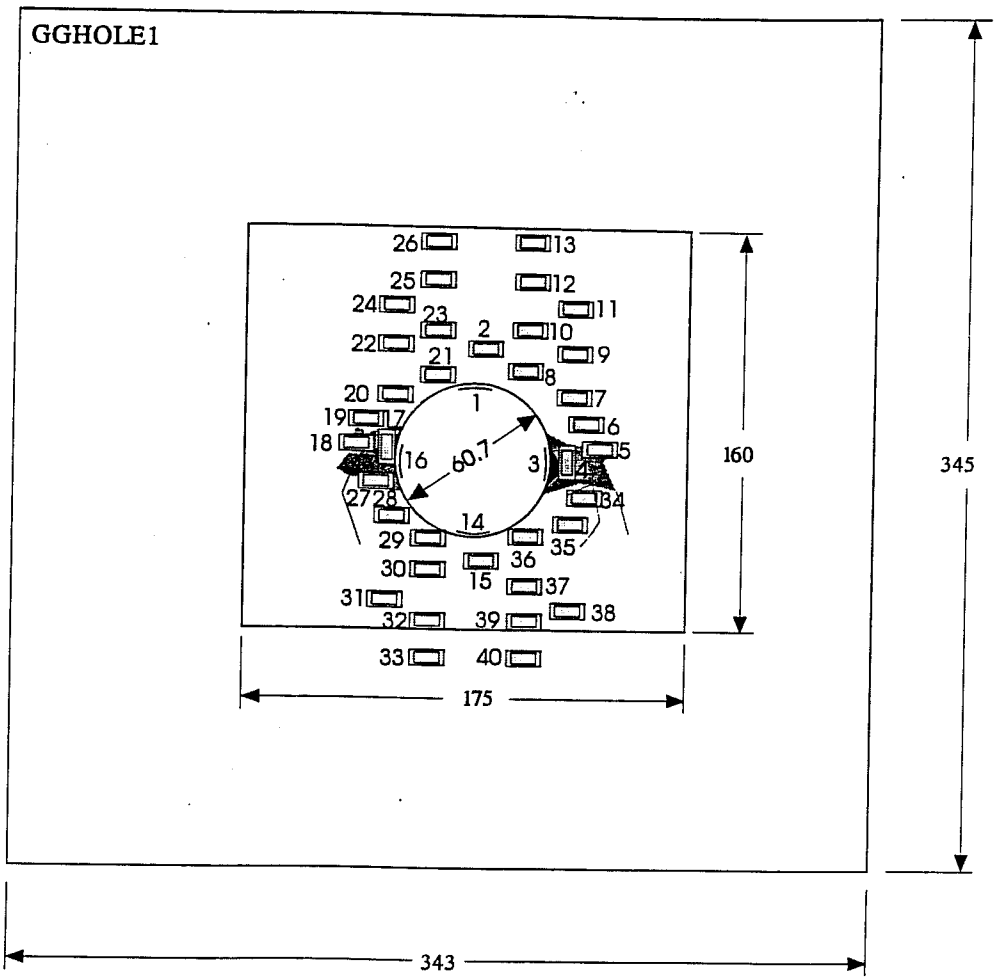

LEGEND

GAUGE SPALLING NOTCH FRACTURE

SCALE

0 25 50 100

NOTE:
OUTER SQUARE IS ORIGINAL SIZE OF BLOCK.
INNER SQUARE IS CUT SIZE.
BLOCK IS 103mm THICK.
GAUGES 1, 3, 14 AND 16 ARE IN HOLE.

ALL DIMENSIONS ARE IN mm

USI CODE NO. 1026.4 15. 1007.25.1.11			
URL - MINE-BY BLOCK TESTING DETAILS EXPERIMENT GGHOLE1			
DR'N E.P. JACOBS	DATE 93/11/16	ATOMIC ENERGY OF CANADA LIMITED RESEARCH COMPANY WHITESHELL NUCLEAR RESEARCH ESTABLISHMENT PINAWA MANITOBA, CANADA	
CHK'D F.A. Bibb	DATE 94/03/10		
SUBMITTED	DATE		
APP'D G.B. Lau	DATE 94/03/23	JOB NO. 49W30	SCALE 1:2.5
DWG. NO A4-1026-SK157		SHT 1	CONT ON / REV 0

FIGURE B-1: Block Sample GGHOLE1 Gauges and Crack Locations

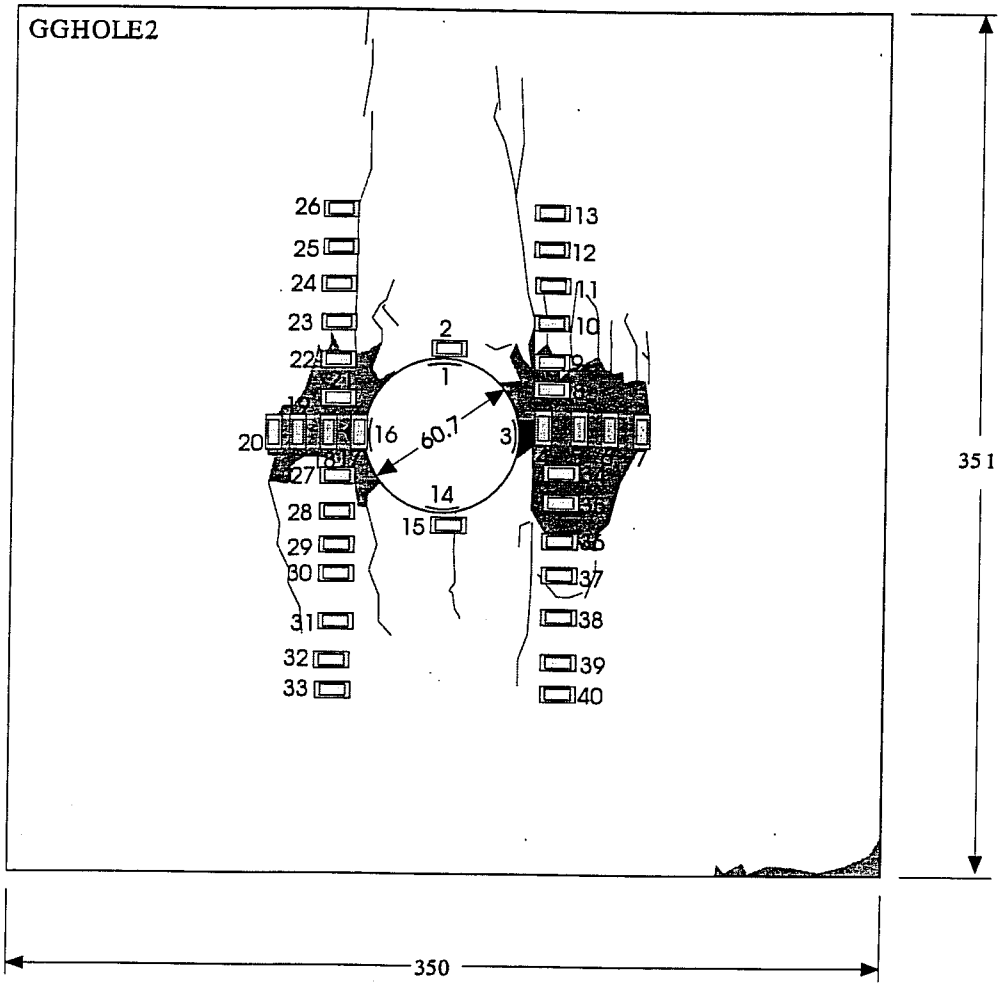

LEGEND

GAUGE SPALLING NOTCH FRACTURE

SCALE

0 25 50 100

NOTE:
BLOCK IS 107mm THICK.
GAUGES 1, 3, 14 AND 16 ARE IN HOLE.

ALL DIMENSIONS ARE IN mm

USI CODE NO. 1026.4 15.1007.25.1.11			
URL - MINE-BY BLOCK TESTING DETAILS EXPERIMENT GGHOLE2			
DR'N E.P. JACOBS	DATE 93/11/15	ATOMIC ENERGY OF CANADA LIMITED RESEARCH COMPANY WHITESHELL NUCLEAR RESEARCH ESTABLISHMENT PINAWA MANITOBA, CANADA	
CHK'D	DATE 94/03/16		
SUBMITTED	DATE		
APP'D	DATE 94/03/23	JOB NO. 49W30	SCALE 1:2.5
DWG. NO A4-1026-SK158		1 / 0	

FIGURE B-2: Block Sample GGHOLE2 Gauges and Crack Locations

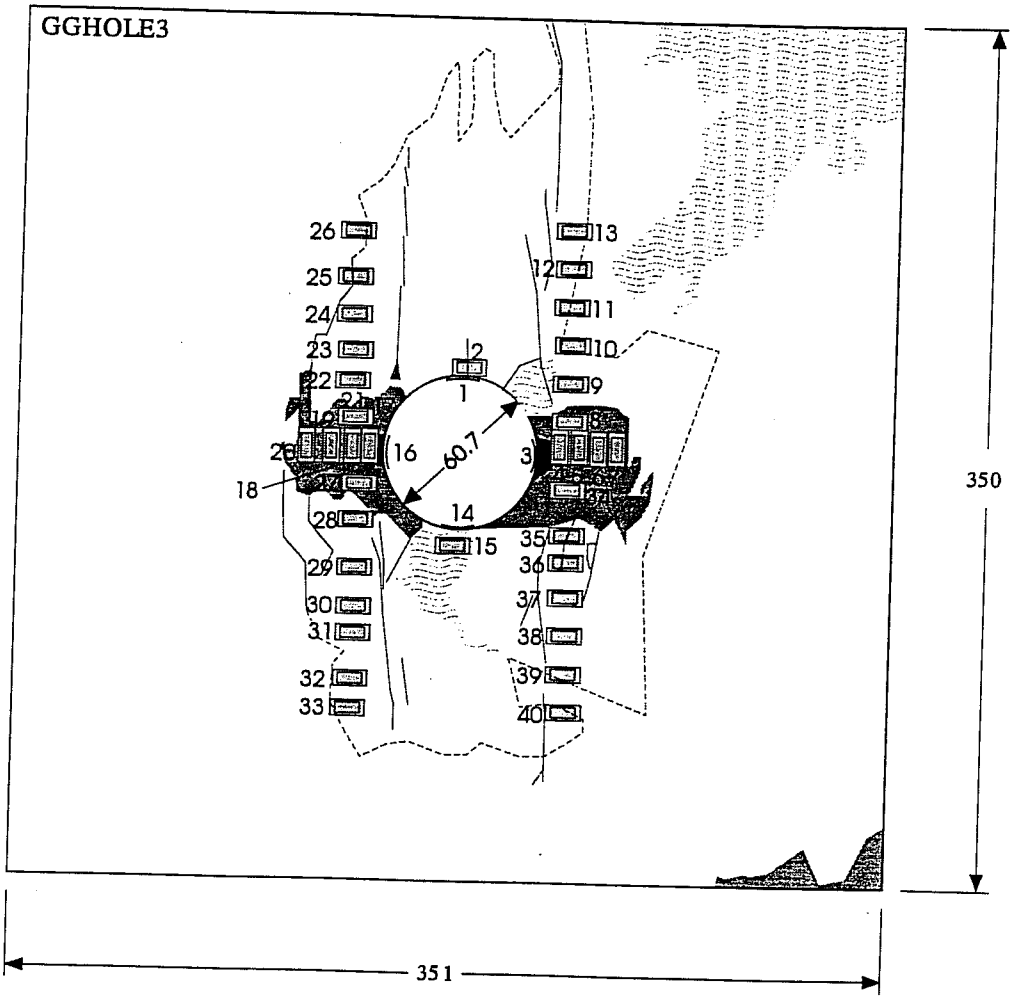

LEGEND

GAUGE | SPALLING | NOTCH | MAFIC | FRACTURE

HIGH DENSITY MICROCRACKING

SCALE

0 25 50 100

NOTE:
BLOCK IS 106mm THICK.
GAUGES 1, 3, 14 AND 16 ARE IN HOLE.

ALL DIMENSIONS ARE IN mm

USI CODE NO. 1026.4 15. 1007.25. 1. 11			
URL - MINE-BY BLOCK TESTING DETAILS EXPERIMENT GGHOLE3			
DR'N E.P. JACOBS	DATE 93/11/15	ATOMIC ENERGY OF CANADA LIMITED RESEARCH COMPANY WHITESHELL NUCLEAR RESEARCH ESTABLISHMENT PINAWA MANITOBA, CANADA	
CHK'D T.A. Bibb	DATE 94/02/16		
SUBMITTED	DATE		
APP'D G.B. Mountain	DATE 94/03/23	JOB NO. 49W30	SCALE 1:2.5
DWG. NO A4-1026-SK159	SHT 1	CONT ON /	REV 0

FIGURE B-3: Block Sample GGHOLE3 Gauges and Crack Locations

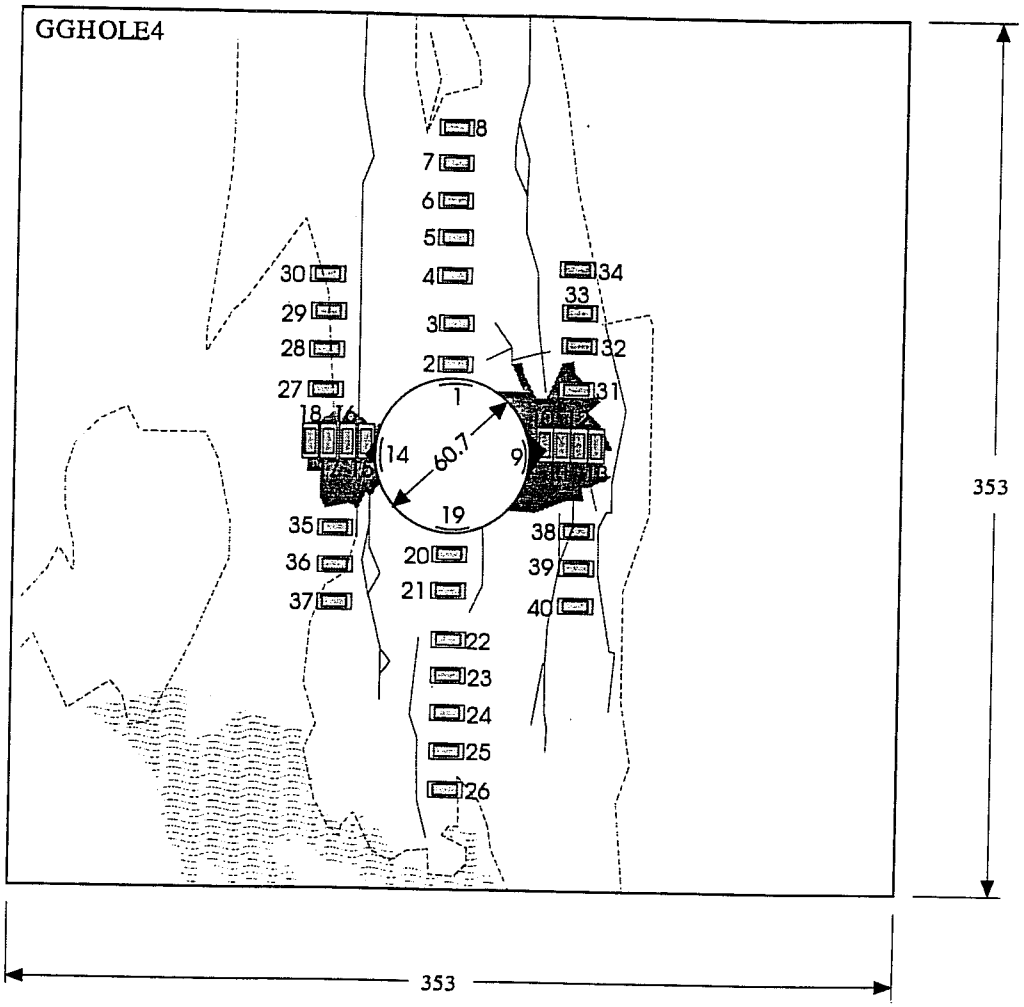

LEGEND

GAUGE SPALLING NOTCH MAFIC FRACTURE

HIGH DENSITY MICROCRACKING

SCALE

0 25 50 100

NOTE:
BLOCK IS 107mm THICK.
GAUGES 1, 9, 14 AND 19 ARE IN HOLE.

ALL DIMENSIONS ARE IN mm

USI CODE NO. 1026.4 15.1007.25.1.11			
URL - MINE-BY BLOCK TESTING DETAILS EXPERIMENT GGHOLE4			
DR'N E.P. JACOBS DATE 93/11/15	ATOMIC ENERGY OF CANADA LIMITED RESEARCH COMPANY WHITESHELL NUCLEAR RESEARCH ESTABLISHMENT PINAWA MANITOBA, CANADA		
CHK'D T.A. Bidwell DATE 94/03/16			
SUBMITTED DATE			
APP'D C.B. Martin DATE 94/03/23	JOB NO. 49W30	SCALE 1:2.5	
DWG. NO A4-1026-SK160	1	/	0

FIGURE B-4: Block Sample GGHOLE4 Gauges and Crack Locations

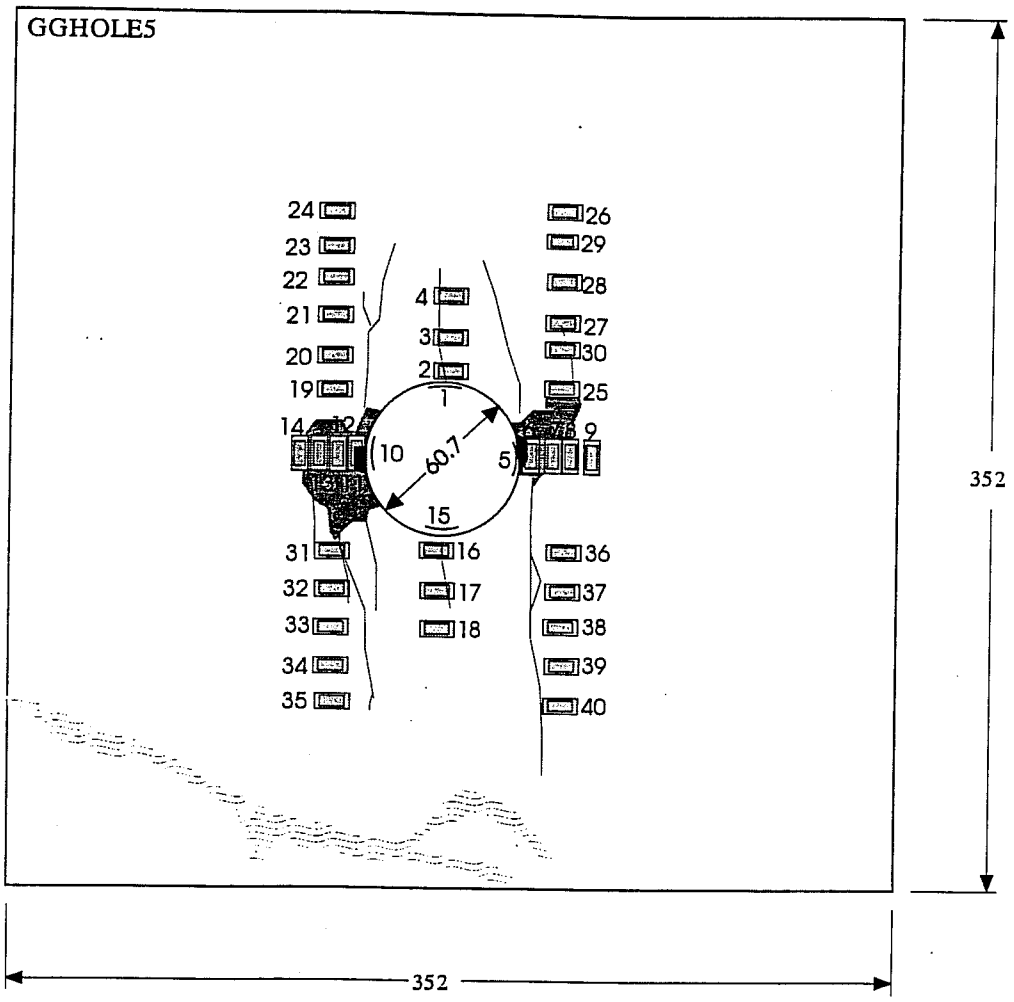

LEGEND

GAUGE SPALLING NOTCH MAFIC FRACTURE

SCALE

0 25 50 100

NOTE:
BLOCK IS 109mm THICK.
GAUGES 1, 5, 10 AND 15 ARE IN HOLE.

ALL DIMENSIONS ARE IN mm

USI CODE NO. 1026.4 15. 1007.25.1.11			
URL - MINE-BY BLOCK TESTING DETAILS EXPERIMENT GGHOLE5			
DR'N E.P. JACOBS DATE 93/11/15	ATOMIC ENERGY OF CANADA LIMITED RESEARCH COMPANY WHITESHELL NUCLEAR RESEARCH ESTABLISHMENT PINAWA MANITOBA, CANADA		
CHK'D J.A.P. Hahn DATE 94/03/16			
SUBMITTED — DATE			
APP'D A.S. Martino DATE 94/03/23	JOB NO. 49W30	SCALE 1:2.5	
DWG. NO A4-1026-SK161	1	/	0

FIGURE B-5: Block Sample GGHOLE5 Gauges and Crack Locations

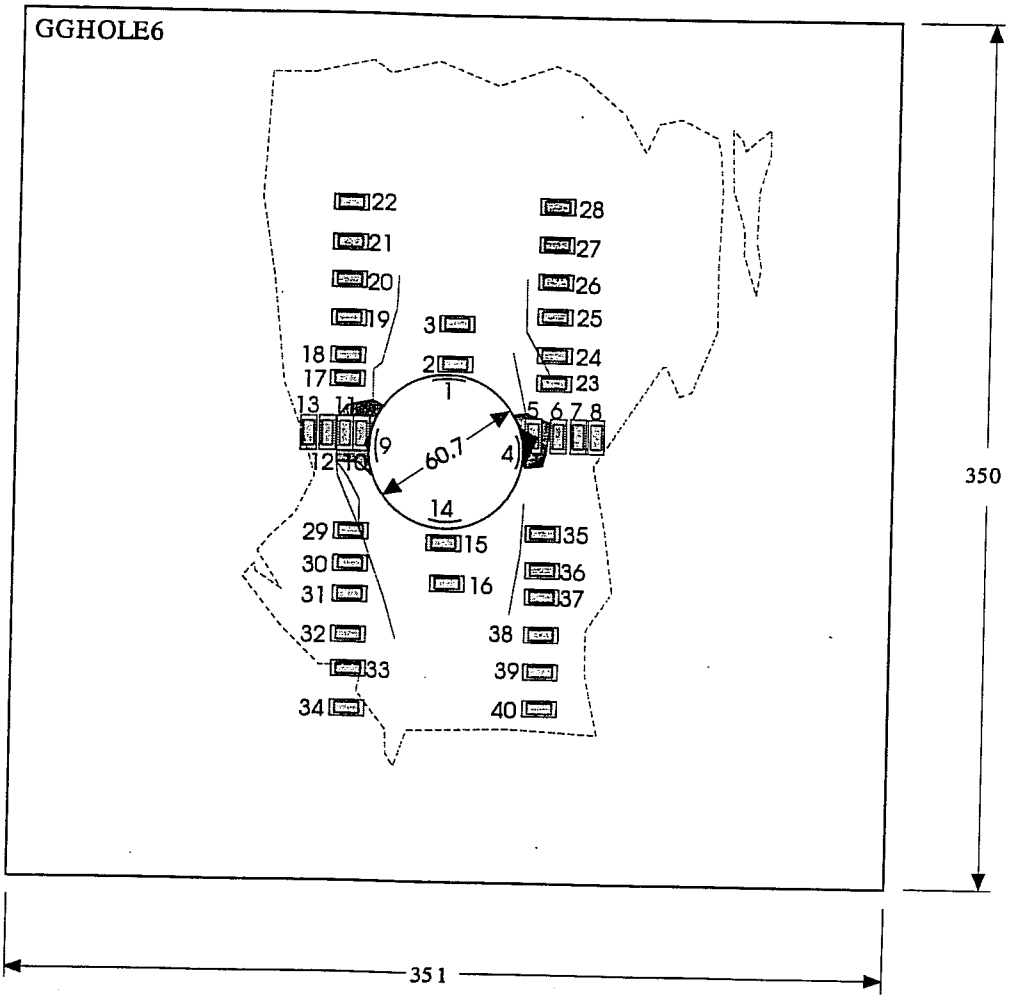

LEGEND

GAUGE SPALLING NOTCH FRACTURE

HIGH DENSITY MICROCRACKING

SCALE

0 25 50 100

NOTE:
BLOCK IS 109mm THICK.
GAUGES 1, 4, 9 AND 14 ARE IN HOLE.

ALL DIMENSIONS ARE IN mm

USI CODE NO. 1026.415.1007.25.1.11			
URL - MINE-BY BLOCK TESTING DETAILS EXPERIMENT GGHOLE6			
DR'N E.P. JACOBS	DATE 93/11/15	ATOMIC ENERGY OF CANADA LIMITED RESEARCH COMPANY WHITESHELL NUCLEAR RESEARCH ESTABLISHMENT PINAWA MANITOBA, CANADA	
CHK'D T.A. Brown	DATE 94/03/16		
SUBMITTED	DATE		
APP'D S.J. Bhatt	DATE 94/03/23	JOB NO. 49W30	SCALE 1:2.5
DWG NO A4-1026-SK162		1 / 0	

FIGURE B-6: Block Sample GGHOLE6 Gauges and Crack Locations

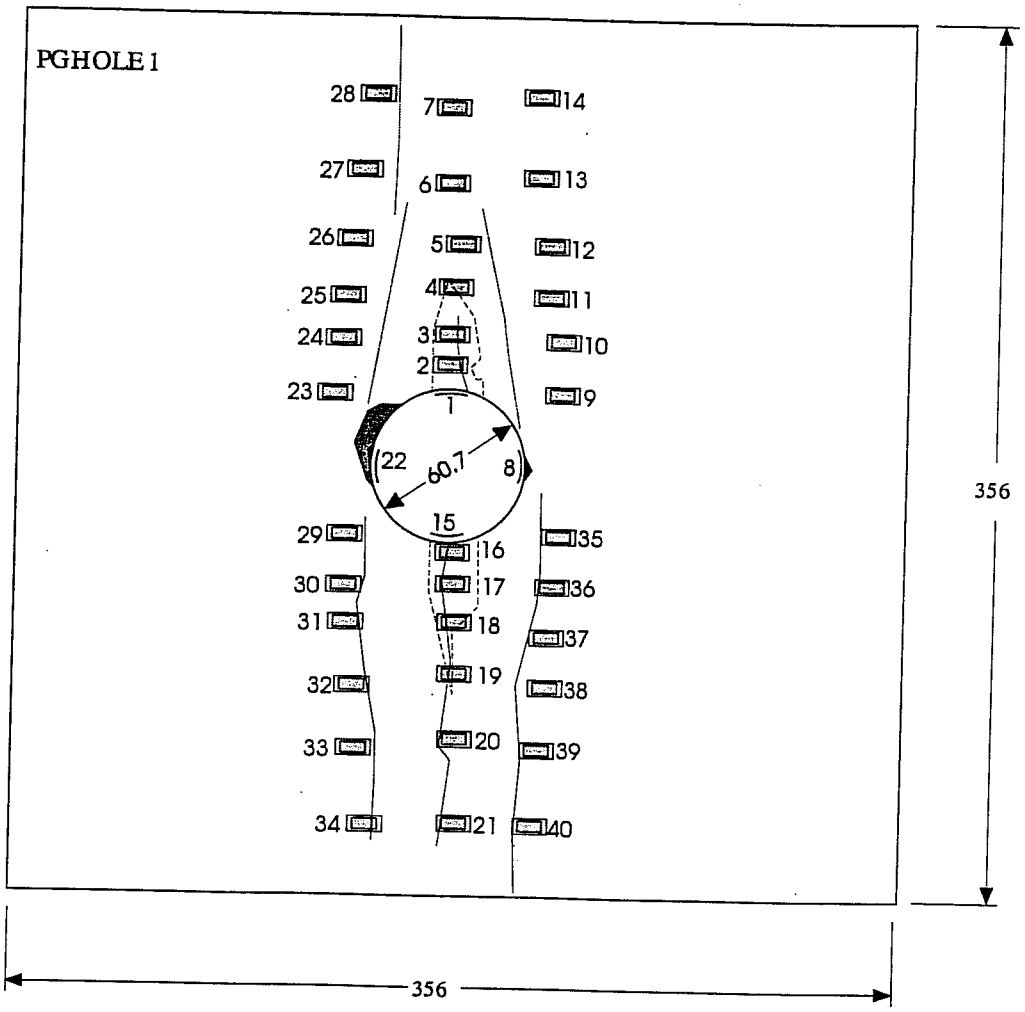

LEGEND

GAUGE SPALLING NOTCH FRACTURE

HIGH DENSITY MICROCRACKING

SCALE

0 25 50 100

NOTE:
BLOCK IS 108mm THICK.
GAUGES 1, 8, 15 AND 22 ARE IN HOLE.

ALL DIMENSIONS ARE IN mm

USI CODE NO. 1026.4 15. 1007.25.1.11			
URL - MINE-BY BLOCK TESTING DETAILS EXPERIMENT PGHOLE 1			
DR'N E.P. JACOBS DATE 93/11/15	ATOMIC ENERGY OF CANADA LIMITED RESEARCH COMPANY WHITESHELL NUCLEAR RESEARCH ESTABLISHMENT PINAWA MANITOBA, CANADA		
CHK'D DATE 94/03/16			
SUBMITTED DATE			
APP'D DATE 94/03/17	JOB NO. 49W30	SCALE 1:2.5	
DWG. NO A4-1026-SK163	1	/	0

FIGURE B-7: Block Sample PGHOLE1 Gauges and Crack Locations

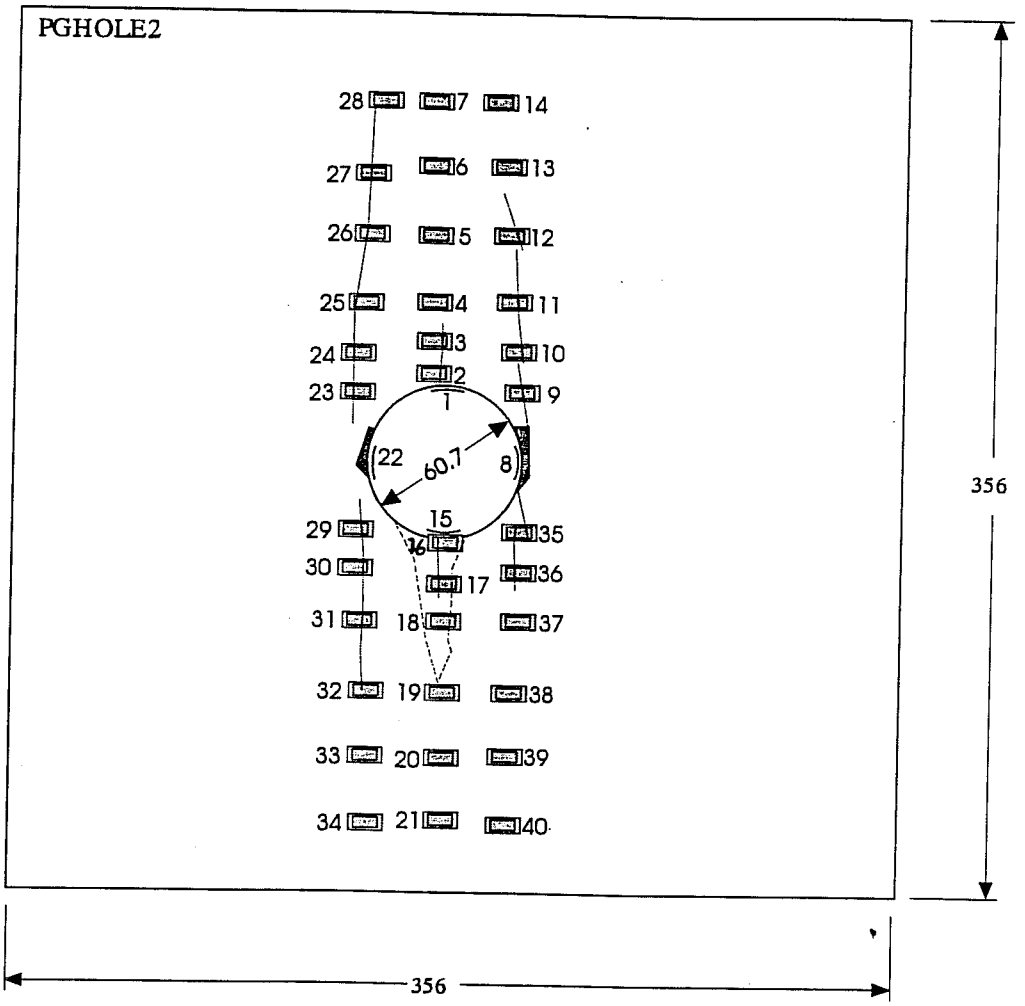

LEGEND

GAUGE SPALLING NOTCH FRACTURE

HIGH DENSITY MICROCRACKING

SCALE

0 25 50 100

NOTE:
BLOCK IS 108mm THICK.
GAUGES 1, 8, 15 AND 22 ARE IN HOLE.

ALL DIMENSIONS ARE IN mm

USI CODE NO. 1026.4 15.1007.25.1.11			
URL - MINE-BY BLOCK TESTING DETAILS EXPERIMENT PGHOLE2			
DR'N E.P. JACOBS DATE 93/11/15	ATOMIC ENERGY OF CANADA LIMITED RESEARCH COMPANY WHITESHELL NUCLEAR RESEARCH ESTABLISHMENT PINAWA MANITOBA, CANADA		
CHK'D T.A.B. DATE 94/03/16			
SUBMITTED DATE			
APP'D DATE 94/03/23	JOB NO. 49W30	SCALE 1:2.5	
DWG NO A4-1026-SK164	1	/	0

FIGURE B-8: Block Sample PGHOLE2 Gauges and Crack Locations

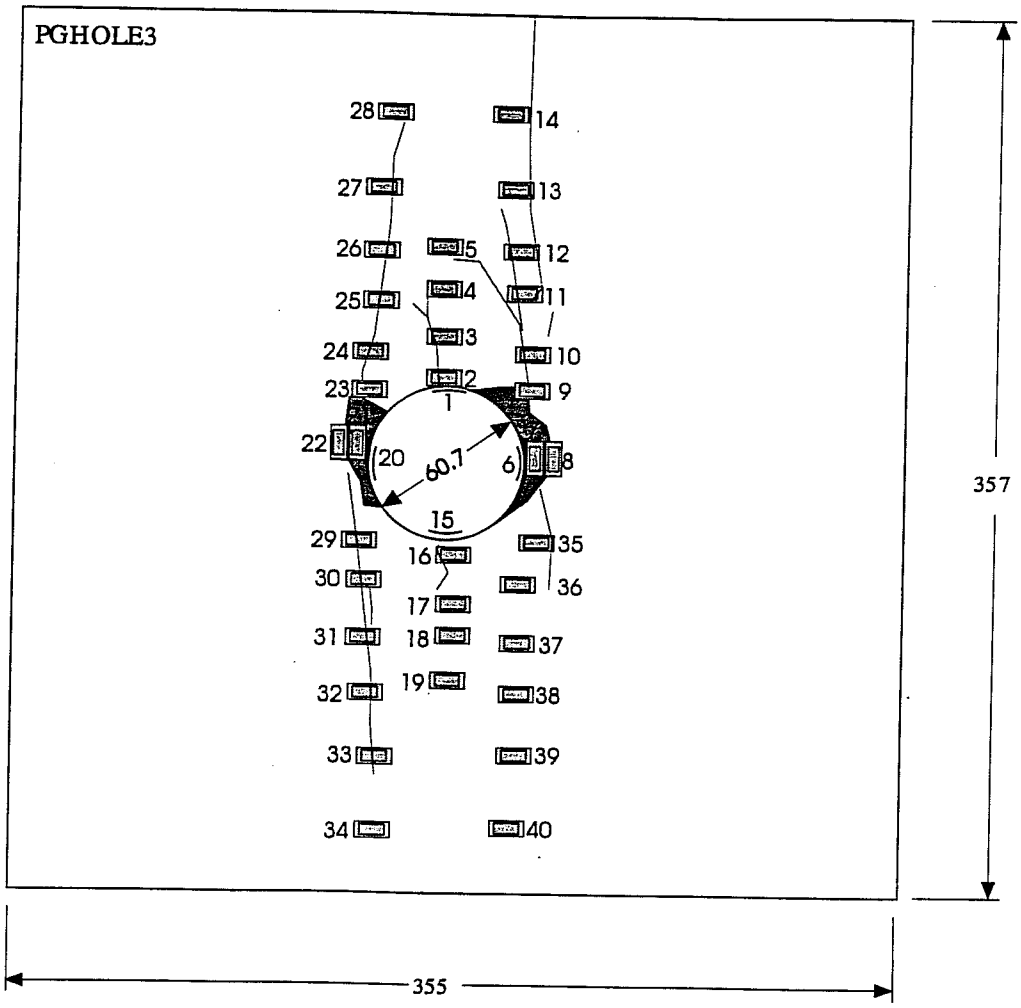

LEGEND

GAUGE SPALLING NOTCH FRACTURE

HIGH DENSITY MICROCRACKING

SCALE

0 25 50 100

NOTE:
BLOCK IS 108mm THICK.
GAUGES 1, 6, 15 AND 20 ARE IN HOLE.

ALL DIMENSIONS ARE IN mm

USI CODE NO. 1026.4 15.1007.25.1.11			
URL - MINE-BY BLOCK TESTING DETAILS EXPERIMENT PGHOLE3			
DR'N E.P. JACOBS DATE 93/11/15	ATOMIC ENERGY OF CANADA LIMITED RESEARCH COMPANY WHITESHELL NUCLEAR RESEARCH ESTABLISHMENT PINAWA MANITOBA, CANADA		
CHK'D ZA Bilek DATE 94/03/16			
SUBMITTED DATE			
APP'D C.B. Haughton DATE 94/03/23	JOB NO. 49W30	SCALE 1:2.5	
DWG. NO A4-1026-SK165	1	/	0

FIGURE B-9: Block Sample PGHOLE3 Gauges and Crack Locations

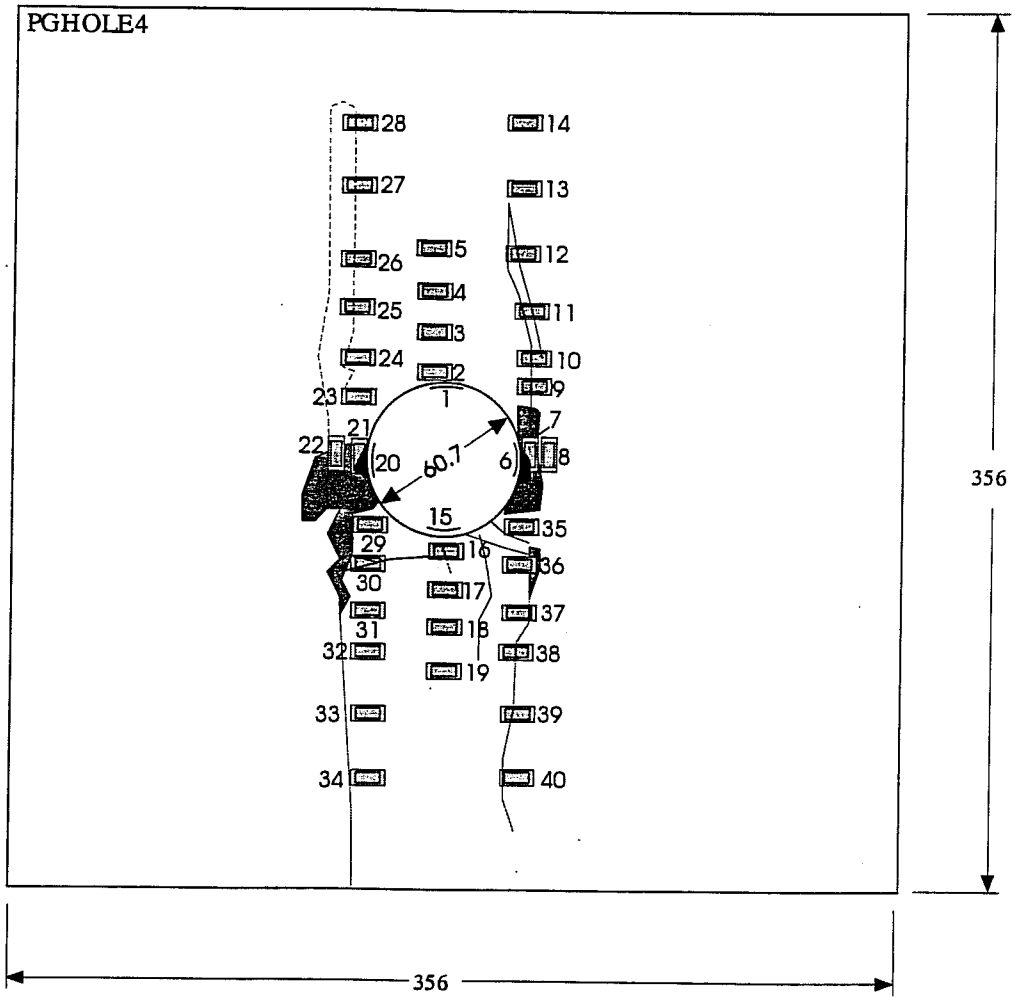

LEGEND

GAUGE SPALLING NOTCH FRACTURE

HIGH DENSITY MICROCRACKING

SCALE

0 25 50 100

NOTE:
BLOCK IS 108mm THICK.
GAUGES 1, 6, 15 AND 20 ARE IN HOLE.

ALL DIMENSIONS ARE IN mm

USI CODE NO. 1026.4 15.1007.25.1.11			
URL - MINE-BY BLOCK TESTING DETAILS EXPERIMENT PGHOLE4			
DR'N E.P. JACOBS DATE 93/11/15	ATOMIC ENERGY OF CANADA LIMITED RESEARCH COMPANY WHITESHELL NUCLEAR RESEARCH ESTABLISHMENT PINAWA MANITOBA, CANADA		
CHK'D F.A.B. DATE 94/03/16			
SUBMITTED DATE			
APP'D [illegible] DATE 94/03/23	JOB NO. 49W30	SCALE 1:2.5	
DWG-NO A4-1026-SK166	1	/	0

FIGURE B-10: Block Sample PGHOLE4 Gauges and Crack Locations

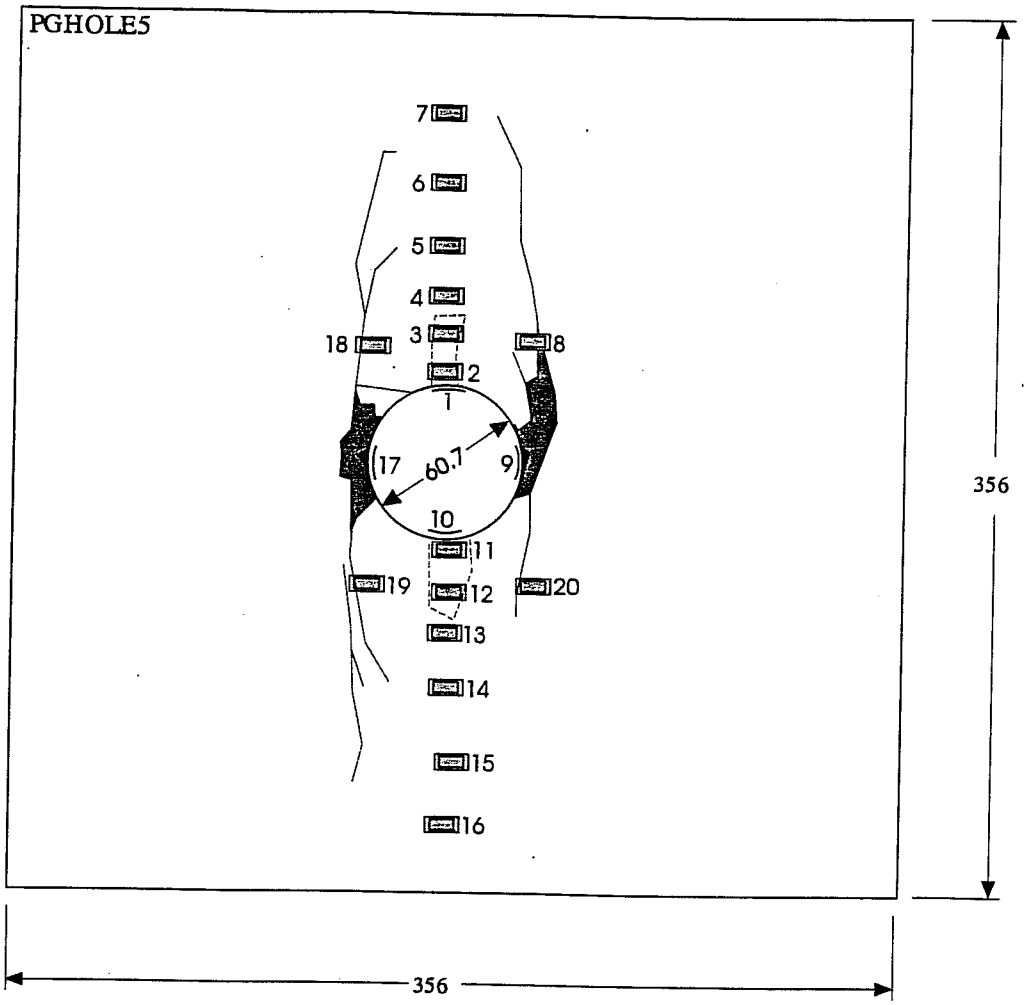

LEGEND

GAUGE SPALLING NOTCH FRACTURE

HIGH DENSITY MICROCRACKING

SCALE

0 25 50 100

NOTE:
BLOCK IS 107mm THICK.
GAUGES 1, 9, 10 AND 17 ARE IN HOLE

ALL DIMENSIONS ARE IN mm

USI CODE NO. 1026.4 15. 1007.25.1.11			
URL - MINE-BY BLOCK TESTING DETAILS EXPERIMENT PGHOLE5			
DR'N E.P. JACOBS	DATE 93/11/15	ATOMIC ENERGY OF CANADA LIMITED RESEARCH COMPANY WHITESHELL NUCLEAR RESEARCH ESTABLISHMENT PINAWA MANITOBA, CANADA	
CHK'D ZA Bilsk	DATE 94/03/16		
SUBMITTED	DATE		
APP'D	DATE 94/03/23	JOB NO. 49W30	SCALE 1:2.5
DWG. NO A4-1026-SK167		1 / 0	

FIGURE B-11: Block Sample PGHOLE5 Gauges and Crack Locations

APPENDIX C

CRACKING IN PHYSICAL MODELS

TABLE C-1

GGHOLE1 LOADING RESULTS

(Confining Pressure = 15 MPa)

Gauge Number	Crack Type	Load at Gauge at Time of Cracking (MPa)
1	Upper Primary	29
2	Upper Primary	-
3	Right Side Spall	94
4	Right Side Spall	Partial Debond
5	Right Side Spall	115
6	Right Side Spall	-
7	Right Side Spall	*
8	Upper Right Remote	*
9	Upper Right Remote	*
10	Upper Right Remote	*
11	Upper Right Remote	*
12	Upper Right Remote	*
13	Upper Right Remote	*
14	Lower Primary	30
15	Lower Primary	33
16	Left Side Spall	100
17	Left Side Spall	115
18	Left Side Spall	125
19	Upper Left Remote	*
20	Upper Left Remote	*
21	Upper Left Remote	*
22	Upper Left Remote	*
23	Upper Left Remote	*
24	Upper Left Remote	*
25	Upper Left Remote	*
26	Upper Left Remote	*
27	Lower Left Remote	81
28	Lower Left Remote	83
29	Lower Left Remote	-
30	Lower Left Remote	*
31	Lower Left Remote	*
32	Lower Left Remote	*
33	Lower Left Remote	*
34	Right Side Spall	95
35	Right Side Spall	95
34	Lower Right Remote	-
35	Lower Right Remote	81
36	Lower Right Remote	82
37	Lower Right Remote	82
38	Lower Right Remote	84
39	Lower Right Remote	*
40	Lower Right Remote	*

Notes

* Crack did not reach gauge or too far from gauge

\- Not Readable

Many readings faint

TABLE C-2

GGHOLE2 LOADING RESULTS

(Confining Pressure = 5 MPa)

Gauge Number	Crack Type	Load at Gauge at Time of Cracking (MPa)
1	Upper Primary	17
2	Upper Primary	18
3	Right Side Spall	76
4	Right Side Spall	67
5	Right Side Spall	99
6	Right Side Spall	117
7	Right Side Spall	119
8	Upper Right Remote	76
9	Upper Right Remote	78
10	Upper Right Remote	78
11	Upper Right Remote	78
12	Upper Right Remote	-
13	Upper Right Remote	-
14	Lower Primary	16
15	Lower Primary	17
16	Left Side Spall	88
17	Left Side Spall	87
18	Left Side Spall	93
19	Left Side Spall	96
20	Left Side Spall	96
21	Upper Left Remote	BAD
22	Upper Left Remote	-
23	Upper Left Remote	-
24	Upper Left Remote	-
25	Upper Left Remote	-
26	Upper Left Remote	-
27	Lower Left Remote	73
28	Lower Left Remote	74
29	Lower Left Remote	76
30	Lower Left Remote	78
31	Lower Left Remote	78
32	Lower Left Remote	79
33	Lower Left Remote	*
34	Lower Right Remote	67
35	Lower Right Remote	67
36	Lower Right Remote	67
37	Lower Right Remote	68
38	Lower Right Remote	BAD
39	Lower Right Remote	69
40	Lower Right Remote	-

Notes

* Crack did not reach gauge or too far from gauge

\- Not Readable

TABLE C-3

GGHOLE3 LOADING RESULTS

(Confining Pressure = 10 MPa)

Gauge Number	Crack Type	Load at Gauge at Time of Cracking (MPa)
1	Upper Primary	21
2	Upper Primary	27
3	Right Side Spall	75
4	Right Side Spall	85
5	Right Side Spall	85
6	Right Side Spall	108
7	Right Side Spall	119
8	Upper Right Remote	67
9	Upper Right Remote	67
10	Upper Right Remote	67
11	Upper Right Remote	68
12	Upper Right Remote	70
13	Upper Right Remote	74
14	Lower Primary	17
15	Lower Primary	22
16	Left Side Spall	70
17	Left Side Spall	80
18	Left Side Spall	88
19	Left Side Spall	94
20	Left Side Spall	94
21	Upper Left Remote	69
22	Upper Left Remote	-
23	Upper Left Remote	-
24	Upper Left Remote	-
25	Upper Left Remote	-
26	Upper Left Remote	-
27	Lower Left Remote	-
28	Lower Left Remote	-
29	Lower Left Remote	-
30	Lower Left Remote	-
31	Lower Left Remote	-
32	Lower Left Remote	-
33	Lower Left Remote	-
34	Lower Right Remote	61
35	Lower Right Remote	62
36	Lower Right Remote	+
37	Lower Right Remote	62
38	Lower Right Remote	62
39	Lower Right Remote	62
40	Lower Right Remote	63

Notes

* Crack did not reach gauge or too far from gauge

\- Not Readable

\+ Splays pass to either side of gauge isolating it
Distinct "smoothing" of the remote reponses
making it much harder to pick out crack events
An event effecting most gauges on the left upper
and lower remotes occurs at 38.43 MPa, this
jump which large obscures the response

TABLE C-4

GGHOLE4 LOADING RESULTS

(Confining Pressure = 0 MPa)

Gauge Number	Crack Type	Load at Gauge at Time of Cracking (MPa)
1	Upper Primary	13
2	Upper Primary	20
3	Upper Primary	40
4	Upper Primary	*
5	Upper Primary	*
6	Upper Primary	*
7	Upper Primary	*
8	Upper Primary	*
9	Right Side Spall	84
10	Right Side Spall	87
11	Right Side Spall	113
12	Right Side Spall	113
13	Right Side Spall	118
14	Left Side Spall	91
15	Left Side Spall	93
16	Left Side Spall	117
17	Left Side Spall	120
18	Left Side Spall	120
19	Lower Primary	11
20	Lower Primary	15
21	Lower Primary	*
22	Lower Primary	*
23	Lower Primary	*
24	Lower Primary	*
25	Lower Primary	*
26	Lower Primary	*
27	Upper Left Remote	63
28	Upper Left Remote	66
29	Upper Left Remote	66
30	Upper Left Remote	66
31	Upper Right Remote	62
32	Upper Right Remote	63
33	Upper Right Remote	63
34	Upper Right Remote	64
35	Lower Left Remote	67
36	Lower Left Remote	67
37	Lower Left Remote	66
38	Lower Right Remote	67
39	Lower Right Remote	68
40	Lower Right Remote	68

Notes

* Crack did not reach gauge or too far from gauge

\- Not Readable

Wiring may have been reversed on gauges 27 and 30

TABLE C-5

GGHOLE5 LOADING RESULTS

(Confining Pressure = 2.5 MPa)

Gauge Number	Crack Type	Load at Gauge at Time of Cracking (MPa)
1	Upper Primary	17
2	Upper Primary	17
3	Upper Primary	20
4	Upper Primary	*
5	Right Side Spall	91
6	Right Side Spall	93
7	Right Side Spall	98
8	Right Side Spall	116
9	Right Side Spall	116
10	Left Side Spall	86
11	Left Side Spall	86
12	Left Side Spall	98
13	Left Side Spall	112
14	Left Side Spall	123
15	Lower Primary	19
16	Lower Primary	21
17	Lower Primary	35
18	Lower Primary	*
19	Upper Left Remote	64
20	Upper Left Remote	64
21	Upper Left Remote	65
22	Upper Left Remote	65
23	Upper Left Remote	73
24	Upper Left Remote	77
25	Upper Right Remote	65
26	Upper Right Remote	65
27	Upper Right Remote	65
28	Upper Right Remote	68
29	Upper Right Remote	*
30	Upper Right Remote	*
31	Lower Left Remote	60
32	Lower Left Remote	67
33	Lower Left Remote	68
34	Lower Left Remote	69
35	Lower Left Remote	70
36	Lower Right Remote	70
37	Lower Right Remote	70
38	Lower Right Remote	72
39	Lower Right Remote	72
40	Lower Right Remote	*

Notes

*	Crack did not reach gauge or too far from gauge
-	Not Readable
+	Gauges show propagation of splay at 50.61 MPa
	The wiring of gauges 26 and 30 were reversed

TABLE C-6

GGHOLE6 LOADING RESULTS

(Confining Pressure = 15 MPa)

Gauge Number	Crack Type	Load at Gauge at Time of Cracking (MPa)
1	Upper Primary	26
2	Upper Primary	30
3	Upper Primary	*
4	Right Side Spall	73
5	Right Side Spall	85
23	Right Side Spall	97
6	Right Side Spall	105
7	Right Side Spall	*
8	Right Side Spall	*
9	Left Side Spall	77
10	Left Side Spall	79
11	Left Side Spall	89
29	Left Side Spall	95
17	Left Side Spall	103
12	Left Side Spall	*
13	Left Side Spall	*
14	Lower Primary	30
15	Lower Primary	42
16	Lower Primary	*
17	Upper Left Remote	-
18	Upper Left Remote	-
19	Upper Left Remote	-
20	Upper Left Remote	-
21	Upper Left Remote	-
22	Upper Left Remote	-
23	Upper Right Remote	81
24	Upper Right Remote	82
25	Upper Right Remote	83
26	Upper Right Remote	83
27	Upper Right Remote	85
28	Upper Right Remote	-
29	Lower Left Remote	84
30	Lower Left Remote	85
31	Lower Left Remote	-
32	Lower Left Remote	*
33	Lower Left Remote	*
34	Lower Left Remote	*
35	Lower Right Remote	83
36	Lower Right Remote	86
37	Lower Right Remote	-
38	Lower Right Remote	*
39	Lower Right Remote	*
40	Lower Right Remote	*

Notes

* Crack did not reach gauge or too far from gauge

\- Not Readable

Many readings faint

TABLE C-7

PGHOLE1 LOADING RESULTS

(Confining Pressure = 0 MPa)

Gauge Number	Crack Type	Load at Gauge at Time of Cracking (MPa)
1	Upper Primary	19
2	Upper Primary	21
3	Upper Primary	24
4	Upper Primary	31
5	Upper Primary	35
6	Upper Primary	43
7	Upper Primary	46
8	Right Side Spall	91
9	Right Side Spall	*
9	Upper Right Remote	80
10	Upper Right Remote	80
11	Upper Right Remote	80
12	Upper Right Remote	80
13	Upper Right Remote	80
14	Upper Right Remote	80
15	Lower Primary	15
16	Lower Primary	15
17	Lower Primary	23
18	Lower Primary	24
19	Lower Primary	31
20	Lower Primary	37
21	Lower Primary	45
22	Left Side Spall	80
23	Left Side Spall	90
23	Upper Left Remote	65
24	Upper Left Remote	67
25	Upper Left Remote	70
26	Upper Left Remote	80
27	Upper Left Remote	80
28	Upper Left Remote	80
29	Left Side Spall	102
29	Lower Left Remote	79
30	Lower Left Remote	80
31	Lower Left Remote	80
32	Lower Left Remote	80
33	Lower Left Remote	80
34	Lower Left Remote	80
35	Right Side Spall	*
35	Lower Right Remote	80
36	Lower Right Remote	80
37	Lower Right Remote	80
38	Lower Right Remote	80
39	Lower Right Remote	80
40	Lower Right Remote	80

Notes

* Crack did not reach gauge or too far from gauge

\- Not Readable

TABLE C-8

PGHOLE3 LOADING RESULTS

(Confining Pressure = 15 MPa)

Gauge Number	Crack Type	Load at Gauge at Time of Cracking (MPa)
1	Upper Primary	43
2	Upper Primary	50
3	Upper Primary	*
4	Upper Primary	*
5	Upper Primary	*
6	Right Side Spall	116
7	Right Side Spall	116
8	Right Side Spall	116
9	Right Side Spall	110
9	Upper Right Remote	87
10	Upper Right Remote	88
11	Upper Right Remote	88
12	Upper Right Remote	90
13	Upper Right Remote	93
14	Upper Right Remote	94
15	Lower Primary	47
16	Lower Primary	51
17	Lower Primary	*
18	Lower Primary	*
19	Lower Primary	*
20	Left Side Spall	117
21	Left Side Spall	115
22	Left Side Spall	-
23	Left Side Spall	*
23	Upper Left Remote	88
24	Upper Left Remote	88
25	Upper Left Remote	89
26	Upper Left Remote	90
27	Upper Left Remote	96
28	Upper Left Remote	*
29	Lower Left Remote	104
30	Lower Left Remote	96
31	Lower Left Remote	104
32	Lower Left Remote	-
33	Lower Left Remote	*
34	Lower Left Remote	*
35	Right Side Spall	*
35	Lower Right Remote	96
36	Lower Right Remote	*
37	Lower Right Remote	*
38	Lower Right Remote	*
39	Lower Right Remote	*
40	Lower Right Remote	*

Notes

* Crack did not reach gauge or too far from gauge

\- Not Readable

Upper right remote growth seen during face spalling

TABLE C-9

PGHOLE4 LOADING RESULTS

(Confining Pressure = 5 MPa)

Gauge Number	Crack Type	Load at Gauge at Time of Cracking (MPa)
1	Upper Primary	30
2	Upper Primary	31
3	Upper Primary	*
4	Upper Primary	*
5	Upper Primary	*
6	Right Side Spall	96
7	Right Side Spall	98
8	Right Side Spall	-
9	Right Side Spall	-
9	Upper Right Remote	75
10	Upper Right Remote	76
11	Upper Right Remote	76
12	Upper Right Remote	77
13	Upper Right Remote	77
14	Upper Right Remote	*
15	Lower Primary	37
16	Lower Primary	-
17	Lower Primary	*
18	Lower Primary	*
19	Lower Primary	*
20	Left Side Spall	88
21	Left Side Spall	88
22	Left Side Spall	88
23	Left Side Spall	-
23	Upper Left Remote	*
24	Upper Left Remote	*
25	Upper Left Remote	*
26	Upper Left Remote	*
27	Upper Left Remote	*
28	Upper Left Remote	*
29	Left Side Spall	85
29	Lower Left Remote	-
30	Lower Left Remote	82
31	Lower Left Remote	82
32	Lower Left Remote	83
33	Lower Left Remote	86
34	Lower Left Remote	87
35	Right Side Spall	92
35	Lower Right Remote	77
36	Lower Right Remote	77
37	Lower Right Remote	77
38	Lower Right Remote	77
39	Lower Right Remote	78
40	Lower Right Remote	78

Notes

* Crack did not reach gauge or too far from gauge

\- Not Readable

TABLE C-10

PGHOLE5 LOADING RESULTS

(Confining Pressure = 10 MPa)

Gauge Number	Crack Type	Load at Gauge at Time of Cracking (MPa)
1	Upper Primary	29
2	Upper Primary	34
3	Upper Primary	*
4	Upper Primary	*
5	Upper Primary	*
6	Upper Primary	*
7	Upper Primary	*
8	Upper Right Remote	86
8	Right Side Spall	105
9	Right Side Spall	-
10	Lower Primary	34
11	Lower Primary	38
12	Lower Primary	*
13	Lower Primary	*
14	Lower Primary	*
15	Lower Primary	*
16	Lower Primary	*
17	Left Side Spall	102
18	Upper Left Remote	87
19	Lower Left Remote	91
18	Left Side Spall	104
19	Left Side Spall	-
20	Lower Right Remote	-
20	Right Side Spall	115

Notes

* Crack did not reach gauge or too far from gauge

\- Not Readable

TABLE C-11

GENERAL FRACTURE DEVELOPMENT
OBSERVATIONS ON BLOCK SAMPLES

Block Name	Confining Pressure (MPa)	Maximum Axial Load (MPa)	Comments
PGHOLE1	0	108.61	All cracks well developed, straight crack paths Upper and lower primaries and remotes occur with Few visible microcracks around crack paths Outer boundary of sidewall slabbing controlled by remotes Sidewall notch 3.5 mm deep
PGHOLE2	5	117.00	Loaded instanteously to max load Primary is faint with 2-3 step outs Remote reasonably clear Sidewall notch about 4 mm deep
PGHOLE3	15	127.09	Primary is not visible on face , but visible inside hole Remote is visible but has splays and microcrack bands Remotes show about 3 step-outs per 10 cm Sidewall notch 3.5 mm deep
PGHOLE4	5	123.03	Primary shows some wander in crack path One remote shows as a microcrack band rather than a distinct crack Sidewall spalling not completely controlled by remote cracks Sidewall notch 5 mm deep
PGHOLE5	10	122.80	Primary is faintly visible Remotes are visible but crack paths show wandering Sidewall spalling bounded by remote cracks Sidewall notch 5 mm deep
GGHOLE1	15	135.00	Primary not visible Remotes are very faint Sidewall notch about 5 mm deep Dense microcracking is visible around the hole
GGHOLE2	5	123.15	Primary faint on face, clearer in hole Remotes show multiple cracks and crack path wander A microcrack band is associated with the cracks Sidewall slabbing notch controlled by remote cracks Sidewall notch 5 mm deep
GGHOLE3	10	124.69	Primary is faint Remotes are visible and have microcrack bands associated with them Notches are 6 and 9 mm deep on either side

Continued...

TABLE C-11 (concluded)

Block Name	Confining Pressure (MPa)	Maximum Axial Load (MPa)	Comments
GGHOLE4	0	130.54	Microcrack bands associated with fractures Primary is weakly visible and crack path wanders Remotes show crack path wander, Upper right remote shows multiple splays or parallel cracks rather than a single crack Sidewall slabbing not controlled by remote cracks Sidewall notch about 8 mm deep
GGHOLE5	2.5	123.23	Primary faint on face but clear inside hole Remote clear but crack path wanders Sidewall spalling not bounded by remote cracks Sidewall notch about 5 mm deep
GGHOLE6	15	110.20	Primary faint on face, visible in hole Remotes are visble but have large microcrack bands associated with them Sidewall spalling not controlled by remote cracks Sidewall notch about 2.5 mm deep

APPENDIX D

CRACK LENGTH VERSUS LOAD VALUES

TABLE D-1

VALUES USED IN FIGURE 5.4

Sample PGHOLE1 Lower Primary	
Applied Load (MPa)	Linear Length (cm)
15	0
15	0.8
23	2.1
24	3.8
31	5.9
37	8.6
45	11.7

Sample GGHOLE4 Upper Primary	
Applied Load (MPa)	Linear Length (cm)
13	0
20	0.3
40	1.9

TABLE D-2

VALUES USED IN FIGURE 5.5

Sample PGHOLE3 Upper Left Remote	
Applied Load (MPa)	Linear Length (cm)
88	0
88	1.4
89	3.7
90	5.5
96	8.5

Sample GGHOLE1 Lower Left Remote	
Applied Load (MPa)	Linear Length (cm)
81	0
81	1
82	1.9
82	3.6
84	4.5

Sample PGHOLE3 Upper Right Remote	
Applied Load (MPa)	Linear Length (cm)
87	0
88	1.7
88	4
90	5.8
93	8.9
94	11.3

Sample GGHOLE6 Upper Right Remote	
Applied Load (MPa)	Linear Length (cm)
81	0
82	1.2
83	2.9
83	4.1
85	5.5

TABLE D-3

VALUES USED IN FIGURE 5.6

Sample PGHOLE4 Upper Right Remote	
Applied Load (MPa)	Linear Length (cm)
75	0
76	1.3
76	5.3
77	5.4
77	8

Sample GGHOLE2 Upper Right Remote	
Applied Load (MPa)	Linear Length (cm)
76	0
78	1.5
78	2.9
78	4.4

Sample PGHOLE4 Lower Left Remote	
Applied Load (MPa)	Linear Length (cm)
82	0
82	1.6
82	3.4
83	4.9
86	7.5
87	10.2

Sample GGHOLE2 Lower Left Remote	
Applied Load (MPa)	Linear Length (cm)
73	0
74	1.3
76	2.7
78	4.2
78	5.8
79	7.4